THE UNIVERSITY OF CHICAGO

SYMMETRY ENRICHED TOPOLOGICAL PHASES AND THEIR EDGE THEORIES

A DISSERTATION SUBMITTED TO
THE FACULTY OF THE DIVISION OF THE PHYSICAL SCIENCES
IN CANDIDACY FOR THE DEGREE OF
DOCTOR OF PHILOSOPHY

DEPARTMENT OF PHYSICS

BY
CHRISTOPHER HEINRICH

CHICAGO, ILLINOIS
JUNE 2017

To my parents

Crescat scientia; vita excolatur

TABLE OF CONTENTS

LIST OF FIGURES viii

LIST OF TABLES x

ACKNOWLEDGMENTS xi

ABSTRACT xiii

1 INTRODUCTION 1
1.1 Background 1
1.1.1 Phases of matter 1
1.1.2 Topological phases 2
1.1.3 Symmetry protected topological phases 4
1.1.4 Symmetry enriched topological phases 5
1.2 Questions and main results 7
1.2.1 Overview of main questions 7
1.2.2 Symmetry-enriched string nets 8
1.2.3 Protected edge modes with $\mathbb{Z}_2$ symmetry 9
1.2.4 Solvable models for neutral modes 11

2 SYMMETRY-ENRICHED STRING NETS 13
2.1 Introduction 13
2.2 Toric code with $e \leftrightarrow m$ symmetry 15
2.2.1 The model 16
2.2.2 Properties of the Hamiltonian 20
2.2.3 Ground state wave function 22
2.2.4 Excitations and string operators 24
2.2.5 Symmetry action on anyons 27
2.2.6 Braiding statistics 27
2.3 Relationship to doubled Ising string-net model 30
2.3.1 Review of doubled Ising string-net model 31
2.3.2 The gauged toric code model 33
2.3.3 Equivalence between gauged toric code and doubled Ising string-net model 35
2.3.4 Ungauging the doubled Ising string-net model 37
2.4 General construction 40
2.4.1 Drinfeld center, string-net models, and G-extensions 41
2.4.2 Symmetry enriched string-net models 44
2.4.3 Properties 47
2.5 Examples 49
2.5.1 Bosonic $\mathbb{Z}_2$ SPT phase 50
2.5.2 Toric code with a non-permuting $\mathbb{Z}_2$ symmetry 51
2.5.3 Quantum double of S_3 53

2.5.4 Quantum double of A_4 . . . 56
2.6 Conclusion . . . 58

3 PROTECTED EDGE MODES WITH $\mathbb{Z}_2$ SYMMETRY . . . 60
3.1 Background and motivation . . . 60
3.1.1 Chiral boson edge theories with $\mathbb{Z}_2$ symmetry . . . 60
3.1.2 Gapping perturbations and null vectors . . . 61
3.1.3 Edge theories of bosonic $\mathbb{Z}_2$ SPT phases . . . 63
3.1.4 Motivating example . . . 64
3.2 Main results and applications . . . 66
3.2.1 The auxiliary vector χ_+ . . . 67
3.2.2 General criterion . . . 69
3.2.3 Examples . . . 70
3.3 Derivation of results . . . 72
3.3.1 A few simplifications . . . 72
3.3.2 Derivation . . . 73
3.3.3 Proving $K = W = \sigma^x$ is gapped . . . 80
3.4 Abelian $\mathbb{Z}_2$ SETs . . . 81
3.4.1 Proof of sufficiency . . . 82

4 SOLVABLE MODELS FOR NEUTRAL MODES IN FRACTIONAL QUANTUM HALL EDGES . . . 84
4.1 Introduction . . . 84
4.2 Models and main results . . . 86
4.3 Toy model: infinite U . . . 90
4.3.1 Review of general formalism . . . 90
4.3.2 Solving the toy model . . . 92
4.3.3 Low energy phonon modes . . . 98
4.3.4 Expression for density operator . . . 99
4.3.5 Charge and neutral modes . . . 101
4.4 Toy model: finite U . . . 102
4.4.1 RG analysis of low energy theory . . . 103
4.4.2 Fate of neutral mode . . . 105
4.4.3 Finite U corrections . . . 107
4.5 Generalized models . . . 110
4.5.1 General impurity lattices . . . 111
4.5.2 Random impurities . . . 118
4.6 Conclusion . . . 123

5 CONCLUSION . . . 125
5.1 Summary of results . . . 125
5.2 Future directions . . . 126

A APPENDICES FOR CHAPTER 2 128
A.1 Ground state degeneracy 128
A.2 Derivation of ground state wave function 131
A.3 The other toric code with $e \leftrightarrow m$ symmetry 132
A.4 Derivation of string operators 133

B APPENDICES FOR CHAPTER 3 140
B.1 Derivation of SU(2) symmetry 140
B.1.1 Review: the SU(2) symmetry 140
B.1.2 Transformation law for b 143
B.2 A lemma about bosonic Abelian topological phases 145
B.3 Putting K, W, χ and χ_+ into standard form 147
B.4 Proving ν is integer 151
B.4.1 A special case 152
B.4.2 The general case 155
B.5 Proving $K_\pm$ have Lagrangian subgroups in the SET case 156
B.5.1 Statement of the result 156
B.5.2 Proof 156

C APPENDICES FOR CHAPTER 4 159
C.1 Degeneracy 159
C.1.1 General method for computing degeneracy 159
C.1.2 Application to impurity model 160
C.2 Regularizing the impurity scattering terms 163
C.3 Deriving the approximation (4.93) 166

REFERENCES 169

LIST OF FIGURES

1.1 A schematic diagram of anyon braiding. On the left side the particle a braids around particle b, and on the right side particle a braids around the vacuum. The difference between these processes is the statistical phase $e^{i\theta_{a,b}}$ 3

1.2 A diagram illustrating the relationship between symmetry and anyons. The focus of this thesis has been on phases with symmetry and anyons, shown in the upper right. 6

2.1 (color online) The Hilbert space of the symmetric toric code model is built out of two-state spins τ_p and three-state spins μ_l living on the plaquettes p and links l of the honeycomb lattice. The Hamiltonian is a sum of three terms, P_l, Q_v, B_p, which act on the green, blue, and red spins, respectively. 17

2.2 The four types of vertices that obey the fusion rules. 18

2.3 (a) The vertices counted by N_{p1}. (b) The vertices counted by N_{p2}. For a vertex to be counted, its initial state must match the picture on the left and final state match the picture on the right or vice versa. External legs of p are shown in bold. 20

2.4 (color online) Two examples of the function $f(X)$. Here the string states are drawn in the continuum rather than on the lattice. 22

2.5 The vertices counted by $N_{e1}, ..., N_{e6}$. Vertices marked with 'left' are only counted if the external leg (shown in bold) adjoins γ from the left, and similarly for those marked with 'right.' The vertices counted by $N_{m1}, ..., N_{m6}$ can be obtained from the above set by flipping all the plaquette spins: $|+\rangle \leftrightarrow |-\rangle$. 26

2.6 An example of paths β, γ used to find the mutual statistics of e and m. Applying the two string operators in two different orders gives results that differ by the mutual statistical phase $e^{i\theta_{e,m}}$. 29

2.7 The gauge field degrees of freedom, ν_{pq}, live on the links $\langle pq \rangle$ of the dual *triangular* lattice connecting neighboring plaquette spins (we omit link spins for clarity). . 33

2.8 Building a symmetry enriched string-net model involves two steps. First we construct the string-net model for the G-extension $\mathcal{D}$ of $\mathcal{C}$. Next we 'ungauge' the string-net model to obtain a G-symmetric model with anyon excitations given by $\mathcal{Z}(\mathcal{C})$. 41

2.9 By rotating oriented links 90 degrees counterclockwise, an orientation on the original hexagonal lattice gives an orientation on the dual triangular lattice. The latter allows us to define link variables g_l, given any configuration of plaquette spins $\{g_p\}$ and any link l of the original hexagonal lattice. 46

4.1 Toy model for a FQH edge with impurity scattering: two counter-propagating chiral Luttinger liquids with parameters k_1 and k_2 together with a regular lattice of impurity scatterers with spacing ℓ. 86

4.2 Phonon bandstructure of the toy model in the limit $U \to \infty$, for the case $k_1 = 1, k_2 = 3$ and $v = \ell = 1$. The zeros of the $n = 0$ band correspond to low energy phonon modes: $k = 0$ corresponds to a right-moving charge mode, while $k = \pi/\ell$ corresponds to a left-moving neutral mode. 95

4.3 Generalized impurity lattice model with three impurities per unit cell. The unit cell has length ℓ while the spacings between the impurities are ℓ_1, ℓ_2 and ℓ_3. . . 111

4.4 A schematic figure illustrating the difference between band structures with an odd and even number of impurities per unit cell. In the odd case (a), the phonon bands have zeros at $k = 0$ and $k = \pi/\ell$. In the even case (b), the phonon bands have both zeros at $k = 0$. 114
4.5 Random impurity model: two counter-propagating chiral Luttinger liquids in a circular geometry of length L, together with M randomly positioned impurity scatterers. 119

A.1 The 'T-junction' operator $W_{\sigma\bar{\sigma}\perp\psi\bar{\psi}}$ is made up of two string operators $W_{\sigma\bar{\sigma}}$, $W_{\psi\bar{\psi}}$ which meet at a point p. 135

LIST OF TABLES

2.1 The mapping U (2.44) between the Hilbert space of the gauged toric code model and the Hilbert space of the modified string-net model. 37
2.2 Anyon types and corresponding topological data for the quantum double $\mathcal{Z}(S_3)$. 53
2.3 Anyon types and corresponding topological data for the quantum double $\mathcal{Z}(A_4)$. 56

ACKNOWLEDGMENTS

I would first like to first express my gratitude for all of the physicists and scientists that have uncovered the laws of nature which I have had the pleasure to study, especially those early scientists who faced persecution and resistance for developing their bold new ideas. All of this knowledge would have been lost on me had it not been for countless dedicated instructors. Starting with Cindy Kvale in highschool, and throughout the rest of my education, I have had access to some of the best teachers in the world, and I am very grateful for all of them.

I would like to extend my deepest gratitude to my most dedicated instructor, and PhD advisor, Michael Levin. When I joined Michael's group over three years ago, I knew a small fraction of what I know now, and it required great patience, kindness and wisdom on his behalf to get me here. As a scientist and instructor, Michael combines deep creativity, physical insights, and an unfailing commitment to clear and precise communication. I am very grateful for having had the opportunity to work so closely with him, and am a much better scientist, thinker, and writer as a result.

I am grateful for my committee members, Emil Martinec, Dave Schuster, and Dam Thanh Son. I have had the fortune of knowing them as instructors, and have enjoyed interacting with them throughout the years at the Kadanoff Center Journal Club. I especially appreciate the time they have taken to serve on my thesis committee.

My time during my PhD would have been much less enjoyable without the company of many friends and classmates. I would like to especially mention Alex Edelman, Misha Laskin and Brent Perreault, my closest peers in the study of theoretical condensed matter physics. I have enjoyed many discussions, seminars, conferences and arguments in the company of these close friends, and many others at the University of Chicago. I also benefitted greatly from my participation in the Journal Club, and especially thank Jingyuan Chen, Michael Geracie and Dung Nguyen for many illuminating discussions.

My interest in physics goes back as long as I can remember, and I owe a tremendous amount to my parents for recognizing this interest so early on, and for encouraging and

supporting me along the way. Whether it was buying me books about black holes, enrolling me in science summer camps, or paying for my education, I surely would not be here it if were not for their constant love and support.

Lastly, I would like to express my deep gratitude for my wife and closest companion, Chen. We met as classmates here at the University of Chicago, and her passion, patience and wisdom have made me a much better scientist and human. I can confidently say that I would not have made it through my PhD if I had been without her love and companionship. Thank you.

ABSTRACT

In this thesis we investigate topological phases of matter that have a global, unbroken symmetry group – also known as symmetry enriched topological (SET) phases. We address three questions about these phases: (1) how can we build exactly solvable models that realize them? (2) how can we determine if their edge theories can be gapped without breaking the symmetry? and (3) how do we understand the phenomenon of decoupled charge and neutral modes which occurs in certain fractional quantum Hall states?

More specifically, we address the first question by constructing exactly solvable models for a wide class of symmetry enriched topological (SET) phases, which we call *symmetry-enriched string nets*. The construction applies to 2D bosonic SET phases with finite unitary onsite symmetry group G, and we conjecture that our models realize every phase in this class that can be described by a commuting projector Hamiltonian. As an example, we present a model for a phase with the same anyon excitations as the toric code and with a $\mathbb{Z}_2$ symmetry which exchanges the e and m type anyons. We further illustrate our construction with a number of additional examples.

For the second question, we focus on the edge theories of 2D SET phases with $\mathbb{Z}_2$ symmetry. The central problem we seek to solve is to determine which edge theories can be gapped without breaking the symmetry. Previous attempts to answer this question in special cases relied on constructing perturbations of a particular type to gap the edge. This method proves the edge can be gapped when the appropriate perturbations can be found, but is inconclusive if they cannot be found. We build on this previous work by deriving a necessary and sufficient algebraic condition for when the edge can be gapped. Our results apply to $\mathbb{Z}_2$ symmetry protected topological phases as well as Abelian $\mathbb{Z}_2$ SET phases.

Finally, in chapter 4, we describe solvable models that capture how impurity scattering in certain fractional quantum Hall edges can give rise to a neutral mode — i.e. an edge mode that does not carry electric charge. These models consist of two counter-propagating chiral Luttinger liquids together with a collection of discrete impurity scatterers. Our main result

is an exact solution of these models in the limit of infinitely strong impurity scattering. From this solution, we explicitly derive the existence of a neutral mode and we determine all of its microscopic properties including its velocity. We also study the stability of the neutral mode and show that it survives at finite but sufficiently strong scattering. Our results are applicable to a family of Abelian fractional quantum Hall states of which the $\nu = 2/3$ state is the most prominent example.

CHAPTER 1

INTRODUCTION

1.1 Background

1.1.1 Phases of matter

Condensed matter physics is the study of what happens when a large number of particles are put together and interact. The behavior of a large number of particles is often strikingly different than the behavior of a few particles, and it is often difficult or impossible to predict how large numbers of particles will behave even if you understand the behavior of a few particles perfectly. Furthermore, the conditions under which these particles interact, such as the temperature or the influence of external fields, can lead to an incredibly diverse array of beautiful and unusual phenomena. Some familiar examples of such phenomena include waves on a lake, the electrical conductance of a copper wire, or the transition from liquid water to ice. All of these are condensed matter phenomena since they only occur when you have a large number of particles together – it makes no sense to ask if a single water molecule is liquid or frozen, or if a single atom of copper can conduct electricity.

Physicists realized early on that it was possible to group together different materials based on them having common properties. This grouping is useful because it allows one to tame the complexity in nature, and develop theories that explain the properties of many different materials belonging to the same group. For example, both copper and iron conduct electricity, and so both are called 'metals', despite having different chemical properties. Furthermore, the band theory of solids, which explains their electrical conduction properties, applies equally well in either case. These groups of different materials with similar properties are known as 'phases of matter'. An equivalent definition of condensed matter physics, then, is that it seeks to answer two fundamental questions: what are all the possible phases of matter, and what are the properties of these phases?

For quantum phases of matter, i.e. phases of matter at zero temperature, an important distinction can be made between two general classes: gapped phases and gapless phases. Gapped phases, such as insulators, have an energy gap separating the ground state from the first excited state, meanwhile gapless phases, such as metals, have no such gap. In this thesis we will primarily be concerned with gapped quantum phases, and their gapless boundary modes.

Significant progress was made towards classifying all gapped phase of matter by Landau in the thirties, with his symmetry-breaking theory of phase transitions[39]. He argued that phases of matter could be classified according to the symmetries they broke. Such symmetry breaking phases can be characterized by an *order parameter* which has a non-zero expectation value in the ordered state. The symmetry breaking theory of phases transitions successfully describes many phases of matter including ferromagnets, superconductors, crystals and superfluids.

Despite its many successes, physicists eventually discovered phases of matter which evaded classification by symmetry breaking. These new phases, which lack an order parameter, and an associated broken symmetry, are now known as *topological phases*. Physicists have now discovered many distinct topological phases, and classifying and understanding these phases is one of the central themes of modern condensed matter physics.

1.1.2 Topological phases

Perhaps the biggest experimental discovery in condensed matter physics during the last 40 years was the discovery of the integer and fractional quantum Hall effects [34, 60]. Quite unexpectedly, von Klitzing et al found that when you put a 2D electron gas into a very strong magnetic field, and cool it to near absolute zero, the Hall conductance becomes perfectly quantized to integer multiples of e^2/h [34]. Even more surprisingly, just a few years later, Tsui et al[60] found that the conductance could be quantized at certain fractional multiples of e^2/h, the most prominent example being $\frac{1}{3}e^2/h$. These discoveries revolutionized condensed

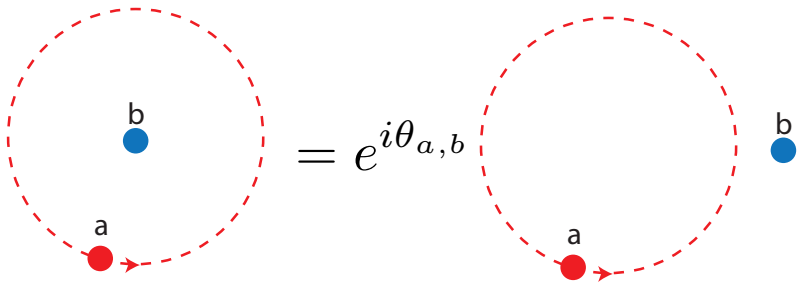

Figure 1.1: A schematic diagram of anyon braiding. On the left side the particle a braids around particle b, and on the right side particle a braids around the vacuum. The difference between these processes is the statistical phase $e^{i\theta_{a,b}}$

matter physics, and opened up a whole new era in our understanding of phases of matter.

Almost 40 years later, the fractional quantum Hall effect continues to inspire new theoretical and experimental work. Even more fascinating than the exact quantization of the Hall conductance, is the physical mechanism behind this quantization and the associated phenomena of fractional charge and fractional braiding statistics. The first paper to explain the fractional quantum Hall effect was a seminal work by Laughlin[40], which introduced ground state wave functions with properties very similar to those observed experimentally. In this work it was argued that the fractionally quantized Hall conductance was due to the existence of fractionally charged quasiparticles, with charge $e/3$. It was later realized that in addition to being fractionally charged, these particles also have fractional braiding statistics[1]. By fractional braiding statistics, we mean that there are two quasiparticles a and b such that when one is braided all the way around the other the wave function is *not* multiplied by $+1$ as it is for bosons and fermions, but by some phase factor $e^{i\theta_{a,b}}$, as shown in Figure 1.1.

We are now in a position to define a topological phase. A topological phase is a *gapped many-body phase with quasiparticles obeying fractional braiding statistics.* Quasiparticles with this property are known as *anyons.*[1] An interesting consequence of the definition is that topological phases have topological ground state degeneracy – that is, when these

1. In some cases, $\theta_{a,b}$ can be a matrix, in which case the anyons a and b are called *non-Abelian* anyons.

phases are placed on topologically non-trivial manifolds such as a torus, their ground states are degenerate, and the degeneracy is protected against arbitrary perturbations as long as the energy gap remains open [12, 68].

While the most prominent experimental examples of topological phases are given by fractional quantum Hall states, many other theoretical models for different topological phases are known[48, 32]. One of the simplest and most well known examples is the toric code [32]. The toric code phase is conventionally realized in an exactly solvable lattice model with 2-state spins located on the links of the square lattice. The Hamiltonian is a sum of commuting projector operators A_v and B_p which act on the vertices and plaquettes of the square lattice: $H = -\sum_v A_v - \sum_p B_p$. The ground state of the system satisfies $A_v = B_p = 1$, and is four-fold degenerate on a torus. This system has four distinct species of anyons, conventionally labeled as $\{1, e, m, em\}$, which correspond to defects with $A_v = -1$ or $B_p = -1$ or both. These particles have the special property that braiding an e-particle all the way around an m-particle changes the phase of the wave function by $e^{i\theta_{e,m}} = -1$, in other words, these particles obey fractional statistics. We will return to the toric code in chapter 2 where we introduce an exactly solvable model with the same anyon excitations, and a $\mathbb{Z}_2$ symmetry that exchanges e and m.

1.1.3 Symmetry protected topological phases

One of the most surprising developments in condensed matter physics during the last 20 years was the theoretical prediction[30] and subsequent experimental discovery[36] of 2D topological insulators [21]. It had always been assumed that there was only one type of two dimensional time reversal invariant band insulator, and the discovery of a distinct phase, now known as the *topological insulator*, revolutionized the way we think about symmetries in condensed matter physics. One of the distinguishing properties of a topological insulator is that it has protected gapless boundary modes, while the conventional insulator does not. Time reversal and charge conservation symmetry play a crucial role in this story, if either

of these symmetries is broken then the distinction between topological and conventional insulators disappears, and the resulting phase is a conventional insulator.

This observation motivated a generalization of topological insulators to a broad class of phases now known as *symmetry protected topological phases*, which can exist in any dimension and can be built out of bosons or fermions. More specifically, a gapped many-body system is said to belong to a non-trivial symmetry protected topological (SPT) if it satisfies the following three criteria. First, the Hamiltonian is invariant under some set of symmetries which are not broken explicitly or spontaneously. Second, the ground state of the Hamiltonian cannot be connected to a trivial insulator without breaking the symmetries or closing the energy gap. And finally, the ground state *can* be connected to a trivial state without closing the gap if the symmetries are broken in the process. In other words, the last property implies that the state has no intrinsic topological order.

SPT phases have now been extensively studied and are believed to be classified in many cases. In an important work by Chen et al[10], a wide class of exactly solvable models were presented for bosonic SPT phases with symmetry group G in any dimension d. Perhaps the simplest example is a 2D bosonic SPT with $\mathbb{Z}_2$ symmetry. There are believed to be two possible phases for this class, one trivial and one non-trivial, and the non-trivial phase has been proven to have protected, gapless edge modes [43].

1.1.4 Symmetry enriched topological phases

Not long after the discovery of topological insulators, and the subsequent explosion of interest in SPT phases, physicists began to wonder how phases with anyons (topological phases) and phases with unbroken symmetries (SPT phases) fit together. Most research had previously focused on one or the other, but when both are present there can be a rich interplay between anyons and symmetry (Fig. 1.2). Such phases with unbroken symmetries and anyons are known as *symmetry enriched topological* (SET) *phases*, and are the main focus of this thesis.

There are two ways that unbroken symmetries can interplay with anyons in an SET

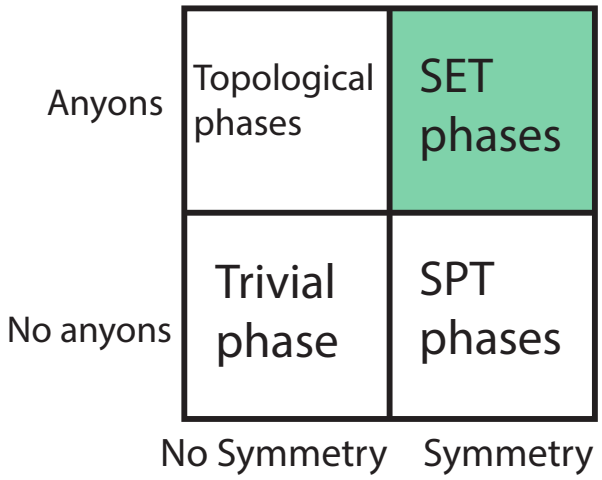

Figure 1.2: A diagram illustrating the relationship between symmetry and anyons. The focus of this thesis has been on phases with symmetry and anyons, shown in the upper right.

phase. The first way, which is commonly referred to as *symmetry fractionalization*, leads to anyons acquiring a fractional charge. When an anyon that carries fractional charge is braided around symmetry defect lines, the wave function acquires a phase not equal to the identity. One of the most famous examples of *symmetry fractionalization* occurs in FQH states. In addition to having anyons, these phases also have a $U(1)$ symmetry associated with charge conservation. In a state with filling factor $\nu = 1/3$ for example, the lowest energy excitations carry fractional charge $\frac{e}{3}$, and braiding a pair of these charges around each other leads to a phase factor of $e^{\frac{2\pi i}{3}}$.

The other way that symmetry can act is by *permuting* the set of anyons. This permutation action can be difficult to treat since the anyons can be transformed in a non-trivial way. As a result, SET phases with permutation action are less well understood, and a central theme of the thesis is to study this fascinating class of phases. A simple example of a phase in this class is the toric code phase with a $\mathbb{Z}_2$ symmetry that permutes the e and m particles.

1.2 Questions and main results

1.2.1 Overview of main questions

Three basic questions one can ask about SET phases are: (1) how can we classify them? (2) how can we build theoretical models that realize them? and (3) how do we study and characterize their properties? These three questions are not unrelated, and in general, answering any one of them will shed light on the others. The first question of classification is an interesting one, but is not one we will tackle directly in this thesis. There has been progress made in this direction, particularly in Ref. [3], in which a mathematical classification of SET phases was proposed and studied. In this thesis we report significant progress towards the second and third question.

In chapter 2, we address the question of how to build exactly solvable models for SET phases. Exactly solvable models are useful because they can be used to study a particular phase in depth, either analytically or numerically, and also because they provide a concrete physical proof that such a phase can actually be realized as the ground state of some local, Hermitian Hamiltonian. We present a construction for building models for SET phases which takes certain mathematical data as input, and outputs an exactly solvable model with a number of nice properties that facilitate analytical study.

In chapter 3, we address the question of characterizing SET phases. One of the most basic and important questions one can ask about an SET phase involves the behavior at its boundary with the vacuum. In particular, if the phase is defined on a manifold with boundary, how can we determine if the boundary excitations can be gapped without breaking the symmetry? This is an important question because the existence of gapless boundary modes can lead to a variety of interesting transport phenomena, as revealed by topological insulators and fractional quantum Hall states. We answer this question for Abelian SETs with $\mathbb{Z}_2$ symmetry by introducing an invariant ν. This invariant can be computed using standard data for parametrizing edge theories of SET phases, and has a simple interpretation:

when ν is equal to zero mod 2 the boundary can be gapped without breaking the symmetry and when ν is non-zero mod 2 the boundary cannot be gapped.

Finally, in chapter 4 we further address the question of characterizing SET phases by investigating more deeply a phenomenon that occurs on the edges of certain fractional quantum Hall states. The phenomenon we investigate is that of decoupled charge and neutral modes, which occurs in certain FQH edge states, most notable the $\nu = 2/3$ state. We present exactly solvable models for impurity scattering in these edge states which capture this phenomenon. The main result is an exact solution of these models in the limit of infinitely strong impurity scattering. From this solution, we explicitly derive the existence of a neutral mode and we determine all of its microscopic properties including its velocity. We also study the stability of the neutral mode and show that it survives at finite but sufficiently strong scattering.

The contents of chapters 2 and 4 are adapted from Ref. [22] and Ref. [23] respectively. Meanwhile, the results from chapter 3 will be included in a future publication. Mathematical details are left for the appendices. We now proceed to introduce each chapter in more detail, including additional background material and concrete statements of the main results.

1.2.2 Symmetry-enriched string nets

A useful approach for studying gapped quantum phases, especially those with interactions, is to construct exactly solvable lattice models that realize them [32, 48, 33, 18, 62, 10]. Among other applications, such models have been used to prove that certain phases exist and are anomaly free [18, 7]. In addition, exactly solvable models have revealed new properties of previously known phases [6, 47]. In most cases, the solvability of these models comes from the fact that their Hamiltonians can be written as a sum of commuting projection operators P_i, i.e. $H = -\sum_i P_i$. We will refer to Hamiltonians of this type as 'commuting projector' models.

The solvable model approach has been developed primarily in the context of two types of

phases: (1) topological phases without symmetries and (2) symmetry protected topological phases. In the former case, the string-net models of Ref. [48] are known to realize a large class of two dimensional topological phases. Likewise, in the latter case, the cohomology models of Ref. [10] can realize symmetry-protected topological (SPT) phases in arbitrary spatial dimension with finite unitary onsite symmetry. These constructions are especially appealing because they are conjectured to realize *all* phases of type (1) and (2) that can be built from commuting projector models.

In view of these successes, it is natural to try to build solvable models for symmetry-*enriched* topological (SET) phases. Some progress has been made in this direction and a number of solvable models for SET phases have been written down [53, 24, 59, 58]. However, these constructions are not as general as they could be since they do not include all phases that can be realized with commuting projector models.

In chapter 2 we construct exactly solvable models for more general 2D SET phases, which we call 'symmetry enriched string-net' models. Our construction applies to 2D SET phases that are built out of bosonic degrees of freedom and have a finite unitary onsite symmetry group. We conjecture that, within this class of SET phases, our models realize every phase that can be described by a commuting projector Hamiltonian. As an example, we present an exactly solvable model for an SET phase that has eluded previous constructions, namely a phase with the same anyon excitations as the toric code [32] and an onsite $\mathbb{Z}_2$ symmetry which exchanges the e and m anyon excitations.

1.2.3 Protected edge modes with $\mathbb{Z}_2$ symmetry

One of the most important properties of a two dimensional gapped phase of matter is whether or not it supports protected, gapless edge modes. Protected edge modes lead to interesting transport phenomena, and they also indicate that there is some non-trivial phase in the bulk. For example, topological insulators have protected edge modes as long as time reversal is unbroken, leading to a quantized spin Hall current [30]. Likewise, fractional quantum Hall

states also have protected edge modes which carry the quantized Hall current in systems with boundaries. Thus, given an edge theory for a 2D phase of matter, one of the questions we would like to answer is whether or not its edge theory can be gapped without breaking the physical symmetries. If the edge theory cannot be gapped, then the edge modes are protected and gapless.

In the case of bosonic $\mathbb{Z}_2$ SPT phases, important progress towards understanding when the boundaries can be gapped was made in Refs. [43, 50]. These papers proved (1) there are two distinct bosonic $\mathbb{Z}_2$ SPT phases and (2) the model in the trivial phase has a gapped symmetric boundary while the model in the non-trivial phase has a gapless boundary, as long as the $\mathbb{Z}_2$ symmetry is unbroken.

Likewise, for the case of Abelian topological phases without symmetry, important progress was made in Ref. [42]. In this paper, a necessary and sufficient condition was derived for when an Abelian topological phase can have a gapped boundary. In particular, in order to have a gapped boundary, the set of anyons must contain a Lagrangian subgroup – that is, a subset of anyons $\mathcal{M}$ which (1) have trivial braiding statistics with respect to every other particle in $\mathcal{M}$ and (2) every anyon not contained in $\mathcal{M}$ has non-trivial braiding statistics with respect to at least one anyon in $\mathcal{M}$.

Despite these advances, it was unclear how to generalize these results to arbitrary $\mathbb{Z}_2$ SPT edge theories, or to topological phases with a $\mathbb{Z}_2$ symmetry, i.e. $\mathbb{Z}_2$ SETs. In chapter 3, we build on this previous work and address the question: given the edge theory of a 2D Abelian SET with a $\mathbb{Z}_2$ symmetry, how can you determine if it can be gapped without breaking the symmetry. Our main result is two necessary and sufficient conditions for when such a phase can have a gapped edge. In particular, the phase must (1) contain a Lagrangian subgroup invariant under the symmetry and (2) the value of a particular invariant must be equal to zero. This invariant, which we label ν, is defined in terms of the data parametrizing the phase.

1.2.4 Solvable models for neutral modes

Perhaps the most well known examples of gapless edge states occur at the boundary of quantum Hall states. These edge states are guaranteed to be gapless, as long as the $U(1)$ charge conservation symmetry is unbroken, since they are responsible for carrying the quantized Hall current. Every state has at least one edge mode, but the structure of these modes varies from state to state. For example, the Laughlin states are believed to have a single chiral edge mode,[65] while integer quantum Hall states have multiple chiral edge modes — one for every filled Landau level [19].

Because these edge states are guaranteed to be gapless as long as the symmetry is unbroken, we seek to address a more fine grained question about the structure of these modes for a family of fractional quantum Hall states, of which the $\nu = 2/3$ state is the most prominent example. The $\nu = 2/3$ state is interesting because it is believed to have two *counter-propagating* chiral edge modes — one which is identical to the $\nu = 1$ integer quantum Hall state, and one which looks like the edge mode of a $\nu = 1/3$ Laughlin state, but with opposite chirality [64, 66, 52, 26]. This edge theory for the $\nu = 2/3$ state poses a basic question because it predicts charge propagation in both directions along the edge, in disagreement with experiment [2].

This question was first addressed by Kane, Fisher and Polchinski in Ref. [29]. In that work, the authors argued that what is missing from the clean edge theory, is impurity-induced electron scattering between the $\nu = 1$ and $\nu = 1/3$ edge modes. The authors showed that random impurity scattering can drive the edge to a special disorder dominated fixed point where one of the edge modes is electrically *neutral* while the other carries charge; the charge mode propagates in the direction determined by the external magnetic field while the neutral mode propagates in the opposite 'upstream' direction. This mode structure can explain why current flow is only observed in one direction on the $\nu = 2/3$ edge. It is also consistent with experiments on the $\nu = 2/3$ edge which have found evidence for upstream energy-carrying neutral modes.

While the analysis of Ref. [29] is powerful, it leaves some important questions unanswered. In particular, it does not give a microscopic picture for how a neutral mode emerges from impurity scattering. In this chapter, we seek to provide such a picture using concrete models. The models we consider are built out of two counter-propagating chiral Luttinger liquids together with a collection of discrete impurity scatterers. Our main result is an exact solution of these models in the limit of infinitely strong impurity scattering, which we obtain using a formalism introduced in Ref. [15]. From this solution, we explicitly derive the existence of a neutral mode and we determine all of its microscopic properties including its velocity. Importantly, we also study the stability of the neutral mode and we show that it survives at finite, but sufficiently strong impurity scattering, as long as this scattering has a random spatial dependence.

CHAPTER 2

SYMMETRY-ENRICHED STRING NETS

2.1 Introduction

The interplay between symmetry and topology in gapped quantum many body systems has been a subject of intense investigation recently. Spurred by the theoretical prediction and experimental discovery of topological insulators,[20, 55] a large class of gapped quantum many body systems in which symmetry and topology play a crucial role have been predicted and classified. At the heart of this classification is the concept of a gapped *phase*: two gapped many body systems are said to belong to the same phase if one can continuously interpolate between their Hamiltonians while maintaining a finite energy gap and preserving all physical symmetries.

In this chapter we construct exactly solvable models for 2D SET phases, which we call 'symmetry enriched string-net' models. Our construction applies to the simplest class of 2D SET phases, namely those that are built out of bosonic degrees of freedom and have a finite unitary onsite symmetry. We conjecture that, within this class of SET phases, our models realize every phase that can be described by a commuting projector Hamiltonian. (In fact, our conjecture is even stronger: we believe that our models realize every phase whose underlying topological order can be realized by a commuting projector model.) As an example, we present an exactly solvable model for an SET phase that has eluded previous constructions, namely a phase with the same anyon excitations as the toric code[32] and an onsite $\mathbb{Z}_2$ symmetry which exchanges the e and m (i.e. $\mathbb{Z}_2$ charge and $\mathbb{Z}_2$ flux) anyon excitations.

To understand the basis of our conjecture, we need to recall recent work on the classification of 2D SET phases.[3] According to this work, every SET phase with anyon excitations $\mathcal{A}$ and finite unitary onsite symmetry group G is associated with a mathematical object known as a 'braided G-crossed extension of $\mathcal{A}$.[3, 59] Roughly speaking, this object describes

the collective fusion and braiding data of the anyon excitations in $\mathcal{A}$ along with extrinsic symmetry defects. It is known that if two models are described by distinct braided G-crossed extensions then they belong to distinct SET phases. It has also been conjectured that the converse is true.[3] If this is the case, then braided G-crossed extensions provide a complete classification of 2D SET phases.[1]

Using this language, we can precisely characterize the generality of our models. Consider a topological phase with anyon excitations $\mathcal{A}$ that is realizable with a string-net model and has no symmetries. Then, with our construction, we can build a symmetry enriched string-net model realizing every braided G-crossed extension of $\mathcal{A}$. Our conjecture now follows immediately from this result if we make two assumptions: (1) string-net models realize every topological phase (without symmetry) that can be realized by commuting projector models and (2) the above classification is correct.

The general idea behind our construction is as follows. Suppose we want to construct a model for a particular SET phase with symmetry group G. We can build such a model in two steps. The first step is to build a string-net model that realizes the *gauged* SET phase — that is, the phase obtained by gauging the global G-symmetry of the SET phase of interest. In general, this step can be challenging, but mathematical results guarantee that such a string-net model exists. The second step is to 'ungauge' the resulting string-net model: that is, to construct a model that has a symmetry group G, and with the property that gauging this symmetry gives back the string-net model (or at least something that belongs to the same phase). Conveniently, this second step can be accomplished rather easily by making small modifications to the string-net Hilbert space and Hamiltonian. Once we make these modifications, the resulting lattice model realizes the SET phase of interest.

We now comment on the relationship between our results and previous work. Exactly solvable models realizing certain SET phases were written down in Ref. [24]. This construction was then extended in Ref. [58] to include certain anyon permuting symmetries, but

1. See Ref. [37] for a different approach to classification.

not all. The previous constructions of SET phases that are perhaps most similar to ours are given in Refs. [53] and [9]. The models of Ref. [53] realize a subset of the SET phases discussed in this chapter, and in these cases their models are essentially equivalent to ours. Meanwhile, the models of Ref. [9] are similar to ours in that they realize SET phases by extending the string-net construction. However, our construction has the advantage of providing a more algorithmic way of building models and making the symmetry manifest. It is also worth noting that the 2D group cohomology SPT models[10] and string-net models[48] can be considered as special cases of our construction by taking the limits $\mathcal{A} = 0$ and $G = 0$ respectively.

This chapter is organized as follows. To warm-up, we present a simple example of our construction in section 2.2. This example is an exactly solvable model for a toric code SET phase with a $\mathbb{Z}_2$ symmetry which exchanges the e and m anyon excitations. In section 2.3, we explain the relationship between this toric code model and the string-net model that it descends from, namely the *doubled Ising* string-net model. After this warm-up, we outline the general construction in section 2.4. We then illustrate the general construction with additional examples in section 2.5. Technical arguments are given in the appendices.

2.2 Toric code with $e \leftrightarrow m$ symmetry

Before discussing the general construction, it is useful to first see a concrete example. The example that we present is an exactly solvable model that has the same types of anyon excitations as the toric code[32] and has a global onsite $\mathbb{Z}_2$ symmetry which exchanges the 'e' and 'm' type anyons (also known as the $\mathbb{Z}_2$ charge and $\mathbb{Z}_2$ flux). We will refer to this example as the 'symmetric toric code' model.

Like all of the symmetry enriched string-net models, the symmetric toric code model is derived from a parent string-net model — in this case, the doubled Ising string-net model. That being said, in this section we will make every effort to analyze the symmetric toric code model from first principles, without referring to the doubled Ising string-net model.

We postpone the discussion of the connection between the two models to section 2.3.

We note here that there are actually two *distinct* toric code SET phases with an $e \leftrightarrow m$ symmetry, which differ in a very minor way.[3] For simplicity, we focus on just one of them in the main text, but we briefly discuss the other in appendix A.3.

2.2.1 The model

The model is a spin system built out of *two-state* spins that live on the plaquettes of the honeycomb lattice and *three-state* spins that live on the links of the honeycomb lattice. We will denote the basis states of the two-state spins by $|+\rangle$ and $|-\rangle$, and the basis states of the three-state spins by $|1\rangle$, $|\psi\rangle$, and $|\sigma\rangle$. In this notation, the basis states for the full Hilbert space are labeled as $|\{\tau_p^z, \mu_l\}\rangle$ where $\tau_p^z = \pm$ parameterizes the states of the plaquette p and $\mu_l = 1, \psi, \sigma$ parameterizes the states of the link l (Fig. 2.1).

We will sometimes find it convenient to describe the link degrees of freedom using an alternative language involving strings. In particular, if a link is in the state $|\psi\rangle$, we will say that it is occupied by a ψ string, and likewise if the link is in the state $|\sigma\rangle$, we will say it is occupied by a σ string. If a link is in the state $|1\rangle$, we will say that it is unoccupied. Using this language, every state of the link spins μ_l corresponds to a configuration of ψ and σ strings drawn on the honeycomb lattice.

The Hamiltonian of the model,

$$H = -\sum_l P_l - \sum_v Q_v - \sum_p B_p, \tag{2.1}$$

is expressed as a sum over operators associated with the links (l), vertices (v), and plaquettes (p) of the honeycomb lattice. We now explain how each of these operators are defined.

The link operator P_l acts on three spins — namely the ones living on the link l and the

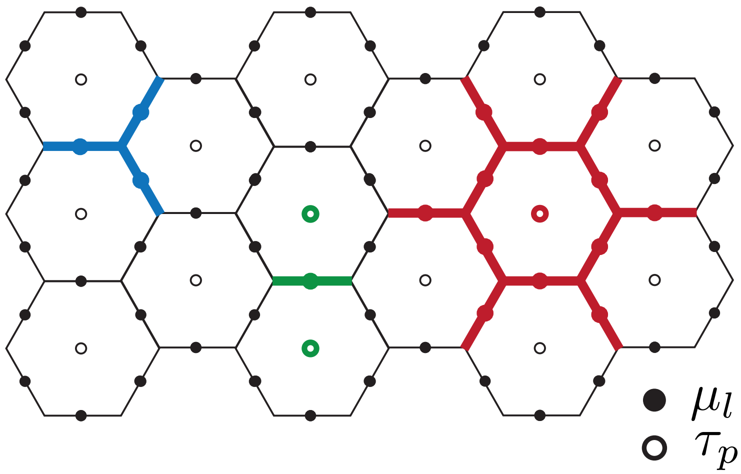

Figure 2.1: (color online) The Hilbert space of the symmetric toric code model is built out of two-state spins τ_p and three-state spins μ_l living on the plaquettes p and links l of the honeycomb lattice. The Hamiltonian is a sum of three terms, P_l, Q_v, B_p, which act on the green, blue, and red spins, respectively.

two adjacent plaquettes p and q (green spins in Fig. 2.1). It is defined by

$$P_l = \frac{1}{2}(1 + (-1)^{N_{l\sigma}} \cdot \tau_p^z \tau_q^z) \tag{2.2}$$

Here τ_p^z and τ_q^z are the standard Pauli operators for the plaquette spins p and q, and $N_{l\sigma}$ is a link spin operator defined by $N_{l\sigma}|1\rangle = N_{l\sigma}|\psi\rangle = 0$ and $N_{l\sigma}|\sigma\rangle = |\sigma\rangle$.

If we examine the above definition we can see that P_l has a simple interpretation: P_l projects onto states such that either (1) τ_p^z and τ_q^z are anti-aligned and the link l is in the state $|\sigma\rangle$ or (2) τ_p^z and τ_q^z are aligned, and the link l is *not* in the state $|\sigma\rangle$. In other words, P_l projects onto states in which the σ strings coincide with the *domain walls* between the plaquette spins.

The vertex operator Q_v acts on the three spins living on the links adjacent to v (blue spins in Fig. 2.1). It is defined by

$$Q_v \left| {}_{i}\!\!\prec^{j}_{k} \right\rangle = \delta_{ijk} \left| {}_{i}\!\!\prec^{j}_{k} \right\rangle \tag{2.3}$$

where δ_{ijk} is a fully symmetric three-index tensor whose only nonzero elements are

$$\delta_{111} = \delta_{1\psi\psi} = \delta_{1\sigma\sigma} = \delta_{\psi\sigma\sigma} = 1, \tag{2.4}$$

together with cyclic permutations. In the string language, we will refer to the states with $\delta_{ijk} = 1$ as obeying the 'fusion rules', and those with $\delta_{ijk} = 0$ as violating the fusion rules (see Fig. 2.2). Thus, Q_v is a projection operator that projects onto states that obey the fusion rules at v.

The B_p operator acts on the plaquettes of the honeycomb lattice (red spins in Fig. 2.1) and is a linear combination of three terms:

$$B_p = a_1 B_p^1 + a_\psi B_p^\psi + a_\sigma B_p^\sigma \tau_p^x, \tag{2.5}$$

where $a_1 = a_\psi = \frac{1}{4}$ and $a_\sigma = \frac{\sqrt{2}}{4}$. Each term, B_p^s, takes the form

$$B_p^s = \mathcal{P}_p \tilde{B}_p^s \mathcal{P}_p \tag{2.6}$$

where

$$\mathcal{P}_p = \prod_{v \in p} Q_v \tag{2.7}$$

is a projection operator which projects onto states that obey the fusion rules at the 6 vertices adjoining p. Before giving formal definitions of these operators, it is worth noting that the B_p^s operators are identical to the B_p^s operators in the doubled Ising string-net model, a connection we will explore further in section 2.3.

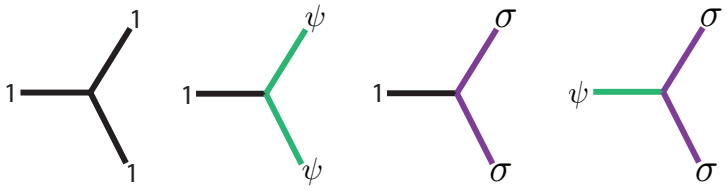

Figure 2.2: The four types of vertices that obey the fusion rules.

The first operator, $\tilde{B}_p^1$, is the simplest:

$$\tilde{B}_p^1 = \mathbf{1}. \tag{2.8}$$

The second operator, $\tilde{B}_p^\psi$, is more complicated. This operator acts on 12 link spins — 6 of which lie along the boundary of the plaquette p and 6 of which lie on the 'external legs' that adjoin p. Importantly, $\tilde{B}_p^\psi$ acts differently on the boundary spins than it does on the external leg spins: in particular, while $\tilde{B}_p^\psi$ changes the state of the boundary spins, it does not affect the state of the spins on the external legs. Thus, the nonvanishing matrix elements of $\tilde{B}_p^\psi$ can be parameterized as

$$\left\langle \quad \right| \tilde{B}_p^\psi \left| \quad \right\rangle = B_{p,ghijkl}^{\psi,g'h'i'j'k'l'}(abcdef)$$

The explicit formula for these matrix elements is

$$B_{p,ghijkl}^{\psi,g'h'i'j'k'l'}(abcdef) = \delta_{\psi gg'}\delta_{\psi hh'}\cdots\delta_{\psi ll'}\cdot(-1)^{N_{p1}} \tag{2.9}$$

where N_{p1} denotes the number of vertices of p of the type shown in Fig. 2.3a. The matrix elements for $\tilde{B}_p^\sigma$ have a similar structure and are given by

$$B_{p,ghijkl}^{\sigma,g'h'i'j'k'l'}(abcdef) = \delta_{\sigma gg'}\cdots\delta_{\sigma ll'}\cdot 2^{-\frac{N_{p\sigma}}{4}}(-1)^{N_{p2}} \tag{2.10}$$

Here, $N_{p\sigma}$ denotes the number of external legs $a, b, \ldots, f$ that are in the state $|\sigma\rangle$ while N_{p2} denotes the number of vertices of p for which the initial state has a vertex of the type shown on the left of Fig. 2.3b and a final state vertex of the type shown on the right of Fig. 2.3b or vice versa.

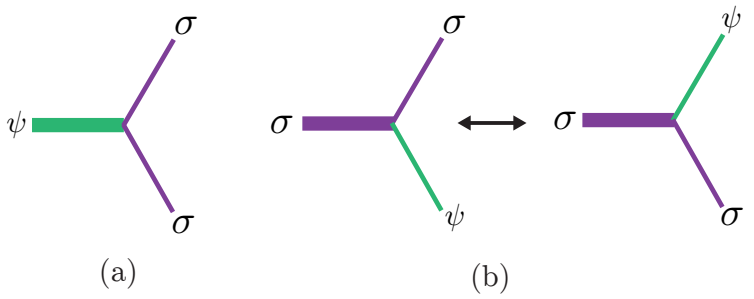

Figure 2.3: (a) The vertices counted by N_{p1}. (b) The vertices counted by N_{p2}. For a vertex to be counted, its initial state must match the picture on the left and final state match the picture on the right or vice versa. External legs of p are shown in bold.

2.2.2 Properties of the Hamiltonian

The Hamiltonian H (2.1) defined above has several interesting properties. Among the most important of these is that it possesses a global $\mathbb{Z}_2$ symmetry. This symmetry is defined by

$$S = \prod_p \tau_p^x, \tag{2.11}$$

where τ_p^x denotes the Pauli operator acting on the plaquette spin p. We can think of S as a conventional Ising symmetry which flips all the plaquette spins: $|+\rangle \leftrightarrow |-\rangle$. To see that $[S, H] = 0$, note that every term in H either (1) does not act on the plaquette spins at all (i.e., Q_v, B_p^1, B_p^ψ), or (2) acts on the plaquette spins in a way that is manifestly symmetric under S (i.e., P_l, $B_p^\sigma \tau_p^x$).

Another important property is that H is a sum of mutually commuting operators. Indeed, from the expressions for P_l and Q_v given in Eq. 2.2 and 2.3 it is clear that

$$[P_l, P_{l'}] = [Q_v, Q_{v'}] = [P_l, Q_v] = 0, \tag{2.12}$$

since these operators are all diagonal in the $|\{\tau_p^z, \mu_l\}\rangle$ basis. It is also easy to see that

$$[B_p, Q_v] = [B_p, P_l] = 0. \tag{2.13}$$

The first equality follows from the fact that the plaquette operators include a factor of $\mathcal{P}$ on both sides. The second equality requires a little more work, but can be verified by separately considering each of the three terms in the definition of B_p. In particular, one can see that B_p^1 and B_p^ψ both commute with P_l, since they commute with $(-1)^{N_{l\sigma}}$ for every link l. Likewise, one can see that $B_p^\sigma \tau_p^x$ commutes with P_l by noting that B_p^σ *anti-commutes* with $(-1)^{N_{l\sigma}}$ if l is adjacent to p and commutes with $(-1)^{N_{l\sigma}}$ otherwise. The only relation left to establish is

$$[B_p, B_{p'}] = 0 \tag{2.14}$$

The easiest way to prove this relation is to use the fact that the B_p^s operators are identical to the string-net plaquette operators for the doubled Ising string-net model. String-net plaquette operators are known to commute with each other,[48] so we know that $[B_p^s, B_{p'}^{s'}] = 0$, implying the above identity.

A third property of H is that the operators P_l, Q_v and B_p are all *projectors*. Indeed, we've already pointed this out for the case of P_l and Q_v. As for B_p, the easiest way to see that it is a projector is to again invoke the fact that the B_p^s operators are identical to string-net plaquette operators, which are known to obey the identity

$$B_p^s B_p^{s'} = \sum_{t=1,\psi,\sigma} \delta_{ss't} B_p^t \tag{2.15}$$

Using this identity, together with the fact that the coefficients a_s obey the relation $\sum_{ss'} \delta_{ss't} a_s a_{s'} = a_t$, it is easy to check that $B_p^2 = B_p$, i.e. B_p is a projector.

Given that H is a sum of commuting projectors, we know that the lowest energy states are those that obey

$$P_l|\Psi\rangle = Q_v|\Psi\rangle = B_p|\Psi\rangle = |\Psi\rangle, \tag{2.16}$$

for all links l, vertices v and plaquettes p. In addition, we know that these states are separated from the excited states by a gap of at least $\Delta \geq 1$. Thus, the only property of the

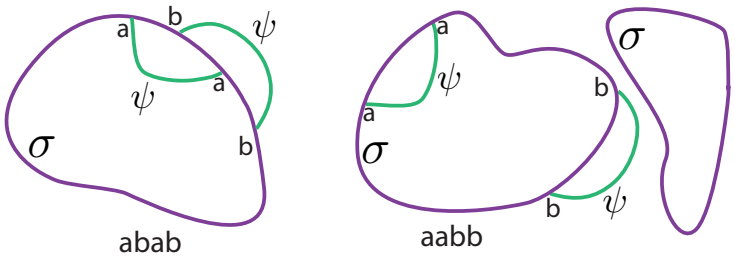

Figure 2.4: (color online) Two examples of the function $f(X)$. Here the string states are drawn in the continuum rather than on the lattice.

low energy spectrum left to determine is the ground state degeneracy of the model, i.e. the number of states that obey (2.16). This degeneracy D can be conveniently computed using the formula

$$D = \mathrm{Tr}\left(\prod_l P_l \prod_v Q_v \prod_p B_p\right) \tag{2.17}$$

We carry out this calculation in Appendix A.1, and we find that the degeneracy depends on the global topology in which the model is defined. For example, if the model is defined in an infinite plane or spherical geometry, the ground state degeneracy is $D = 1$. In contrast, if the model is defined in a torus geometry, the ground state degeneracy is $D = 4$. More generally, we find that the ground state degeneracy on a surface of genus g is $D = 4^g$.

We can draw two conclusions from this calculation. First, we conclude that H does not break the symmetry S *spontaneously* since the ground state is non-degenerate in an infinite plane or sphere geometry. Second, we conclude that H realizes a topological phase (i.e. supports anyon excitations) since the ground state degeneracy is different for different topologies.

2.2.3 Ground state wave function

Interestingly, we can write down an explicit formula for the ground state wave function of the symmetric toric code model in an infinite plane or spherical geometry. Let $|X\rangle = |\{\tau_p^z, \mu_l\}\rangle$

be an arbitrary configuration of spins τ_p^z and strings μ_l. The amplitude for $|X\rangle$ in the ground state vanishes unless X satisfies two conditions: (1) the σ strings lie along the domain walls of the τ_p^z spins, and (2) the $1, \psi, \sigma$ strings obey the fusion rules at each vertex (Fig. 2.2). Note that condition (2) implies that σ strings form closed loops and ψ strings either form closed loops or else their ends lie on σ loops. If these conditions are satisfied, then the amplitude for $|X\rangle$ is given by[2]

$$\Psi(X) \equiv \langle X|\Psi\rangle = \sqrt{2}^{N_\sigma(X)} f(X) \tag{2.18}$$

where $N_\sigma(X)$ is the number of σ loops contained in X (Fig. 2.4) and $f(X)$ takes the values 0 or ± 1. More specifically, $f(X) = 0$ whenever there is at least one σ loop in X which has an odd number of ψ strings ending on it, and $f(X) = \pm 1$ otherwise. Determining whether $f(X) = +1$ or -1 is a little bit trickier. To determine this sign, we compute a ± 1 factor for each σ loop in X and then multiply them all together. The $\pm$ sign corresponding to each σ loop can be calculated as follows. Suppose that there are $2n$ vertices where the ψ strings end on the σ loop. We can divide these vertices into two groups corresponding to the cases where the ψ strings are incident from the outside of the loop or the inside of the loop. We then label the vertices in one group by 'a', and the vertices in the other group by 'b' (which one is which isn't important). We then go around the loop (in either direction) starting at some arbitrary point, reading off the sequence of a's and b's. We then count how many pairwise exchanges of a's and b's are necessary to rearrange the sequence so that a's and b's are separated into two blocks, i.e. $aa\cdots abb\cdots b$. The $\pm$ sign associated with the loop is given by the parity of the number of these exchanges (Fig. 2.4). We explain how to derive Eq. (2.18) in appendix A.2.

2. For simplicity, we do not bother to normalize the wave function.

2.2.4 Excitations and string operators

In this section, we show that the model supports four topologically distinct types of anyon excitations. We label these excitations by $\{1,\ e,\ m,\ em\}$, where 1 denotes the trivial excitation, and e, m, em denote the three nontrivial excitations. We argue that this is a complete list and that there are no other topologically distinct anyons.

We begin by describing the *string* operators that create each of these anyon excitations (for a derivation of these operators see appendix A.4). In general, these string operators act nontrivially along an open path γ, and when we apply them to the ground state, they create a pair of anyon excitations, with one at each end of the path γ.[32] The string operator that creates e-type anyons is defined by

$$W_e^\gamma = \mathcal{P}_\gamma \cdot \prod_{l\in\gamma} (f_l)^{\frac{1}{4}(1+\tau^z_{p_l})(1+\tau^z_{q_l})} (-1)^{\sum_{i=1}^6 N_{ei}} \cdot \mathcal{P}_\gamma \tag{2.19}$$

where γ is an (open) path on the honeycomb lattice and $\mathcal{P}_\gamma$ denotes the projection operator

$$\mathcal{P}_\gamma = \prod_{v\in\gamma} Q_v \cdot \prod_{l\in\gamma} P_l \tag{2.20}$$

Let us explain the notation in the formula for W_e^γ: the index l runs over links that are contained in γ, while p_l and q_l denote the two plaquettes adjacent to link l. The link spin operator f_l is defined as

$$f_l = |\psi\rangle\langle 1| + |1\rangle\langle\psi| + |\sigma\rangle\langle\sigma| \tag{2.21}$$

while the operators $N_{e1}, ..., N_{e6}$ count the number of vertices that belong to the path γ and that are of the six types shown in Fig. 2.5. One subtlety is that the $N_{e1}, ..., N_{e6}$ operators distinguish between vertices where the external leg enters γ on the 'left' or on the 'right', so to define these operators, we need to fix an orientation on γ. However the choice of orientation is not important: it is possible to show that changing the orientation of γ only changes W_e^γ by local operators acting near the ends of γ.

Translating the formula for W_e^γ into words, the action of W_e^γ on a basis state $|\{\tau_p^z, \mu_l\}\rangle$ can be broken down into several steps. First, the projector $\mathcal{P}_\gamma$ annihilates the state unless (1) the strings obey the fusion rules for all the vertices v in γ, and (2) the σ strings lie along the domain walls of the τ^z spins, for all the links l in γ. The next step is to multiply the state by a $\pm$ sign depending on whether γ contains an even or odd number of vertices of the type shown in Fig. 2.5. The final step is to change the state of the link spins μ_l from $|1\rangle \to |\psi\rangle$ or $|\psi\rangle \to |1\rangle$ if the adjacent plaquette spins satisfy $\tau_{p_l}^z = \tau_{q_l}^z = +1$.

The string operator for the m-type anyons takes a very similar form:

$$W_m^\gamma = \mathcal{P}_\gamma \cdot \prod_{l\in\gamma} (f_l)^{\frac{1}{4}(1-\tau_{p_l}^z)(1-\tau_{q_l}^z)} (-1)^{\sum_{i=1}^6 N_{mi}} \cdot \mathcal{P}_\gamma \tag{2.22}$$

This differs from the expression for W_e^γ in two ways. First, $\tau_{p_l}^z, \tau_{q_l}^z$ are replaced by $-\tau_{p_l}^z, -\tau_{q_l}^z$, and second, the N_{ei} operators are replaced by N_{mi}. The N_{mi} operators count the number of vertices that belong to γ that have a particular type. These types are the same as those corresponding to N_{ei} (Fig. 2.5), except with the plaquette spins flipped: $|+\rangle \leftrightarrow |-\rangle$. [3]

The only remaining string operator that we need to discuss is the one corresponding to em. As the notation suggests, this string operator can be obtained by multiplying together W_e and W_m:

$$W_{em}^\gamma = W_e^\gamma W_m^\gamma \tag{2.23}$$

To justify the above formulas, several points need to be established. First, we need to show that the above string operators only create excitations at their endpoints and nowhere else. Second, we need to show that the anyon excitations created by the string operators are topologically distinct. Finally, we need to show that the string operators create *all* the topologically distinct excitations.

To establish the first point we note that the above string operators have the property

3. Similar string operators were described by Ref. [57], in the context of a phase with $\mathbb{Z}_2$ topological order and translation symmetry broken by densely packed σ loops.

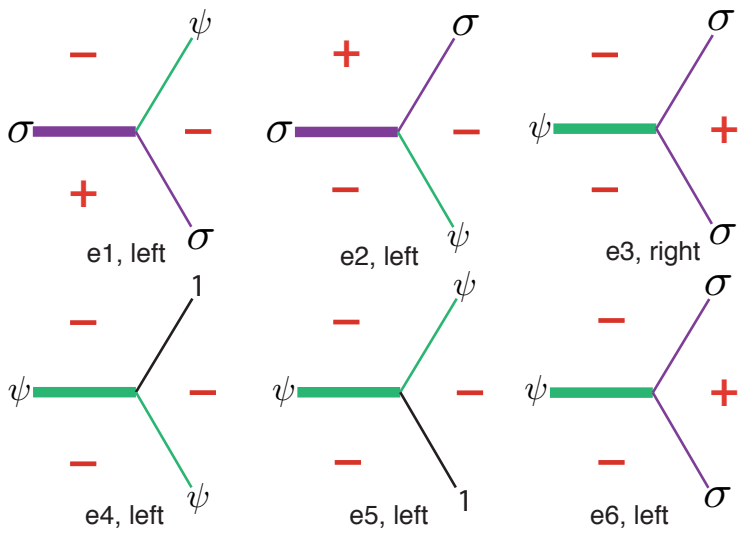

Figure 2.5: The vertices counted by $N_{e1}, ..., N_{e6}$. Vertices marked with 'left' are only counted if the external leg (shown in bold) adjoins γ from the left, and similarly for those marked with 'right.' The vertices counted by $N_{m1}, ..., N_{m6}$ can be obtained from the above set by flipping all the plaquette spins: $|+\rangle \leftrightarrow |-\rangle$.

that they commute with every term in the Hamiltonian except for the six B_p terms that act on the plaquettes adjoining the endpoints of γ. This property can be established either by straightforward (but tedious) algebra, or by using a graphical representation of the string operators as in Ref. [48]. As for the second point, this follows from the braiding statistics calculation presented in the next section: in particular, our calculation shows that the e, m and em excitations all have distinct braiding statistics and are therefore topologically distinct. Finally, to establish the last point, we recall that the ground state degeneracy of the model in a torus geometry is 4. Typically, the ground state degeneracy on a torus is equal to the number of distinct anyon types[4] so we conclude that $\{1, e, m, em\}$ is a complete list of anyons.

A final remark: it is interesting to note that the above string operators have especially simple behavior when acting on states with no σ strings and with $\tau_p^z = +1$ everywhere. Indeed, if we denote these states by $|+, \mu_l\rangle$, we can see from Eq. (2.19), that the action

4. This relation can break down for some systems with non-Abelian anyons, or systems where translational symmetry permutes anyon excitations. We assume that our model does not fall into one of these categories.

of W_e^γ on $|+,\mu_l\rangle$ is simply to flip the link spins from $|1\rangle \leftrightarrow |\psi\rangle$ on all the links along γ. Likewise, the action of W_m^γ on $|+,\mu_l\rangle$ is to multiply the state by a factor of $(-1)^{N_\psi}$, where N_ψ counts the number of ψ strings adjoining γ on the left.

What is particularly interesting is that these formulas precisely agree with the action of the W_e, W_m string operators in the usual toric code string-net model built from string types $\{1,\psi\}$. Furthermore, if we consider symmetry reversed states, $|-,\mu_l\rangle$, where $\tau_p^z = -1$ for all p, this correspondence is reversed. That is, the action of W_e^γ on $|-,\mu_l\rangle$ agrees with the action of W_m in the usual toric code and vice versa. This connection between the string operators in the symmetric toric code and usual toric code is not a coincidence and holds more generally for all the symmetry enriched models that we describe below.

2.2.5 Symmetry action on anyons

With expressions for the e and m string operators in hand, we can derive one of the most interesting features of our model: the $\mathbb{Z}_2$ symmetry S *exchanges* e-type anyons and m-type anyons. To see this, note that the string operators W_e^γ, W_m^γ (2.19-2.22) are related to one another by

$$S^{-1}W_e^\gamma S = {W_m}^\gamma, \quad S^{-1}W_m^\gamma S = {W_e}^\gamma \tag{2.24}$$

We conclude that S *exchanges* e-type anyons and m-type anyons. On the other hand, $S^{-1}W_{em}^\gamma S = W_{em}^\gamma$, so the symmetry leaves em-type particles unchanged.

We note that a toric code with a symmetry exchanging e and m has been studied previously. [67, 59] However, in that case, the symmetry was not an onsite $\mathbb{Z}_2$ symmetry, but rather a spatial symmetry.

2.2.6 Braiding statistics

We now compute the braiding statistics data for the $\{1,e,m,em\}$ anyons, and we show that this data agrees with that of the toric code model. We begin with the mutual statistics of

the anyons — that is, the statistical phase $e^{i\theta_{a,b}}$ associated with braiding anyon a around anyon b where $a, b \in \{1, e, m, em\}$. We compute this statistical phase using a standard approach:[32, 46, 48] we construct the string operators associated with a and b, with one acting on the path β and the other on the path γ (Fig. 2.6), and then we derive the mutual statistics from the string operator commutation algebra using the general relation:

$$W_a^\beta W_b^\gamma = e^{i\theta_{a,b}} W_b^\gamma W_a^\beta \tag{2.25}$$

We start with the mutual statistics of the e and m type anyons. To find their statistics, we need to compare $W_m^\beta W_e^\gamma$ with $W_e^\gamma W_m^\beta$. To make a comparison, it is easiest to consider the action of these operators on a particular state, say $|\{\tau_p^z = +, \mu_l = 1\}\rangle$. First we apply W_e^γ. The result is to flip the link spins from $|1\rangle$ to $|\psi\rangle$ along the path γ:

$$W_e^\gamma |\{+, 1\}\rangle = |\{\tau_p^z = +, \mu_{l\in\gamma} = \psi, \mu_{l\notin\gamma} = 1\}\rangle$$

Next we apply W_m^β. This has no effect on the link spins since W_m^β only flips the link spins when $\tau_p^z = -$. On the other hand, applying W_m^β has the effect of multiplying the state by -1 since $\prod_{l\in\beta}(-1)^{\sum_i N_{mi}} = -1$ for the above state. Thus, we have

$$W_m^\beta W_e^\gamma |\{+, 1\}\rangle = -|\{\tau_p^z = +, \mu_{l\in\gamma} = \psi, \mu_{l\notin\gamma} = 1\}\rangle \tag{2.26}$$

Now consider the opposite ordering. First, we apply W_m^β to $|\{+, 1\}\rangle$. In this case, the state is left unchanged:

$$W_m^\beta |\{+, 1\}\rangle = |\{\tau_p^z = +, \mu_l = 1\}\rangle$$

Note that there is no factor of -1 here because $\prod_{l\in\beta}(-1)^{\sum_i N_{mi}} = +1$ for the above state. If we now apply W_e^γ, we obtain

$$W_e^\gamma W_m^\beta |\{+, 1\}\rangle = |\{\tau_p^z = +, \mu_{l\in\gamma} = \psi, \mu_{l\notin\gamma} = 1\}\rangle \tag{2.27}$$

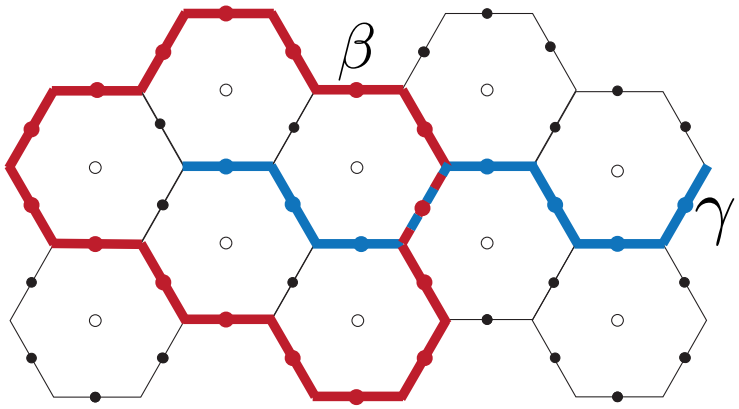

Figure 2.6: An example of paths β, γ used to find the mutual statistics of e and m. Applying the two string operators in two different orders gives results that differ by the mutual statistical phase $e^{i\theta_{e,m}}$.

Again, there is no factor of -1 since $\prod_{l\in\beta}(-1)^{\sum_i N_{ei}} = +1$.

Comparing Eqs. 2.27 and 2.26, we can see that W_e^γ and W_m^β *anti-commute* when acting on the state $|\{+,1\}\rangle$. In fact, this anti-commutation property is more general: these operators anti-commute when acting on *any* state. We have verified this by expressing the string operators in matrix form and computing their anti-commutator numerically. In view of Eq. (2.25), the implication of this result is that the e and m type particles have a mutual statistical phase of

$$e^{i\theta_{e,m}} = -1 \tag{2.28}$$

Following a similar analysis, one can show that W_e^γ and W_e^β *commute* with one another (as do W_m^γ and W_m^β) so that the corresponding statistical phases are

$$e^{i\theta_{e,e}} = e^{i\theta_{m,m}} = +1 \tag{2.29}$$

All of these phases agree with the toric code model.[32] Furthermore, the statistical phases involving the em particle also agree since these are fully determined by the fact that $em = e \times m$ together with the above data.

The only thing left to check is that the anyons in our model have the same *exchange*

statistics as those in the toric code model. In particular, we need to check that the e and m particles are bosons, while the em particle is a fermion. Conveniently we can establish this fact without doing any additional calculation. To see this, note that e and m have to be either bosons or fermions, given the mutual statistics found above. Furthermore symmetry requires that e and m have the same exchange statistics. Thus, the only alternative possibility is that e and m are both fermions, in which case em is also a fermion — by the composition rule for exchange statistics. But we can rule out this three-fermion possibility by noting that if e, m, em were all fermions, then the chiral central charge c_- of our model would have to be $c_- \equiv 4 \pmod 8$, [5] yet we know that the chiral central charge of our model must vanish since the Hamiltonian is a sum of commuting projectors.

2.3 Relationship to doubled Ising string-net model

In this section we discuss the relationship between the symmetric toric code and the doubled Ising string-net model. We present two results. First, we show that if we gauge the global $\mathbb{Z}_2$ symmetry of the symmetric toric code model, the resulting gauge theory can be mapped *exactly* onto a variant of the doubled Ising string-net model. Second, we reverse the logic and we show that the symmetric toric code model can be constructed from the doubled Ising string-net model by applying an 'ungauging' procedure.

Why are these results important? As we explain below, our first result provides an alternative proof that the symmetric toric code model has the properties claimed above, namely (1) it supports anyon excitations with the same braiding statistics as in the conventional toric code, and (2) the $\mathbb{Z}_2$ symmetry exchanges the e and m type particles. Likewise, our second result is significant because it shows how the symmetric toric code model was constructed. Most important of all, both of these results generalize to arbitrary symmetry enriched string-

5. This follows from a general relation that holds for any topological phase, namely $e^{2\pi i c_-/8} = \frac{1}{D}\sum_s d_s^2 \theta_s$ where $D = \sqrt{\sum_s d_s^2}$. Here the sum runs over all anyons s. and θ_s, d_s denote the topological spin and quantum dimension of s. See e.g. Ref. [33] and references therein.

net models and they lie at the heart of our construction and analysis of the more general models in section 2.4.

2.3.1 Review of doubled Ising string-net model

We begin with a brief review of the doubled Ising string-net model. (See Ref. [48] for a general introduction to the string-net formalism). The doubled Ising string-net model is a spin system built out of spins that live on the links of the honeycomb lattice. Each spin can be in *three* states, which we denote by $|1\rangle$, $|\psi\rangle$, and $|\sigma\rangle$. The states of the spins can be equivalently described in terms of 'strings': if a spin is in the state $|\psi\rangle$ or $|\sigma\rangle$, we will say that the corresponding link is occupied by a ψ or σ string, while if the spin is in the state $|1\rangle$, we will say the corresponding link is unoccupied. The Hamiltonian of the model is given by

$$H^{di} = -\sum_v Q_v - \sum_p B_p^{di} \tag{2.30}$$

The first term, Q_v, acts on three links adjacent to a vertex v, and is defined as in Eq. (2.3). This term energetically favors vertices that satisfy the fusion rules shown in Fig. 2.2. The second term, B_p^{di} can be written as a sum

$$B_p^{di} = a_1 B_p^1 + a_\psi B_p^\psi + a_\sigma B_p^\sigma \tag{2.31}$$

where $a_1 = a_\psi = \frac{1}{4}$ and $a_\sigma = \frac{\sqrt{2}}{4}$. The operators $B_p^1, B_p^\psi, B_p^\sigma$ each act on 12 links — 6 of which make up the boundary of a plaquette p and another 6 that lie on the external legs that adjoin p. These operators are defined as in Eqs. (2.6-2.10). (For readers who are familiar with string-net models, we should mention that the definitions of $B_p^1, B_p^\psi, B_p^\sigma$ given in Eqs. (2.6-2.10) are equivalent to the standard definitions of B_p^s in terms of F-symbols).

The ground state of the model, $|\Psi^{di}\rangle$, is a linear superposition of string configurations that obey the fusion rules. The amplitude for each configuration can be computed using the

following 'local rules':

$$\Psi^{di}\left(\quad\right) = \Psi^{di}\left(\quad\right) \tag{2.32}$$

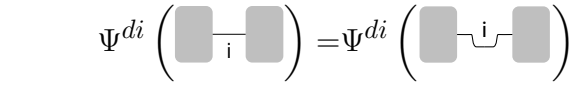

$$\Psi^{di}\left(\quad\right) = d_i \Psi^{di}\left(\quad\right) \tag{2.33}$$

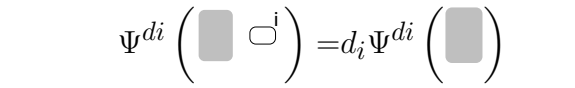

$$\Psi^{di}\left(\quad\right) = \delta_{ij} \Psi^{di}\left(\quad\right) \tag{2.34}$$

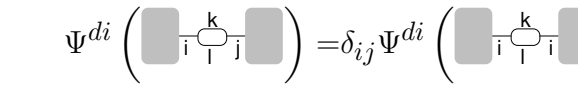

$$\Psi^{di}\left(\quad\right) = \sum_n F^{ijm}_{kln} \Psi^{di}\left(\quad\right) \tag{2.35}$$

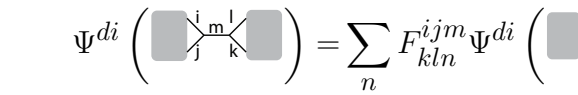

Here d_i is the quantum dimension of the i'th edge label

$$d_1 = d_\psi = 1,\ d_\sigma = \sqrt{2} \tag{2.36}$$

while F^{ijm}_{kln} is the 'F-symbol' for the doubled Ising model, with the following nonzero components:

$$\begin{aligned}
&F^{211}_{211} = F^{121}_{121} = -1,\ F^{11j}_{11k} = \frac{(-1)^{\frac{j\cdot k}{4}}}{\sqrt{2}},\ j,k = 0,2 \\
&F^{220}_{220} = F^{220}_{111} = F^{110}_{221} = F^{121}_{210} = F^{211}_{120} = F^{121}_{101} = F^{211}_{011} = 1 \\
&F^{121}_{012} = F^{211}_{102} = F^{011}_{122} = F^{101}_{212} = F^{101}_{121} = F^{011}_{211} = F^{000}_{000} = 1 \\
&F^{i0i}_{i0i} = F^{0ii}_{0ii} = F^{000}_{iii} = F^{ii0}_{00i} = F^{i0i}_{0i0} = F^{0ii}_{i00} = 1, \quad i = 1,2
\end{aligned} \tag{2.37}$$

where

$$0 = \text{vacuum}, \quad 1 = \sigma, \quad 2 = \psi \tag{2.38}$$

Let us specialize to the case where the model is defined in a sphere or infinite plane geometry. In this case, the above local constraint equations uniquely determine the ground state wave function Ψ^{di} since they allow us to relate the amplitude of any string configuration to the amplitude of the vacuum (empty string) configuration which is defined to be $\Psi^{di}(\text{vacuum}) = 1$, by convention. Using this approach, it is not hard to show that the

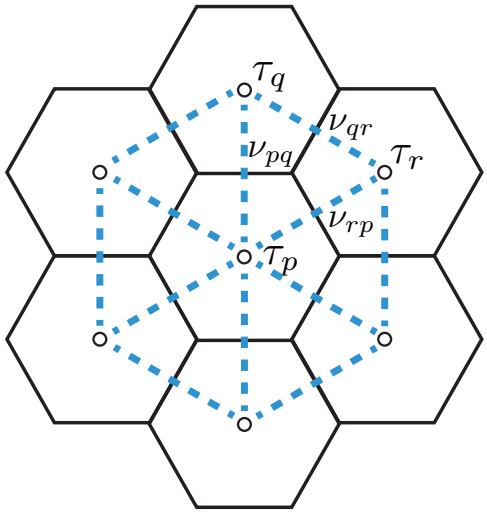

Figure 2.7: The gauge field degrees of freedom, ν_{pq}, live on the links $\langle pq \rangle$ of the dual *triangular* lattice connecting neighboring plaquette spins (we omit link spins for clarity).

ground state amplitude is given by $\Psi^{di}(X) = \sqrt{2}^{N_\sigma(X)} f(X)$, in exact agreement with Eq. (2.18). This agreement is not a coincidence: in fact, the way we derive Eq. (2.18) is to first find the ground state wave function of the doubled Ising string-net model and then use the connection with the symmetric toric code to obtain the ground state of the symmetric toric code model. See appendix A.2 for details.

Physically, the most important property of the doubled Ising string-net model is that it supports 9 different types of anyon excitations. These anyons can be labeled as:

$$\{1, \psi, \sigma\} \times \{1, \bar{\psi}, \bar{\sigma}\} = \{1, \psi, \bar{\psi}, \sigma, \bar{\sigma}, \psi\bar{\psi}, \sigma\bar{\psi}, \psi\bar{\sigma}, \sigma\bar{\sigma}\}$$

The braiding statistics and fusion rules of these anyons are described by the Ising $\times$ $\overline{\text{Ising}}$ topological phase. This is why the model is called the 'doubled Ising' string-net model.

2.3.2 The gauged toric code model

Setting aside the doubled Ising string-net model for the moment, we now explain how to gauge the global $\mathbb{Z}_2$ symmetry of the symmetric toric code model. Following the standard

procedure,[35] the first step is to add a gauge field to the model. This gauge field should be placed on links connecting neighboring lattice sites where the symmetry acts. In our case, the symmetry $S = \prod_p \tau_p^x$ only acts on the plaquette spins, so we put the gauge field on the links $\langle pq \rangle$ of the *triangular* lattice connecting the plaquette spins (Fig. 2.7). Since the gauge group is $\mathbb{Z}_2$, the lattice gauge field is a two-state degree of freedom $\nu_{pq}^z = \pm 1$.

The second step is to perform the minimal coupling procedure, replacing $\tau_p^z \tau_q^z \to \tau_p^z \nu_{pq}^z \tau_q^z$, whenever there are terms in the Hamiltonian that couple neighboring plaquette spins τ_p^z, τ_q^z. The final step is to add to the Hamiltonian the term $-\sum_{\langle pqr \rangle} \nu_{pq}^z \nu_{qr}^z \nu_{rp}^z$, which ensures that the states with zero $\mathbb{Z}_2$ gauge flux have the lowest energy. Applying these steps to the symmetric toric code model gives the following gauged Hamiltonian:

$$H^{\text{gauged}} = -\sum_v Q_v - \sum_p B_p - \sum_l P_l^{\text{gauged}} - \sum_{\langle pqr \rangle} \nu_{pq}^z \nu_{qr}^z \nu_{rp}^z \tag{2.39}$$

where

$$P_l^{\text{gauged}} = \frac{1}{2}(1 + (-1)^{N_{l\sigma}} \cdot \tau_p^z \nu_{pq}^z \tau_q^z) \tag{2.40}$$

Notice that Q_v and B_p are not affected by the minimal coupling procedure since they don't contain any terms like $\tau_p^z \tau_q^z$. Like any gauge theory, the Hamiltonian H^{gauged} is defined on a Hilbert space consisting of *gauge invariant* states, that is, states $|\psi\rangle$ obeying

$$\tau_p^x \prod_q \nu_{pq}^x |\psi\rangle = |\psi\rangle \tag{2.41}$$

for all p.

As an aside, we should mention that we skipped one of the steps in the usual gauging procedure. This step involves multiplying each term in the gauged Hamiltonian by an operator that projects onto states that have vanishing $\mathbb{Z}_2$ gauge flux through all triangular plaquettes contained in the region of support of the term in question.[43, 63] While this step is important when gauging a general spin model, it is not necessary when the Hamiltonian

only includes nearest neighbor $\tau_p^z \tau_q^z$ couplings, as is the case here.

2.3.3 Equivalence between gauged toric code and doubled Ising string-net model

In this section, we establish an exact equivalence between the gauged toric code model and a *modified* version of the doubled Ising string-net model. Using this equivalence, we then present an alternative proof that the symmetric toric code model has the topological and symmetry properties claimed above.

To begin, we explain how the modified doubled Ising string-net model is defined. The modified model differs from the standard Ising string-net model H^{di} in two ways. First, the Hilbert space is bigger: in addition to the three-state spin $\mu_l = 1, \psi, \sigma$, the model also has a two-state spin $\xi_l^z = \pm$ living on each link l of the honeycomb lattice. Also, the Hamiltonian has two extra terms:

$$H^{di'} = H^{di} - \sum_l \frac{1}{2}(1 + \xi_l^z) - \sum_v \prod_{l \in v} \xi_l^z (-1)^{N_{l\sigma}} \tag{2.42}$$

Despite these differences, the ground states of the two models, $\Psi^{di'}$, Ψ^{di}, are almost the same:

$$|\Psi^{di'}\rangle = |\Psi^{di}\rangle \otimes |\{\xi_l^z = +\}\rangle \tag{2.43}$$

To see this, notice that $|\Psi^{di}\rangle \otimes |\{\xi^z = +\}\rangle$ separately minimizes the energy of every term in $H^{di'}$.

The fact that the two ground states $|\Psi^{di'}\rangle$, $|\Psi^{di}\rangle$ are identical up to tensoring with a product state is very important for us because it implies that the two models have the same topological properties, i.e. the same anyon excitations and the same braiding statistics. The two models are thus interchangeable for our purposes.

We now show that the modified string-net model $H^{di'}$ is exactly equivalent to the gauged

toric code model. To this end, we need to construct a unitary mapping U between the Hilbert spaces of the two models that transforms the Hamiltonian $H^{di'}$ into the Hamiltonian H^{gauged}. The easiest way to define the mapping U is in terms of basis states. The Hilbert space of the modified string-net model is spanned by basis states of the form $|\{\xi_l^z, \mu_l\}\rangle$ where $\xi_l^z = \pm$ and $\mu_l = 1, \psi, \sigma$. Likewise, the Hilbert space of the gauged model is spanned by basis states $|\{\tau_p^z \nu_{pq}^z \tau_q^z, \mu_l\}\rangle$ labeled by the gauge invariant quantum numbers $\tau_p^z \nu_{pq}^z \tau_q^z = \pm$ and $\mu_l = 1, \psi, \sigma$. With this notation, the mapping U is defined by

$$U|\{\tau_p^z \nu_{pq}^z \tau_q^z, \mu_l\}\rangle = |\{\xi_l^z, \mu_l\}\rangle \tag{2.44}$$

where $\xi_l^z = (-1)^{N_{l\sigma}} \tau_p^z \nu_{pq}^z \tau_q^z$ and l is the link separating the two plaquettes p, q (see Table 2.1). To see that U transforms $H^{di'}$ into H^{gauged}, note that

$$\begin{aligned}
&U^{-1} \xi_l^z U = (-1)^{N_{l\sigma}} \tau_p^z \nu_{pq}^z \tau_q^z, \quad U^{-1} Q_v U = Q_v, \\
&U^{-1} N_{l\sigma} U = N_{l\sigma}, \quad U^{-1} B_p^1 U = B_p^1, \\
&U^{-1} B_p^\psi U = B_p^\psi, \quad U^{-1} B_p^\sigma U = B_p^\sigma \tau_p^x
\end{aligned} \tag{2.45}$$

Substituting these formulas into (2.42) gives

$$U^{-1} H^{di'} U = H^{\text{gauged}}, \tag{2.46}$$

as claimed.

The equivalence between the gauged toric code model and the modified doubled Ising string-net model provides another proof that the (ungauged) toric code model has the properties claimed above, i.e. (1) it has the same anyon and braiding statistics as the conventional toric code, and (2) the $\mathbb{Z}_2$ symmetry exchanges the e and m particles. The reason this is so is that the mapping between ungauged and gauged models is known to be one-to-one in the sense that the braiding statistics data for the excitations of the gauged model *uniquely*

Gauged toric code	Modified String-net
$\lvert\tau_p^z\nu_{pq}^z\tau_q^z = +1,\ \mu_l = 1\rangle$	$\lvert+, 1\rangle$
$\lvert\tau_p^z\nu_{pq}^z\tau_q^z = +1,\ \mu_l = \psi\rangle$	$\lvert+, \psi\rangle$
$\lvert\tau_p^z\nu_{pq}^z\tau_q^z = -1,\ \mu_l = \sigma\rangle$	$\lvert+, \sigma\rangle$
$\lvert\tau_p^z\nu_{pq}^z\tau_q^z = -1,\ \mu_l = 1\rangle$	$\lvert-, 1\rangle$
$\lvert\tau_p^z\nu_{pq}^z\tau_q^z = -1,\ \mu_l = \psi\rangle$	$\lvert-, \psi\rangle$
$\lvert\tau_p^z\nu_{pq}^z\tau_q^z = +1,\ \mu_l = \sigma\rangle$	$\lvert-, \sigma\rangle$

Table 2.1: The mapping U (2.44) between the Hilbert space of the gauged toric code model and the Hilbert space of the modified string-net model.

determines the braiding statistics and symmetry data for the ungauged model.[3, 13] In particular, if the excitations of a gauged $\mathbb{Z}_2$ symmetric model are described by the Ising $\times$ $\overline{\text{Ising}}$ topological phase, as is the case here, then it is known that the ungauged model must obey properties (1) and (2).[17, 3]

2.3.4 Ungauging the doubled Ising string-net model

In this section we show that the symmetric toric code model can be obtained from the doubled Ising string-net model using a recipe which we will refer to as the 'ungauging' procedure. This ungauging procedure is how we originally constructed the symmetric toric code model. It is also central to our construction of more general symmetry enriched string-net models, as we explain in section 2.4.

The ungauging procedure involves modifying both the Hilbert space and Hamiltonian of the doubled Ising string-net model. The first step is to enlarge the Hilbert space of the doubled Ising string-net model by adding a two-state spin τ_p to every plaquette p of the honeycomb lattice. (The reason that we use *two*-state spins is related to the fact that we are ungauging a $\mathbb{Z}_2$ symmetry. For a general finite symmetry group G, we would add $|G|$-state spins to each plaquette, as we will explain in section 2.4.2).

The next step is to modify the Hamiltonian of the string-net model (Eq. 2.30) by adding

the term $-\sum_l P_l$ where P_l is defined as in (2.2):

$$H \to H^{di} - \sum_l P_l \tag{2.47}$$

This term energetically favors states $|\{\tau_p^z, \mu_l\}\rangle$ in which the domain walls between the τ_p^z plaquette spins coincide with the links l for which $\mu_l = \sigma$. The final step is to replace the B_p^σ term in H^{di} by

$$B_p^\sigma \to B_p^\sigma \tau_p^x \tag{2.48}$$

This replacement is important because it ensures that $[B_p^\sigma, P_l] = 0$. Combining all three steps, we can see that the resulting Hamiltonian H is exactly the symmetric toric code model (2.1).

As the name suggests, the ungauging procedure is designed to produce a model that (1) is invariant under a global $\mathbb{Z}_2$ symmetry, namely $S = \prod_p \tau_p^x$, and (2) has the property that if this $\mathbb{Z}_2$ symmetry is gauged, then the resulting gauge theory supports the same types of anyon excitations and braiding statistics as the model we started with, i.e. the double Ising string-net model. In this respect, the ungauging procedure works as advertised since it produces the symmetric toric code which we already know has properties (1) and (2).

At the same time, it is unsatisfying that the above ungauging procedure can only be applied to the doubled Ising model; it would be more natural if we could 'ungauge' a large class of models in the same way that we can 'gauge' a large class of models. In fact, the ungauging procedure is more general than it appears (though not as general as gauging). For example, we can easily extend the procedure to an arbitrary perturbed doubled Ising Hamiltonian $\tilde{H}^{di}$ such that (a) $\tilde{H}^{di}$ is gapped, (b) $\tilde{H}^{di}$ commutes with $\prod_{l \in v}(-1)^{N_{l\sigma}}$ for every vertex v, and (c) the ground state of $\tilde{H}^{di}$ obeys $\prod_{l \in v}(-1)^{N_{l\sigma}} = 1$. To ungauge a Hamiltonian of this kind, we follow the same steps as above except that (2.48) needs to be replaced with a more general rule. The more general rule states that any term in the Hamiltonian that flips the sign of $(-1)^{N_{l\sigma}}$ along a closed loop γ should be multiplied by $\prod_{p \in \gamma} \tau_p^x$, where the

product runs over plaquettes contained within the loop. One can easily check that this more general procedure produces a model that has properties (1) and (2) above, using the same analysis as in section 2.3.2. (Of course, another way that the ungauging procedure can be generalized is to consider other symmetry groups and string-net models. We discuss how this works in section 2.4).

A few more comments about ungauging: first, we would like to point out that while the ungauging procedure is inverse to gauging at the level of topological properties, it is *not* the strict inverse at a microscopic level. This is clear from the analysis in section 2.3.2 since gauging the symmetric toric code produces a model which differs slightly from the doubled Ising string-net model (but which nevertheless shares the same topological properties).

Another important point is that the ungauging procedure corresponds to a very simple operation on ground state wave functions. Consider a sphere or infinite plane geometry and let $\Psi^{di}(\{\mu_l\})$ denote the ground state wave function of the doubled Ising string-net model (the input for the procedure) and $\Psi(\{\tau_p^z, \mu_l\})$ denote the ground state wave function of the symmetric toric code model (the output for the procedure). Then the two wave functions are related by

$$\Psi(\{\tau_p^z, \mu_l\}) = \begin{cases} \Psi^{di}(\{\mu_l\}) \text{ if } \sigma\text{'s match } \tau_p^z \text{ domain walls} \\ 0 \qquad\qquad \text{otherwise} \end{cases}$$

(See appendix A.2 for a derivation of this identity). On a torus, the situation is more complicated. In this case the doubled Ising string-net model has 9 degenerate ground states, and some of these states have a nonzero amplitude for an odd number of σ loops to wrap around at least one of the non-contractible cycles of the torus. In the ungauged model, however, such a state would cost energy since it is not compatible with a domain wall configuration of plaquette spins. This suggests that on a torus the ground state degeneracy, and therefore the topological order, of the two theories is different. This is consistent with

the calculation of appendix A.1 which shows that the symmetric toric code has a ground state degeneracy of 4 on a torus.

2.4 General construction

In this section we show that the symmetric toric code can be generalized to a large class of exactly solvable models for SET phases. These models are very powerful: they can realize *every* symmetry-enriched topological phase whose underlying topological order can be realized by the string-net construction.

Before we get into details, we need to describe the input data that goes into our construction. Suppose we want to build a model for an SET phase with anyon excitations $\mathcal{A}$. For our construction to work, the collection of anyons $\mathcal{A}$ must be realizable by a string-net model. Equivalently, in mathematical language, $\mathcal{A}$ must be the 'Drinfeld center' of some 'unitary fusion category' $\mathcal{C}$, which we denote by $\mathcal{A} = \mathcal{Z}(\mathcal{C})$. In this language, the input data for our construction is a mathematical object called a 'G-extension' of $\mathcal{C}$ (we will define these terms below).

To see why G-extensions are a sensible choice for input data, it is important to recall a theorem of Ref. [13] which states that there is a one-to-one correspondence between G-extensions of $\mathcal{C}$ and braided G-crossed extensions of $\mathcal{Z}(\mathcal{C})$.[13] As we mentioned in the introduction, the latter objects can be thought of as mathematical descriptions of SET phases with symmetry group G and anyon excitations $\mathcal{A} = \mathcal{Z}(\mathcal{C})$, so this theorem implies that there is a natural correspondence between G-extensions and SET phases. Our construction provides a concrete realization of this correspondence.

The general idea behind our construction is illustrated in Fig. 2.8. Our construction takes as input a G-extension $\mathcal{D}$ of some unitary fusion category $\mathcal{C}$ and it returns as output an exactly solvable model realizing an SET phase with symmetry group G and anyon excitations $\mathcal{A} = \mathcal{Z}(\mathcal{C})$. The construction itself proceeds in two steps. The first step is to build the string-net model corresponding to $\mathcal{D}$. This string-net model realizes a topological phase

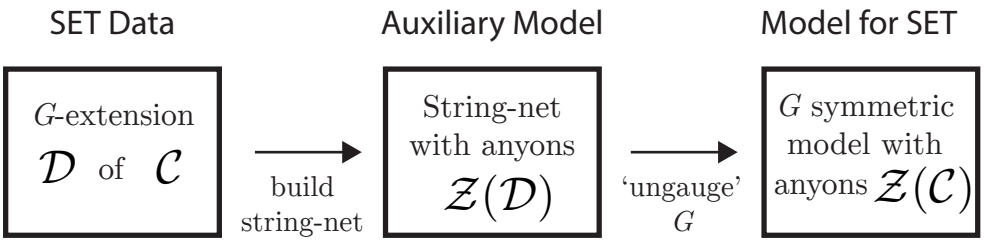

Figure 2.8: Building a symmetry enriched string-net model involves two steps. First we construct the string-net model for the G-extension $\mathcal{D}$ of $\mathcal{C}$. Next we 'ungauge' the string-net model to obtain a G-symmetric model with anyon excitations given by $\mathcal{Z}(\mathcal{C})$.

with anyon excitations given by $\mathcal{Z}(\mathcal{D})$. Crucially, it was shown in Refs. [3, 13] that this collection of anyons is precisely what would be obtained if we gauged the global symmetry of the SET phase of interest. In other words, the string-net model realizes the *gauged* SET phase. Hence, to obtain a model for the ungauged SET phase, all we have to do is reverse the gauging procedure — that is, construct a model that 'gauges' into the string-net model based on $\mathcal{D}$. This is the second step illustrated in Fig. 2.8 and it is accomplished by following a simple recipe which we will describe below.

We now briefly review the definitions of the various terms used above and fill in the details of the construction.

2.4.1 Drinfeld center, string-net models, and G-extensions

The *Drinfeld center* construction is a mathematical procedure that takes as input a unitary fusion category $\mathcal{C}$, and produces, as output, an anyon theory $\mathcal{A} = \mathcal{Z}(\mathcal{C})$.[11] Here, a *unitary fusion category* $\mathcal{C}$ is a finite collection of N simple objects $i, j, k, \ldots$, that includes a trivial simple object 1, together with fusion spaces V_k^{ij} and associativity relations encoded in unitary matrices F_l^{ijk} satisfying certain coherence conditions. An *anyon theory* is also a fusion category, but with the additional data associated with non-degenerate braiding (of anyons).[33] More physically, an anyon theory is the mathematical data used to describe a topological phase without symmetry.

Some simple examples of the Drinfeld center construction are: (1) the toric code, which is the Drinfeld center of $\mathcal{C} = \mathbb{Z}_2$, (2) more generally, the irreducible representations of the quantum double of a finite group $\mathcal{G}$, which is the Drinfeld center of $\mathcal{C} = \mathcal{G}$ and (3) any anyon theory of the form $\mathcal{T} \times \overline{\mathcal{T}}$, which is the Drinfeld center of $\mathcal{T}$. The Drinfeld center is sometimes also referred to as the 'quantum double' construction, though here we will only use the term quantum double in the context of finite groups, as in example (2) above.

String-net models are exactly solvable models that provide a physical realization of the Drinfeld center construction.[48, 31] The input necessary to build a string-net model is a set of string types, fusion rules and F-symbols, obeying certain consistency conditions (see e.g. section 2.3.1). In mathematical language, this input data is precisely a unitary fusion category $\mathcal{C}$, with string types corresponding to simple objects in $\mathcal{C}$. Likewise, the output of the string-net construction is a lattice spin model that realizes precisely the anyon theory $\mathcal{A} = \mathcal{Z}(\mathcal{C})$. This model is built out of $|\mathcal{C}|$-state spins living on the *links* of the honeycomb lattice. The Hamiltonian takes the form

$$H^{\text{snet}} = -\sum_v Q_v - \sum_p B_p^{\text{snet}} \tag{2.49}$$

where the first term, Q_v, is a projection operator that projects onto states that obey the fusion rules of $\mathcal{C}$ at vertex v, and the second term, B_p^{snet}, is the string-net plaquette term:

$$B_p^{\text{snet}} = \sum_{s \in \mathcal{C}} a_s B_p^s, \qquad a_s = \frac{d_s}{\sum_{i \in \mathcal{C}} d_i^2} \tag{2.50}$$

Here d_s denotes the quantum dimension of s and the definition of B_p^s is given in Ref. [48].

A *G-extension* of $\mathcal{C}$ is simply another fusion category $\mathcal{D}$ with an additional property called a G-grading, which is a decomposition of $\mathcal{D}$,

$$\mathcal{D} = \bigoplus_{g \in G} \mathcal{D}_g, \tag{2.51}$$

satisfying $\mathcal{D}_g \times \mathcal{D}_h \subset \mathcal{D}_{gh}$ and $\mathcal{C} = \mathcal{D}_1$, where 1 is the identity of G. We will always assume that the G-grading is *faithful*, i.e. $\mathcal{D}_g$ is non-empty for all $g \in G$.

To get a better feeling for this definition we mention a few examples and make a few comments:

(1) To begin, consider the case where $\mathcal{C} = \mathbb{Z}_2 = \{1, \psi\}$ and $G = \mathbb{Z}_2$. In this case, the Ising fusion category $\mathcal{D} = \{1, \psi, \sigma\}$ provides an example of a $\mathbb{Z}_2$ extension of $\mathcal{C}$ with a $\mathbb{Z}_2$ grading given by $\mathcal{D}_1 = \{1, \psi\}$ and $\mathcal{D}_{-1} = \{\sigma\}$ (Here, the F symbols for $\mathcal{D}$ are given in Eq. [2.37]). In fact, this is precisely the G-extension we used to construct the symmetric toric code model of section 2.2.

(2) Another class of G-extensions which may be more familiar are ordinary group extensions. In this case the category $\mathcal{C}$ and the extended category $\mathcal{D}$ are both groups, and $\mathcal{C}$ is a normal subgroup of $\mathcal{D}$ such that the quotient group $\mathcal{D}/\mathcal{C}$ is isomorphic to G. The F-symbols can be taken to be trivial, i.e. $F \equiv 1$, for both $\mathcal{C}$ and $\mathcal{D}$. For example, the dihedral group $\mathcal{D} = D_{2N}$ is a $\mathbb{Z}_2$ extension of $\mathcal{C} = \mathbb{Z}_N$. The identity component $\mathcal{D}_1$ is the $\mathbb{Z}_N$ subgroup consisting of rotations while the other component $\mathcal{D}_{-1}$ consists of elements that are the composition of a rotation and a reflection.

(3) Note that G-extensions should not be confused with *braided* G-crossed extensions. A G-extension is a fusion category and thus only contains data related to fusion; a braided G-crossed extension is a more complicated structure that contains both fusion and braiding data, and that can be thought of as a mathematical description of an SET phase.

(4) As we mentioned earlier, it is known that there is a one-to-one correspondence between G-extensions of $\mathcal{C}$ and braided G-crossed extensions of $\mathcal{Z}(\mathcal{C})$.[13] This correspondence plays a central role in our construction, so it would be useful if we could turn it into an *explicit* algorithm that produces a G-extension of $\mathcal{C}$ given a braided G-crossed extension of $\mathcal{Z}(\mathcal{C})$. We do not know of such an algorithm, but there are some partial results in this direction that are worth mentioning. Specifically, one such result is that if a braided G-crossed extension has the property that the symmetry action ρ on the anyons is trivial, then the

corresponding G-extension $\mathcal{D}$ is always made up of $|G|$ copies of $\mathcal{C}$, i.e. $\mathcal{D}_g = \mathcal{C}$ for all g.[13] This also implies that if the G-extension $\mathcal{D}$ is *not* made of $|G|$ copies of $\mathcal{C}$ then the action of ρ is non-trivial.

For instance, in the example $\mathcal{D} = \{1, \psi, \sigma\}$ discussed above, the two components of the G-extension are $\mathcal{D}_1 = \{1, \psi\}$ and $\mathcal{D}_{-1} = \{\sigma\}$. The fact that these two components have different size, and are therefore not isomorphic, immediately implies that in the corresponding SET phase, the symmetry has a non-trivial $\mathbb{Z}_2$ action ρ on the topological data characterizing the phase. In general, such a non-trivial action means that either ρ permutes the anyon types of the SET phase or ρ acts non-trivially on the fusion spaces V_k^{ij} and leaves the anyons fixed. In this example, we know that ρ permutes the anyon types because the SET phase corresponding to this G-extension is the symmetric toric code from section 2.2.

2.4.2 Symmetry enriched string-net models

We are now ready to present the general symmetry enriched string-net construction. The input data for our construction is a G-extension $\mathcal{D}$ of a unitary fusion category $\mathcal{C}$. The output is a commuting projector model for an SET phase with symmetry group G and anyon excitations $\mathcal{A} = \mathcal{Z}(\mathcal{C})$.

As mentioned earlier, our construction has two steps. The first step is to build a string-net model with string types corresponding to the simple objects in $\mathcal{D}$. This model is built out of $|\mathcal{D}|$-state spins living on the links of the honeycomb lattice with a Hamiltonian, H^{snet}, given by Eq. (2.49) but with $\mathcal{C}$ replaced by $\mathcal{D}$. The second step is to 'ungauge' this string-net model. We do this by modifying both the string-net Hilbert space and the string-net Hamiltonian. Starting with the Hilbert space, the only modification is that we add $|G|$-state degrees of freedom to the *plaquettes* of the honeycomb lattice. The Hilbert space of our model now consists of two separate tensor factors. One tensor factor is formed by the $|G|$-dimensional Hilbert spaces living on the plaquettes p, each with basis states $|g_p\rangle, g_p \in G$, which we refer to as plaquette spins. The other tensor factor is the $|\mathcal{D}|$-dimensional string-

net Hilbert space living on each link l of the honeycomb lattice with basis states $|s_l\rangle$, $s_l \in \mathcal{D}$. In this notation, the basis states for the full Hilbert space are labeled as $|\{g_p, s_l\}\rangle$.

As for the Hamiltonian, we make two modifications to H^{snet} (Eq. 2.49). First, we add a new term $-\sum_l P_l$. Second, we modify the string-net plaquette term in a particular manner: $B_p^{\text{snet}} \to B_p$. The end result takes the form

$$H = -\sum_l P_l - \sum_v Q_v - \sum_p B_p \tag{2.52}$$

where the sums run over the links (l), vertices (v), and plaquettes (p) of the honeycomb lattice.

In order to explain the three terms listed above, we need to introduce some notation. Our first piece of notation involves the G-grading of $\mathcal{D}$: for each element $s \in \mathcal{D}$, we denote its corresponding group element g in G by g_s. By definition, $s \in \mathcal{D}_{g_s}$.

Another piece of notation has to do with domain walls between plaquette spins. Given any G-spin configuration $\{g_p\}$, we define a G-valued link variable g_l by:

$$g_l = g_{p'}^{-1} g_p \tag{2.53}$$

where p and p' are the two plaquettes that border link l, oriented from p to p' (Figure 2.9). We can think of g_l as defining a domain wall configuration. Note that in order to make this definition unambiguous we need to specify a convention for which plaquette corresponds to p' and which plaquette corresponds to p. To this end, recall that the links in a string-net model always carry an orientation, which we take to be fixed. By rotating the oriented links 90 degrees counterclockwise, we also obtain a fixed orientation of the dual triangular lattice. This orientation allows us to fix a convention for Eq. (2.53), as shown in Figure 2.9.

With this notation, we are now ready to define the different terms in the Hamiltonian

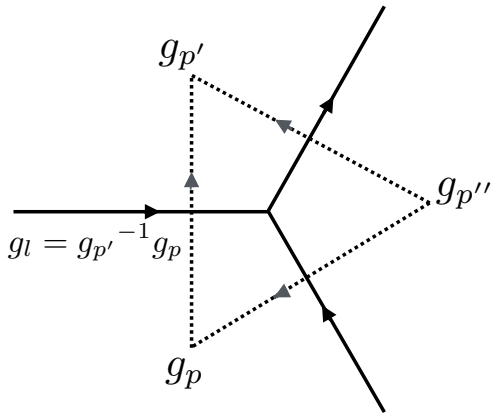

Figure 2.9: By rotating oriented links 90 degrees counterclockwise, an orientation on the original hexagonal lattice gives an orientation on the dual triangular lattice. The latter allows us to define link variables g_l, given any configuration of plaquette spins $\{g_p\}$ and any link l of the original hexagonal lattice.

(2.52). The first term P_l is defined by

$$P_l|X\rangle = \begin{cases} |X\rangle & \text{if } g_l = g_{s_l} \\ 0 & \text{otherwise} \end{cases} \tag{2.54}$$

where $|X\rangle$ is some basis state $|X\rangle = |\{g_p, s_l\}\rangle$, g_l is defined as in Eq. (2.53) and s_l is the $\mathcal{D}$-label on link l. The general interpretation of P_l is as follows: there are two different ways to obtain a G-valued string-net configuration on links. One comes from the domain walls of the plaquette spins, and the other comes from examining the G-grading of the link variables in the $\mathcal{D}$ string-net configuration. The term $-\sum_l P_l$ energetically favors configurations where these two agree. This is a direct generalization of the operator $-\sum_l P_l$ given in the toric code example which favored states for which plaquette spin domain walls coincided with σ strings.

The second term, Q_v, is simply the usual string-net vertex operator. On the other hand, the third term, B_p, is a *modified* version of the usual string-net plaquette operator B_p^{snet}

(Eq. 2.50). In particular,

$$B_p = \sum_{s \in \mathcal{D}} a_s B_p^s \tilde{U}_p^{g_s} \tag{2.55}$$

where $\tilde{U}_p^g$ acts as right-multiplication by g

$$\tilde{U}_p^g : |g_p\rangle \to |g_p g\rangle \tag{2.56}$$

Note that the only difference between B_p and B_p^{snet} is the presence of the operator $\tilde{U}_p^{g_s}$, which acts on the plaquette spins.

We should mention that the above models only apply to the case where the category $\mathcal{D}$ does not have any fusion multiplicity (a category has *fusion multiplicity* if one of the fusion spaces V_k^{ij} has dimension two or greater). If we want to accommodate fusion multiplicity in $\mathcal{D}$, we need to modify the corresponding string-net model H^{snet} by including additional spins that live on the *sites* of the honeycomb lattice.[48, 31, 38] Likewise, these site spins also need to be included in the symmetry-enriched string-net model (2.52). This extension is straightfoward so we omit the details; the main point is that our construction can be applied to arbitrary fusion categories $\mathcal{D}$ as long as one uses suitably generalized string-net models.[31, 38, 49]

2.4.3 Properties

The Hamiltonian H (2.52) defined above has a number of interesting properties. For the most part, the proofs of these properties are very similar to the ones given in detail for the symmetric toric code so we do not repeat the analysis here, but rather simply sketch the main idea.

(1) H has a global G symmetry, where the symmetry action U_g is defined by left multiplication by g:

$$U^g = \bigotimes_p U_p^g \tag{2.57}$$

$$U_p^g : |g_p\rangle \to |gg_p\rangle \tag{2.58}$$

Note that U_g is the natural generalization of the $\mathbb{Z}_2$ symmetry $S = \prod_p \tau_p^x$ in the symmetric toric code model.

(2) All of the terms in H commute. The proof of this statement is nearly identical to the one given for the symmetric toric code in section 2.2.2.

(3) All of the terms in H are projectors. This is clearly the case for P_l and Q_v which were defined as projectors. One can see B_p is a projector by using Eq. (2.15) and following the same reasoning as in the symmetric toric code case.

(4) In an infinite plane or sphere geometry, the operators P_l, Q_v, B_p have a unique simultaneous eigenstate with eigenvalue 1. This state is the unique ground state of H. The existence and uniqueness of this state can be deduced from the existence and uniqueness of string-net ground states in a sphere geometry, together with the fact that gauging H gives a modified string-net model, as discussed in **(6)**. (Note that this result implies that H does not spontaneously break the symmetry, since it has a *unique* ground state).

(5) In a sphere or infinite plane geometry, the ground state amplitude of $X = \{g_p, s_l\}$ is given by

$$\Psi(\{g_p, s_l\}) = \begin{cases} \Psi^{\text{snet}}(\{s_l\}) & \text{if } g_l = g_{s_l} \\ 0 & \text{otherwise} \end{cases}$$

where $\Psi^{\text{snet}}(\{s_l\})$ is the ground state amplitude of $\{s_l\}$ in the string-net model based on $\mathcal{D}$.

(6) Gauging the global symmetry (2.57) of this model results in a topological phase described by the anyon theory $\mathcal{Z}(\mathcal{D})$. This can be seen by introducing G-valued variables

on the links of the dual triangular lattice and performing a minimal coupling procedure as described for the symmetric toric code in section 2.3.2. As in that case, it is straightforward to see that the resulting gauged model is unitarily equivalent to a *modified* string-net model that realizes $\mathcal{Z}(\mathcal{D})$. This modified string-net model contains a $|G|$ dimensional spin, ξ_l, on the links in addition to the usual $\mathcal{D}$-state spin. While the modified model looks different from the usual string-net model, it belongs to the same phase since its ground state is simply the usual string-net ground state tensored with a product state where all of the auxiliary spins ξ_l are in the $|g = 1\rangle$ state. See section 2.3.3 for a precise definition of this modified string-net model and the associated unitary equivalence, in the case of the symmetric toric code.

(7) The Hamiltonian H realizes an SET phase with symmetry group G and anyon excitations $\mathcal{A} = \mathcal{Z}(\mathcal{C})$. Furthermore, this SET phase is precisely the one associated with $\mathcal{D}$ under the correspondence discussed in section 3.1.1. This property follows from property **(6)** together with two mathematical results. The first result is that the anyon theory $\mathcal{Z}(\mathcal{D})$ is exactly what would be obtained by gauging the symmetry of the desired SET phase. The second result is that the anyon theory corresponding to a gauged SET phase uniquely determines the original SET phase. [3, 13]

2.5 Examples

In this section we illustrate the general construction with some additional examples. We start with two simple examples: a bosonic SPT phase with a $\mathbb{Z}_2$ symmetry and a toric code phase with a $\mathbb{Z}_2$ symmetry that does not permute any anyons. We note that solvable models for both of these phases have been written down previously.[43, 10, 24] We then discuss two SET phases that have non-Abelian anyons and anyon-permuting symmetries — one with a $\mathbb{Z}_2$ symmetry and one with a $\mathbb{Z}_3$ symmetry.

2.5.1 Bosonic $\mathbb{Z}_2$ SPT phase

We begin by constructing a model for a bosonic SPT phase with $\mathbb{Z}_2$ symmetry. The first step of our construction is to find the fusion category $\mathcal{C}$ associated with this phase. To this end we note that, like all SPT phases, this phase supports only trivial anyons: $\mathcal{A} = \{1\}$. Trivial anyons can be realized by a trivial string-net model with only one string type, so we conclude that $\mathcal{C} = \{1\}$.

Having found $\mathcal{C}$, the second step is to find the different $\mathbb{Z}_2$-extensions $\mathcal{D}$ of $\mathcal{C}$; each extension will give us a model for a different $\mathbb{Z}_2$ SPT phase. Conveniently the $\mathbb{Z}_2$ extensions of $\mathcal{C} = \{1\}$ are already known: there are two such extensions, both of which are of the form $\mathcal{D} = \mathbb{Z}_2 = \{1, a\}$ with

$$a \times a = 1, \quad a \times 1 = a, \quad 1 \times 1 = 1 \tag{2.59}$$

and with the $\mathbb{Z}_2$ grading given by $\mathcal{D} = \mathcal{D}_1 \oplus \mathcal{D}_{-1}$ with $\mathcal{D}_1 = \{1\}$ and $\mathcal{D}_{-1} = \{a\}$. [6] The difference between the two extensions comes from their F-symbols F_l^{ijk}. In one extension, the F symbol is trivial: $F \equiv 1$. In the other extension, $F_a^{aaa} = -1$, and $F = 1$ otherwise.

Let us focus on the second $\mathbb{Z}_2$ extension, since this is the one that gives the *non-trivial* SPT phase. To build a model for this phase, we first need to construct the string-net model with string types given by $\mathcal{D}$. This string-net model is well-known and is called the 'doubled semion' model.[48] We then need to ungauge the doubled semion model. Following the general recipe, we add two-state spins to the plaquettes of the honeycomb lattice, with states labeled by $\tau_p^z = \pm$. We then modify the Hamiltonian of the doubled semion model by adding the term $-\sum_l P_l$ with

$$P_l = \frac{1}{2}(1 + (-1)^{N_l} \tau_p^z \tau_q^z)$$

6. More generally, for any finite group G, the number of G-extensions of $\{1\}$ is given by $H^3(G, U(1))$ and all the extensions have fusion rules that are isomorphic to G.

Here p, q denote the two plaquettes that adjoin l while the N_l operator is defined by $N_l = 1$ if the link l is occupied with a type a string and $N_l = 0$ otherwise. Finally, we alter the plaquette operator

$$B_p \to \frac{1}{2}(1 + B_p^a \tau_p^x) \tag{2.60}$$

The result is a model for a non-trivial SPT phase with a $\mathbb{Z}_2$ symmetry $S = \prod_p \tau_p^x$.

The above model is closely related to the one written down in Ref. [43] but the Hilbert space is slightly different: in the above model there are two-state spins on both the links and plaquettes of the honeycomb lattice, while the model from Ref. [43] only has spins on the plaquettes. To understand the relationship between the two models, it is useful to think about their ground states. For the model in Ref. [43], the ground state amplitude for a plaquette spin configuration X is given by $\Psi(X) = (-1)^{N(X)}$ where N is the number of domain wall loops in X. In comparison, the ground state amplitude in the above model is given by the same formula, but there is an additional constraint that the occupied links l must lie along the domain walls of the plaquette spins; if this constraint is not satisfied then the amplitude $\Psi = 0$. While the two ground state wave functions are different, it is easy to see that there exists a local unitary transformation that transforms the ground state of the above model into the ground state of the other model tensored with a product state made up of the link spins. Given this connection, we can conclude that the two models describe the same phase.

2.5.2 Toric code with a non-permuting $\mathbb{Z}_2$ symmetry

In this section, we construct a model for a toric code phase with a $\mathbb{Z}_2$ symmetry that does *not* permute the anyons. The first step is to find the fusion category $\mathcal{C}$ corresponding to the toric code. Since the toric code phase can be realized by a string-net model with two string types and $\mathbb{Z}_2$ fusion rules, we have $\mathcal{C} = \mathbb{Z}_2 = \{1, a\}$. As for the F symbol F_l^{ijk}, this is trivial for the toric code model: $F \equiv 1$.

The second step is to find the $\mathbb{Z}_2$ extensions $\mathcal{D}$ of $\mathcal{C}$; each extension will give us a model for a different SET phase. In addition to the two $\mathbb{Z}_2$-extensions with $e \leftrightarrow m$ symmetry discussed in section 2.2 and appendix A.3, we expect four $\mathbb{Z}_2$-extensions with a non-permuting $\mathbb{Z}_2$ symmetry. [51, 3] These four extensions can be found by inspection: two are of the form $\mathcal{D} = \mathbb{Z}_2 \times \mathbb{Z}_2$, and two are of the form $\mathcal{D} = \mathbb{Z}_4$. Within each pair, the two extensions are distinguished from one another by their (extended) F-symbols, F_l^{ijk}, which we omit here for the sake of brevity.

The first two $\mathbb{Z}_2$ extensions give models that describe either the trivial toric code, or a trivial toric code stacked on top of a $\mathbb{Z}_2$ SPT. The other two extensions give models where either the e particle and the em particle carry a half $\mathbb{Z}_2$-charge or the e particle and the m particle carry a half $\mathbb{Z}_2$-charge (the phase where m and em carry a half charge can be obtained by re-labeling, and does not constitute a distinct SET). In all four cases, the $\mathbb{Z}_2$ symmetry does not permute the anyons.

Let us focus on the $\mathbb{Z}_2$ extension corresponding to an SET where the e and the em particles carry half a charge. In this case, $\mathcal{D} = \mathbb{Z}_4 = \{1, a, a^2, a^3\}$ and the $\mathbb{Z}_2$ grading is given by $\mathcal{D} = \mathcal{D}_1 \oplus \mathcal{D}_{-1}$ with $\mathcal{D}_1 = \{1, a^2\}$ and $\mathcal{D}_{-1} = \{a, a^3\}$. The F-symbol is trivial for this extension: $F \equiv 1$. To build a model corresponding to this phase, we need to construct the string-net model with string types given by $\mathcal{D}$. This model is exactly the Kitaev quantum double model[32] with $G = \mathbb{Z}_4$, defined on the honeycomb lattice.

After building this string-net model, we then need to ungauge it. Following the same procedure as before, we do this by attaching additional two-state spins to the plaquettes, with states labeled by $\tau_p^z = \pm$. Next, we add the term $-\sum_l P_l$, with

$$P_l = \frac{1}{2}(1 + (-1)^{N_l}\tau_p^z\tau_q^z)$$

Here p, q denote the two plaquettes that adjoin l while N_l is defined by $N_l = 1$ if the link l is occupied by a or a^3 and $N_l = 0$ otherwise. The last step is to modify the plaquette

Anyon	topological spin	d	Anyon	topological spin	d
$a \equiv 1$	0	1	e	π	3
b	0	1	f	0	2
c	0	2	g	$2\pi/3$	2
d	0	3	h	$4\pi/3$	2

Table 2.2: Anyon types and corresponding topological data for the quantum double $\mathcal{Z}(S_3)$.

operators so that they commute with P_l:

$$B_p \to \frac{1}{4}(B_p^1 + B_p^a \tau_p^x + B_p^{a^2} + B_p^{a^3} \tau_p^x)$$

The resulting model has a $\mathbb{Z}_2$ symmetry $S = \prod_p \tau_p^x$ and describes a toric code phase in which the e and the em particles carry a half $\mathbb{Z}_2$-charge.

2.5.3 Quantum double of S_3

In this section, we consider an SET phase that has the same anyon types as the quantum double of S_3 (see Table 2.2), and has a $\mathbb{Z}_2$ symmetry that exchanges two of the anyons (namely the c and f anyons). The possibility of such an SET phase was discussed previously in Ref. [3]; here we construct an exactly solvable model that realizes it.

As always, the first step in our construction is to find the fusion category $\mathcal{C}$ associated with this topological phase. To this end, we note that the quantum double of S_3 can be realized by a string-net model with three different string types corresponding to the three irreducible representations of S_3.[7] Labeling these representations by $1, a_1, a_2$ where 1 is the trivial representation, a_1 is the two dimensional representation, and a_2 is the one-dimensional representation, we deduce that $\mathcal{C} = \{1, a_1, a_2\}$. The fusion rules can be read off from the representation theory of S_3:

$$a_2 \times a_2 = 1,\ a_1 \times a_2 = a_1,\ a_1 \times a_1 = 1 + a_1 + a_2.$$

7. Actually, the quantum double of S_3 can also be realized by a string-net model with string types corresponding to group *elements* $g \in S_3$. Hence, we could equally well take $\mathcal{C} = S_3$.

Likewise, the F-symbol is given by the $6j$-symbol for S_3.

The second step is to find the $\mathbb{Z}_2$ extensions $\mathcal{D}$ of $\mathcal{C}$. Each extension defines a model for a different SET phase, so if we wanted to be systematic, we would find all such extensions. Here we will be less ambitious and will simply discuss one example: $\mathcal{D} = SU(2)_4$. This extension is particularly interesting because, as we will argue below, it corresponds to an SET phase where the $\mathbb{Z}_2$ symmetry exchanges c and f.

Before proceeding further we need to explain our notation: $SU(2)_4$ denotes the fusion category associated with non-Abelian Chern-Simons theory with gauge group $SU(2)$ at level 4. This fusion category has five simple objects, which can be labeled according to their 'spin' as: $\mathcal{D} = \{1, a_{\frac{1}{2}}, a_1, a_{\frac{3}{2}}, a_2\}$. The fusion rules are given by Eq. (2.63). The $\mathbb{Z}_2$ grading is given by $\mathcal{D} = \mathcal{D}_1 \oplus \mathcal{D}_{-1}$ where

$$\mathcal{D}_1 = \mathcal{C} = \{1, a_1, a_2\} \ , \quad \mathcal{D}_{-1} = \{a_{\frac{1}{2}}, a_{\frac{3}{2}}\}. \tag{2.61}$$

The F-symbol is known but we will not reprint it here.[5]

To build a model for the corresponding SET phase, we need to construct a string-net model with string types given by the simple objects in $\mathcal{D}$. We then need to ungauge this string-net model. Following the same recipe as before, we do this by adding two-state spins to each plaquette, with states labeled by $\tau_p^z = \pm$. Next we modify the string-net Hamiltonian by adding the term $-\sum_l P_l$ with

$$P_l = \frac{1}{2}(1 + (-1)^{N_l}\tau_p^z\tau_q^z)$$

Here p, q denote the plaquettes that adjoin l while N_l is defined by $N_l = 1$ if the edge is occupied by $a_{\frac{1}{2}}$ or $a_{\frac{3}{2}}$ and $N_l = 0$ otherwise. Finally we modify the plaquette operator so

that it commutes with P_l:

$$B_p \to \frac{1}{\sum_i d_i^2}\left(\sum_{s=0,1,2} d_s B_p^s + \tau_p^x \sum_{s=\frac{1}{2},\frac{3}{2}} d_s B_p^s\right) \tag{2.62}$$

The resulting model has a $\mathbb{Z}_2$ symmetry $S = \prod_p \tau_p^x$ and supports the same types of anyons as the quantum double of S_3.

To determine how the symmetry acts on these anyons, notice that the two components in Eq. (2.61) have different sizes, so by the general result discussed in section 3.1.1, the $\mathbb{Z}_2$ action on the topological data must be nontrivial. This means that the $\mathbb{Z}_2$ symmetry either (1) permutes some of the anyons or (2) leaves the anyons fixed but has a nontrivial action on the anyon fusion spaces. Assuming the latter possibility doesn't occur, we deduce that the symmetry must exchange c and f since this is the only anyon permutation that is consistent with the data in Table 2.2.

$\mathcal{D}$ =SU$(2)_k$ for k even

It is worth noting that the above example is part of a larger family of SET phases, all of which have a $\mathbb{Z}_2$ anyon-permuting symmetry. These phases correspond to $\mathbb{Z}_2$-extensions of the form $\mathcal{D} = SU(2)_k$ where k is even and where $\mathcal{C}$ is the subcategory of $\mathcal{D}$ consisting of objects with integer 'spin.' Here, the objects in $SU(2)_k$ can be labeled as $\{a_0 \equiv 1, a_{1/2}, \ldots, a_{k/2}\}$. The fusion rules are[5]

$$a_l \times a_m = \sum_{n=|l-m|}^{\min(l+m,k-l-m)} a_n \tag{2.63}$$

and admit a natural $\mathbb{Z}_2$-grading:

$$\mathcal{D}_1 = \mathcal{C} = \{a_l | l \in \mathbb{Z}\}\ , \quad \mathcal{D}_{-1} = \{a_l | l \in \mathbb{Z} + 1/2\} \tag{2.64}$$

Anyon	topological spin	d	Anyon	topological spin	d
1	0	1	c_1	0	3
b	0	1	c_2	0	3
b^2	0	1	c_3	π	3
a	0	3	c_4	π	3
x_1	0	4	y_1	0	4
x_2	$2\pi/3$	4	y_2	$2\pi/3$	4
x_3	$4\pi/3$	4	y_3	$4\pi/3$	4

Table 2.3: Anyon types and corresponding topological data for the quantum double $\mathcal{Z}(A_4)$.

Following the same reasoning as above, we know that the $\mathbb{Z}_2$ symmetry permutes the anyons (or at least acts nontrivially on the topological data) in these phases since the two components of $\mathcal{D}$ have different sizes. Indeed, $\mathcal{D}_1 = \{a_0, a_1, \ldots, a_{k/2}\}$ contains $k/2+1$ elements, while $\mathcal{D}_{-1} = \{a_{1/2}, a_{3/2}, \ldots, a_{(k-1)/2}\}$ contains only $k/2-1$ elements.

2.5.4 Quantum double of A_4

We now consider an SET phase with the same anyon types as the quantum double of A_4 (see Table 2.3) with a $\mathbb{Z}_3$ symmetry that permutes three of the anyons (namely a, c_1, c_2).

The first step is to find the fusion category $\mathcal{C}$ associated with this phase. To do this, we note that the quantum double of A_4 can be realized by a string-net model with string types corresponding to the four irreducible representations of A_4. Labeling these representations by $\{1, b, b^2, a\}$ where 1 denotes the trivial representation, and b, b^2 denote one dimensional representations, and a denotes a three dimensional representation, we deduce that $\mathcal{C} = \{1, b, b^2, a\}$. The fusion rules can be read off from the representation theory of A_4,

$$b \times b^2 = 1,\ b \times a = b^2 \times a = a,\ a \times a = 1 + b + b^2 + 2a, \tag{2.65}$$

while the F-symbol is given by the $6j$ symbol for A_4.

The next step is to find the $\mathbb{Z}_3$ extensions $\mathcal{D}$ of $\mathcal{C}$. Again, rather than finding all such extensions, we will only discuss one example: $\mathcal{D} = SU(3)_3$. This is a category with 10 simple

objects: $\{1, a, b, b^2, d_1, d_2, d_3, e_1, e_2, e_3\}$. The $\mathbb{Z}_3$ grading is:

$$\mathcal{D}_1 = \mathcal{C} = \{1, a, b, b^2\} \ , \quad \mathcal{D}_\omega = \{d_1, d_2, d_3\}, \\ \mathcal{D}_{\omega^2} = \{e_1, e_2, e_3\} \tag{2.66}$$

where we have labeled the elements of $\mathbb{Z}_3$ as $1, \omega, \omega^2$ with $\omega = e^{2\pi i/3}$. The fusion rules are:

$$\begin{aligned} &d_i \times a = \sum_{j=1}^{3} d_j, \ e_i \times a = \sum_{j=1}^{3} e_j, \quad e_i \times b = e_{(i \bmod 3)+1} \\ &d_i \times e_j = a + b^{(i-j) \bmod 3}, \quad d_i \times b = d_{(i \bmod 3)+1} \\ &d_1 \times d_2 = d_3 \times d_3 = e_2 + e_3, \ d_1 \times d_3 = d_2 \times d_2 = e_1 + e_2 \\ &d_2 \times d_3 = d_1 \times d_1 = e_1 + e_3, \ e_1 \times e_2 = e_3 \times e_3 = d_2 + d_3 \\ &e_1 \times e_3 = e_2 \times e_2 = d_1 + d_2, \ e_2 \times e_3 = e_1 \times e_1 = d_1 + d_3 \end{aligned} \tag{2.67}$$

We omit the F symbol for brevity.

To build a model for the associated SET phase, we need to construct the string-net model with string labels in $\mathcal{D}$ and fusion rules given by Eq. (2.67). We then need to ungauge this string-net model. Following the general procedure, the first step is to add a *three-state* spin to each plaquette. We denote the basis states for this spin by $|1\rangle, |\omega\rangle, |\omega^2\rangle$ where $\omega = e^{2\pi i/3}$. We also define two generalized Pauli operators that act on these basis states:

$$\begin{aligned} C_p &= |1\rangle\langle 1| + \omega \ |\omega\rangle\langle\omega| + \omega^2 \ |\omega^2\rangle\langle\omega^2| \\ S_p &= |\omega\rangle\langle 1| + |\omega^2\rangle\langle\omega| + |1\rangle\langle\omega^2| \end{aligned} \tag{2.68}$$

Next, we add the term $-\sum_l P_l$ to the string-net Hamiltonian, where

$$P_l = \frac{1}{3} \sum_{k=0}^{2} \left(\omega^{-N_l} C_{p'}^{-1} C_p \right)^k \tag{2.69}$$

Here p, p' denote the two plaquettes that adjoin l, and we assume the orientation convention shown in Fig. 2.9. The operator N_l is defined by $N_l = 0, 1, 2$ depending on whether link l is occupied by a string in $\mathcal{D}_1, \mathcal{D}_\omega, \mathcal{D}_{\omega^2}$ respectively. Notice that P_l projects onto states that satisfy $C_{p'}^{-1} C_p = \omega^{N_l}$ — that is, states in which the $\mathbb{Z}_3$ domain walls between the plaquette spins coincide with the $\mathbb{Z}_3$ grading of the string types on the links. The last step is to modify the string-net plaquette term so that it commutes with P_l:

$$B_p \to \frac{1}{\sum_s d_s^2} \left(\sum_{j=0}^{2} \sum_{s \in \mathcal{D}_{\omega^j}} d_s S_p^j B_p^s \right) \tag{2.70}$$

Here s ranges over all labels in $\mathcal{D}$ and d_s is the associated quantum dimension.

The model obtained from this procedure has a $\mathbb{Z}_3$ symmetry $S = \prod_p S_p$ and supports the same types of anyon excitations as the quantum double of A_4. Furthermore, by the same reasoning as in the previous two examples, we know that the $\mathbb{Z}_3$ symmetry acts non-trivially on the topological data in this model. Presumably this means that the symmetry permutes the anyons a, c_1 and c_2 since this is the only non-trivial permutation that is consistent with Table 2.3.

2.6 Conclusion

In this chapter we have constructed a large class of exactly solvable models for 2D bosonic SET phases with finite, unitary onsite symmetry group. These models are very general and can realize every SET phase (or more precisely, every braided G-crossed extension) in this class whose underlying topological order can be realized by a string-net model. As an example of our construction, we have presented an exactly solvable model with the same anyon excitations as the toric code model and a $\mathbb{Z}_2$ symmetry that permutes the anyons e and m.

An interesting corollary of our construction is that it proves that all of the above SET phases are physically realizable in 2D systems. This is significant because mere algebraic

consistency of the topological data does not guarantee the existence of a physical realization: in principle, there could be additional obstructions to realizing an SET phase in a physical system that are not captured by the known mathematical structure. Our construction proves that no such obstructions exist, at least in the above cases.

One shortcoming of our current construction is that if one wants to construct a model for a specific SET phase, one needs to know the corresponding G-extension ahead of time. For example, in the case of the symmetric toric code we had to know that the correct G-extension to realize a phase with $e \leftrightarrow m$ symmetry was the Ising category $\mathcal{D} = \{1, \psi, \sigma\}$. In practice, however, one is more likely to be faced with a situation where one is interested in an SET phase with certain physical properties but one does not have any a priori knowledge of the corresponding G-extension. In this case, one would first need to translate from the known physical properties to the corresponding G-extension before applying our construction, and this is not necessarily an easy task.

Given this issue it would be desirable to construct models starting from a more convenient set of input data. For example, one might want to start from a particular symmetry action on a set of anyons (e.g. $e \leftrightarrow m$), and construct all possible models that realize this action. This is a challenging problem, but it may be possible to make progress using previously known mathematical results[13] on the relationship between symmetry actions and G-extensions.

Apart from this technical issue, perhaps the most interesting direction for future work would be to generalize our construction to a larger class of SET phases. For instance, it would be desirable to generalize these models to include continuous and/or anti-unitary symmetries — especially since many physical symmetries of interest fall into these classes. Another potentially interesting set of generalizations would be to extend these models to higher dimensional or fermionic systems.

CHAPTER 3

PROTECTED EDGE MODES WITH $\mathbb{Z}_2$ SYMMETRY

3.1 Background and motivation

3.1.1 Chiral boson edge theories with $\mathbb{Z}_2$ symmetry

We begin by reviewing the K-matrix formulation of chiral boson edge theories. A general chiral boson edge theory is described by N fields Φ_i obeying commutation relations of the form

$$[\Phi_i(x), \partial_y \Phi_j(y)] = 2\pi i K^{-1}_{ij} \delta(x-y), \tag{3.1}$$

together with a Hamiltonian density of the form

$$\mathcal{H} = \sum_{ij} \frac{V_{ij}}{4\pi} \partial_x \Phi_i \partial_x \Phi_j \tag{3.2}$$

Here K is a $N \times N$ symmetric, non-degenerate integer matrix while V is a $N \times N$ symmetric, positive definite real matrix. One can think of K as describing the topological properties of the bulk and edge, while V contains non-universal information, such as the velocities of the edge modes. In general, V will not play an important role in this paper since we will be primarily interested in the topological structure of the edge.

An important ingredient in any edge theory is the set of local operators. For the above edge theories, the fundamental local operators are of the form $e^{i\Theta_j(x)}$ where $\Theta_j = \sum_k K_{jk}\Phi_k$. All other local operators, such as $\partial_x \Phi_i$, can be constructed by taking derivatives and products of these operators. Physically, $e^{i\Theta_j(x)}$ can be interpreted as a creation operator for the jth species of electron. Here, we use the term 'electron' to denote the underlying microscopic particles from which the system is built, whether or not they are actually electrons.

We now review how to incorporate a $\mathbb{Z}_2$ symmetry into this formalism. A general $\mathbb{Z}_2$ transformation S can be characterized by its action on the electron operators $e^{i\Theta_j}$. In this

paper, we will assume that this symmetry action is of the following general form:

$$S^{-1}e^{i\Theta_j}S = e^{i\pi\chi_j}\prod_k e^{iW_{kj}\Theta_k} \tag{3.3}$$

Here W is an $N \times N$ integer matrix and χ is an N component real vector. The matrix W can be thought of as describing how the electron operators are mixed by the $\mathbb{Z}_2$ symmetry, while χ describes the additional phases that are accumulated.

Consistency demands that W and χ satisfy certain constraints. To derive these constraints, we take the logarithmic derivative of Eq. (3.3) with respect to x and then multiply by K^{-1}_{ij} which gives

$$S^{-1}(\partial_x\Phi_i)S = \sum_k W_{ik}\partial_x\Phi_k \tag{3.4}$$

From this transformation law, we can easily see that W satisfies the constraints

$$W^TKW = K, \quad W^2 = 1 \tag{3.5}$$

where the first constraint comes from the fact that the symmetry must preserve the commutation relations (3.1), while second constraint comes from requiring that $S^2 = 1$. We note that the relation $S^2 = 1$ also gives constraints on χ, but we will not need them here.

To summarize, a general chiral boson edge theory with $\mathbb{Z}_2$ symmetry is characterized by a triplet (K, W, χ) obeying certain constraints (3.5). The matrix K describes the commutation relations of the underlying fields and W, χ describe how the $\mathbb{Z}_2$ symmetry transformations act on these fields.

3.1.2 Gapping perturbations and null vectors

One of the goals of this paper is to determine which of the above edge theories can be gapped without breaking the $\mathbb{Z}_2$ symmetry and which cannot. To investigate this question,

it is useful to have a library of perturbations that can be used to gap chiral boson edge theories. A simple class of such gapping perturbations are those that scatter 'electrons' between different modes on the edge. These scattering terms take the form $U\cos(\Lambda^T\Theta - \alpha)$ where Λ is an N component integer vector and α is an arbitrary phase.

One can show that each scattering term $U\cos(\Lambda^T\Theta - \alpha)$ can gap at most a single pair of modes, so we need a minimum of $N/2$ terms to gap an edge theory with N modes. Conveniently, there are simple sufficient[1] conditions under which a sum of $N/2$ scattering terms

$$\mathcal{H}' = \sum_{i=1}^{N/2} U\cos(\Lambda_i^T\Theta - \alpha_i) \tag{3.6}$$

is guaranteed to gap the edge if U is sufficiently large. In particular, it is known that the above perturbation will gap the edge provided that (1) the vectors $\Lambda_1, ..., \Lambda_{N/2}$ are linearly independent and (2) they satisfy

$$\Lambda_i^T K \Lambda_j = 0 \quad \text{for all } i \text{ and } j \tag{3.7}$$

Such vectors are commonly referred to as 'null-vectors.'

While the above conditions guarantee that the perturbation $\mathcal{H}'$ will gap the edge, we need to impose two more conditions to ensure that the gapped edge does not break the $\mathbb{Z}_2$ symmetry. The first condition is that

$$S^{-1}\mathcal{H}'S = \mathcal{H}'. \tag{3.8}$$

This condition guarantees that the perturbation does not break the symmetry explicitly. The second condition is that the set of null vectors $\{\Lambda_1, ..., \Lambda_{N/2}\}$ is *primitive*, that is, there

1. In fact, these conditions are both necessary and sufficient [42].

is no solution to the equation

$$a_1\Lambda_1 + \ldots + a_{N/2}\Lambda_{N/2} = k\Lambda \tag{3.9}$$

where a_i are integers with no common divisors, k is an integer that is greater than 1, and Λ is an integer vector. This primitivity condition ensures that the perturbation does not break the symmetry *spontaneously*. [45]

If a perturbation $\mathcal{H}'$ satisfying the above conditions exists, then it follows that the edge can be gapped without breaking the $\mathbb{Z}_2$ symmetry. However, it is important to keep in mind that the converse statement is not true in general, i.e. the absence of an appropriate set of null vectors does not imply that the edge cannot be gapped.

3.1.3 Edge theories of bosonic $\mathbb{Z}_2$ SPT phases

In this paper, we will focus on edge theories of bosonic SPT phases — that is, SPT phases that are built out of bosonic 'electrons.' In this case, there are some additional constraints on the K-matrix. In particular,

$$K_{ii} = 0 \pmod 2, \quad |\det(K)| = 1, \quad \text{sig}(K) = 0. \tag{3.10}$$

where 'sig' stands for signature. Here, the first constraint comes from our restriction to phases built out of bosons, while the second constraint comes from the fact that SPT phases do not support quasiparticles with nontrivial statistics. The last constraint comes from the fact that SPT phases have vanishing chiral central charge.

We now discuss two important examples of bosonic SPT edge theories. The first example is:

$$K = \begin{pmatrix} 0 & 1 \\ 1 & 0 \end{pmatrix}, \; W = \begin{pmatrix} 1 & 0 \\ 0 & 1 \end{pmatrix}, \; \chi = \begin{pmatrix} 1 \\ 0 \end{pmatrix} \tag{3.11}$$

The corresponding $\mathbb{Z}_2$ symmetry transformation is given by

$$S^{-1}e^{i\Theta_1}S = -e^{i\Theta_1} \tag{3.12}$$

$$S^{-1}e^{i\Theta_2}S = e^{i\Theta_2} \tag{3.13}$$

From a topological standpoint, the most important feature of this edge theory is that it can be gapped without breaking the $\mathbb{Z}_2$ symmetry. Indeed, the perturbation $U\cos(\Theta_2)$ does the job, according to the null vector conditions described in the previous section. Therefore this edge theory can be identified as the boundary of a *trivial* $\mathbb{Z}_2$ SPT phase.[43]

Another important example of a bosonic SPT edge theory is given by:

$$K = \begin{pmatrix} 0 & 1 \\ 1 & 0 \end{pmatrix},\ W = \begin{pmatrix} 1 & 0 \\ 0 & 1 \end{pmatrix},\ \chi = \begin{pmatrix} 1 \\ 1 \end{pmatrix} \tag{3.14}$$

The corresponding $\mathbb{Z}_2$ symmetry transformation is:

$$S^{-1}e^{i\Theta_1}S = -e^{i\Theta_1} \tag{3.15}$$

$$S^{-1}e^{i\Theta_2}S = -e^{i\Theta_2} \tag{3.16}$$

In contrast to the first example, it is known that this edge theory cannot be gapped without breaking the $\mathbb{Z}_2$ symmetry. Thus, it can be identified as the edge theory of the *nontrivial* $\mathbb{Z}_2$ SPT phase.[43, 50]

3.1.4 Motivating example

In this section we discuss a third example of a bosonic $\mathbb{Z}_2$ SPT edge theory which demonstrates some of the challenges in determining whether or not such edge theories can be

gapped. This example is given by

$$K = \begin{pmatrix} 0 & 1 \\ 1 & 0 \end{pmatrix}, \; W = \begin{pmatrix} 0 & 1 \\ 1 & 0 \end{pmatrix}, \; \chi = \begin{pmatrix} 0 \\ 0 \end{pmatrix} \tag{3.17}$$

This data corresponds to a symmetry transformation that *exchanges* the two electron operators, $e^{i\Theta_1}, e^{i\Theta_2}$:

$$S^{-1} e^{i\Theta_1} S = e^{i\Theta_2} \tag{3.18}$$

$$S^{-1} e^{i\Theta_2} S = e^{i\Theta_1} \tag{3.19}$$

We ask: can this edge theory be gapped without breaking the $\mathbb{Z}_2$ symmetry? Equivalently, is this edge theory the boundary of a trivial or non-trivial SPT phase?

The most straightforward way to investigate this question is to search for null-vector perturbations (4.49) that can gap the edge theory (3.17) without breaking the symmetry. Because $N = 2$, we need a single null vector, which we denote by $\Lambda^T = (a, b)$. To be null, Λ must satisfy the following equation

$$\begin{pmatrix} a & b \end{pmatrix} \begin{pmatrix} 0 & 1 \\ 1 & 0 \end{pmatrix} \begin{pmatrix} a \\ b \end{pmatrix} = 2ab = 0 \tag{3.20}$$

Hence, the only way Λ can be a null vector is if $a = 0$ or $b = 0$. However the corresponding perturbation (4.49) for $a = 0$ ($\cos[b\Theta_2]$) or $b = 0$ ($\cos[a\Theta_1]$) clearly break the $\mathbb{Z}_2$ symmetry, since this symmetry exchanges $e^{i\Theta_1}$ and $e^{i\Theta_2}$. We conclude that there is no way to (symmetrically) gap the above edge theory using null-vector perturbations of the form (4.49).

Given that the null-vector perturbations are not capable of gapping (3.17), one might wonder if this edge theory is actually the boundary of the *non-trivial* SPT phase. If that is the case, then one should be able to find a perturbation that gaps the composite edge theory

obtained by taking the direct sum of (3.17) and the nontrivial SPT edge theory (3.14). [2] This composite edge theory is given by

$$K = \begin{pmatrix} 0 & 1 & 0 & 0 \\ 1 & 0 & 0 & 0 \\ 0 & 0 & 0 & 1 \\ 0 & 0 & 1 & 0 \end{pmatrix}, \; W = \begin{pmatrix} 0 & 1 & 0 & 0 \\ 1 & 0 & 0 & 0 \\ 0 & 0 & 1 & 0 \\ 0 & 0 & 0 & 1 \end{pmatrix}, \; \chi = \begin{pmatrix} 0 \\ 0 \\ 1 \\ 1 \end{pmatrix}$$

However, following the same arguments as in Eq. (3.20), one can again show that there is no choice of null vectors which gives a symmetric perturbation.

We conclude that the standard null-vector analysis does not provide a definitive answer as to whether the edge theory (3.17) corresponds to a trivial or nontrivial $\mathbb{Z}_2$ SPT phase. This example shows that it is not always easy to determine whether bosonic $\mathbb{Z}_2$ SPT edge theories are trivial or nontrivial (i.e. gappable or non-gappable), even in simple cases. This motivates a more general and systematic analysis of bosonic $\mathbb{Z}_2$ SPT edge theories, which we will present below. As part of this general analysis, we will resolve the question of the above edge theory: we show that it is in fact trivial and can be gapped using a more complicated perturbation (see section 3.3.3).

3.2 Main results and applications

The example from the previous section raises the following question: given a general bosonic SPT edge theory with a $\mathbb{Z}_2$ symmetry, how can one determine if it can be gapped or not? Equivalently, how can one determine if it is the boundary of the trivial or non-trivial SPT phase? In this section, we present a simple algebraic criterion that answers this question. We begin by introducing an important auxiliary quantity, which we denote by χ_+.

2. Here we use the fact that $\mathbb{Z}_2$ bosonic SPT phases have a $\mathbb{Z}_2$ group structure, so the direct sum of two nontrivial SPT edge theories is always trivial.

3.2.1 The auxiliary vector χ_+

In this section we define an additional quantity χ_+ for describing bosonic SPT edge theories with $\mathbb{Z}_2$ symmetry. This quantity is completely determined by the standard data for these edge theories, (K, W, χ), and therefore carries no additional information. However, it is still useful for our purposes, as we will see below.

Formally, we define χ_+ as any N component vector that satisfies the following conditions

$$\begin{aligned} W^T \chi_+ &= \chi_+, \\ S^{-1} e^{i\Lambda_+^T \Theta} S &= e^{i\Lambda_+^T \Theta} \cdot e^{i\pi \Lambda_+^T \chi_+}, \end{aligned} \tag{3.21}$$

where the second equality holds for all integer vectors Λ_+ with $W\Lambda_+ = \Lambda_+$. The physical meaning of χ_+ is similar to χ in that it describes the extra phases that are acquired by the electron operators under the $\mathbb{Z}_2$ symmetry S. The main difference is that χ_+ only describes the symmetry transformation properties of a *subset* of electron operators, namely those that are transformed into themselves multiplied by a phase.

A few comments about χ_+: first, we should mention that there is generally more than one choice of χ_+ obeying the conditions (3.21). That said, different choices of χ_+ should be regarded as physically equivalent and in particular we will see that our criterion does not depend on the choice of χ_+.

We should also point out that not all values of χ_+ are physically possible. More specifically, using the fact that $S^2 = 1$, one can show that χ_+ always obeys the relation

$$2\chi_+ = \mathrm{diag}(KW) \pmod 2 \tag{3.22}$$

Finally, we would like to mention an *explicit* formula for χ_+. To use this formula, one first has to perform a change of basis so that (K, W, χ) are in a particular form. In particular, as we show in appendix B.3, it is always possible to put K, W, χ into the following standard

form:

$$W = \begin{pmatrix} -\mathbf{1_m} & 0 & 0 & 0 \\ 0 & \mathbf{1_{n_+ - n_- + m}} & 0 & 0 \\ 0 & 0 & 0 & \mathbf{1_{n_- - m}} \\ 0 & 0 & \mathbf{1_{n_- - m}} & 0 \end{pmatrix}, \tag{3.23}$$

$$K = \begin{pmatrix} A & 0 & B & -B \\ 0 & C & D & D \\ B^T & D^T & E & F \\ -B^T & D^T & F & E \end{pmatrix}, \tag{3.24}$$

and

$$\chi = \begin{pmatrix} 0_m \\ \chi_2 \\ 0_{n_- - m} \\ 0_{n_- - m} \end{pmatrix} \tag{3.25}$$

Here, in the first equation, $\mathbf{1_m}$ denotes an $m \times m$ identity matrix, and m, n_+, n_- are non-negative integers satisfying $n_+ + n_- = N$ and $m \leq n_-$. In the second equation, A, C, E are integer square matrices with the same dimensions as the diagonal blocks of W. Finally, in the third equation, 0_m denotes a column vector with m zeros, while χ_2 is a column vector with $n_+ - n_- + m$ components.

Once K, W and χ are in the above standard form, the vector χ_+ is given by:

$$\chi_+ = \begin{pmatrix} 0_m \\ \chi_2 \\ \mathrm{diag}(F)/2 \\ \mathrm{diag}(F)/2 \end{pmatrix} \pmod 2 \tag{3.26}$$

This formula can be derived straightforwardly by solving Eqs. (3.21).

3.2.2 General criterion

With this background, we can now state our criterion: a $\mathbb{Z}_2$ bosonic SPT edge theory (K, W, χ_+) can be gapped if and only if

$$\nu = 0 \pmod 2 \tag{3.27}$$

where ν is defined by

$$\nu = \frac{1}{2}\chi_+^T K^{-1}\chi_+ + \frac{1}{4}\text{sig}((1-W^T)K(1-W)) \tag{3.28}$$

and 'sig' stands for signature.[3]

While it may not be obvious from the above formula, it is possible to show that ν is always an integer for any consistent edge theory (see appendix B.4). This means that ν can only take the values 0 or 1 (mod 2), with the two cases corresponding to a trivial or non-trivial bulk SPT phase, respectively. For this reason, we will refer to ν (mod 2) as the $\mathbb{Z}_2$ *index* of the edge theory (K, W, χ_+).

This $\mathbb{Z}_2$ index has several important properties:

1. ν (mod 2) does not depend on the choice of χ_+. This result is important because it means that the $\mathbb{Z}_2$ index is *unambiguous*.

2. ν is additive under 'stacking' of edge theories. That is, consider two theories $\{K_a, W_a, (\chi_+)_a\}$ and $\{K_b, W_b, (\chi_+)_b\}$, and let $\{K_{a+b}, W_{a+b}, (\chi_+)_{a+b}\}$ denote their direct sum. Then, the corresponding $\mathbb{Z}_2$ indices are related by $\nu_{a+b} = \nu_a + \nu_b$. This result is to be expected since the $\mathbb{Z}_2$ index of the bulk SPT phases is also additive under stacking.

3. The matrix $(1-W^T)K(1-W)$ also has vanishing eigenvalues, but we define the signature by considering only the eigenvalues that are strictly positive and strictly negative.

3.2.3 Examples

The edge theory (3.17)

We start by analyzing the edge theory (3.17) from section 3.1.4. The first step is to compute χ_+ for this example. Comparing the form of (K, W, χ) to Eqs. (3.23-3.25), we see that $m = 0$, $n_+ = n_-$ and $F = 1$. Therefore, by Eq. 3.26,

$$\chi_+ = \begin{pmatrix} 1/2 \\ 1/2 \end{pmatrix} \tag{3.29}$$

Now computing ν we find

$$\nu = \frac{1}{2} \begin{pmatrix} 1/2 & 1/2 \end{pmatrix} \begin{pmatrix} 0 & 1 \\ 1 & 0 \end{pmatrix} \begin{pmatrix} 1/2 \\ 1/2 \end{pmatrix} + \frac{1}{4} \text{sig} \begin{pmatrix} -2 & 2 \\ 2 & -2 \end{pmatrix} \tag{3.30}$$

$$= \frac{1}{4} + \frac{1}{4}(-1) = 0 \tag{3.31}$$

Hence, according to our criterion, this edge theory can be gapped.

For completeness, we now show how to compute χ_+ directly from Eqs. 3.21, instead of Eq. 3.26. The first step is to choose $\Lambda_+^T = (1, 1)$ as a vector satisfying $W\Lambda_+ = \Lambda_+$. Next, we examine the symmetry transformation properties of the operator

$$e^{i\Lambda_+^T \Theta} = e^{i(\Theta_1 + \Theta_2)} \tag{3.32}$$

To this end, it is useful to decompose this operator into a product of $e^{i\Theta_1}$ and $e^{i\Theta_2}$. Recall that, for two operators X and Y such that $[X, Y]$ is a scalar, we have the following relation

$$e^{X+Y} = e^X e^Y e^{-\frac{1}{2}[X,Y]} \tag{3.33}$$

In our case, the relevant commutator involves two fields located at the *same* position, and

is given by

$$[\Theta_i(x), \Theta_j(x)] = i\pi K_{ij}\text{sign}(i-j) \tag{3.34}$$

Thus, we have

$$e^{i(\Theta_1+\Theta_2)} = e^{i\Theta_2}e^{i\Theta_1}e^{\frac{1}{2}i\pi} = e^{i\Theta_1}e^{i\Theta_2}e^{-\frac{1}{2}i\pi} \tag{3.35}$$

With these identities, we can easily compute the symmetry transformation properties of (3.32):

$$\begin{aligned} S^{-1}e^{i(\Theta_1+\Theta_2)}S &= S^{-1}e^{i\Theta_2}e^{i\Theta_1}S \cdot e^{\frac{1}{2}i\pi} \\ &= e^{i\Theta_1}e^{i\Theta_2} \cdot e^{\frac{1}{2}i\pi} \\ &= -e^{i(\Theta_1+\Theta_2)} \end{aligned} \tag{3.36}$$

Comparing with Eq. (3.21), we deduce that $\Lambda_+^T\chi_+ = 1 \pmod 2$. At the same time, the condition $W^T\chi_+ = \chi_+$ implies that χ_+ must be of the form $\chi_+^T = (a, a)$. We conclude that $\chi_+^T = (1/2, 1/2)$ in agreement with Eq. (3.29).

Theories without permutation: $W = \mathbb{1}$

We now examine the invariant in the case that $W = \mathbb{1}$, the identity matrix. This corresponds to the case where there is no permutation of the fields, and only a shift. For the W matrix in Eq. 3.23, this corresponds to the case where $m = n_- = 0$ and thus $n_+ = N$. The form of the invariant simplifies considerably in this case:

$$\nu = \chi^T K^{-1}\chi \tag{3.37}$$

(Here, the reason we have used χ instead of χ_+ in the above equation is because $\chi = \chi_+$ when $W = \mathbb{1}$).

3.3 Derivation of results

3.3.1 A few simplifications

In order to establish our criterion, we need to prove two claims:

1. If $\nu = 0 \pmod 2$, the edge theory (K, W, χ_+) can be gapped.

2. If $\nu = 1 \pmod 2$, the edge theory (K, W, χ_+) cannot be gapped.

Actually, we will now argue that it is enough to just prove claim (1): to see this, consider the composite edge theory obtained by taking a direct sum of (K, W, χ_+) and the nontrivial SPT edge theory (3.14). If (K, W, χ_+) has $\nu = 1 \pmod 2$, then this composite edge theory has $\nu = 0 \pmod 2$ since ν is additive under stacking and the edge (3.14) has $\nu = 1$. Hence, claim (1) implies that the composite edge theory can be gapped, which in turn implies that the edge theory (K, W, χ_+) cannot be gapped.

In fact, it suffices to prove claim (1) in the special case $\nu_- = 0$ where $\nu_\pm$ are defined by

$$\begin{aligned}\nu_+ &= \frac{1}{2}\chi_+^T K^{-1}\chi_+ \\ \nu_- &= \frac{1}{4}\mathrm{sig}((1-W)K(1-W^T))\end{aligned}$$

One way to see this is to recall the edge theory (3.17). This is the edge theory of a trivial $\mathbb{Z}_2$ SPT, as we prove in section 3.3.3. At the same time, the calculation in section 3.2.3 shows that this theory has $\nu_+ = \frac{1}{4}$ and $\nu_- = -\frac{1}{4}$. Thus, if (K, W, χ_+) is an edge theory with $\nu_- = \frac{n}{4}$, for some positive integer n, then we can take the direct sum of (K, W, χ_+) with n copies of (3.17), in order to make ν_- of the combined theory equal to zero. This 'stacking' will not affect whether the edge can be gapped since (3.17) is the edge theory of a trivial $\mathbb{Z}_2$ SPT.

3.3.2 Derivation

In view of the above simplifications, we only need to show that the edge theories with ν even and $\nu_- = 0$ can be gapped. Our strategy for proving this will be to establish the existence of a set of linearly independent integer vectors $\{\Lambda_+^{(1)}, ..., \Lambda_+^{(n_+/2)}, \Lambda_-^{(1)}, ..., \Lambda_-^{(n_-/2)}\}$ with three properties:

1. The vectors are mutually null: $(\Lambda_\pm^{(j)})^T K \Lambda_\pm^{(k)} = 0$ for all j, k.
2. The vectors are even/odd under W: $W\Lambda_\pm^{(j)} = \pm\Lambda_\pm^{(j)}$.
3. $(\Lambda_+^{(j)})^T \chi_+ = 0 \pmod 2$ for all j.

Using the above null vectors, we will construct a perturbation (4.49) that gaps the edge without breaking the $\mathbb{Z}_2$ symmetry. Here n_+ and n_- denote the dimensions of the $+1$ and -1 eigenspaces of W.

Even and odd subspaces: $K_\pm$

To simplify the problem of finding the null vectors $\Lambda_\pm^{(i)}$, we now define two matrices $K_\pm$ that describe the action of K within the $+1$ and -1 eigenspaces of W. First let

$$\Xi_\pm = \{\Lambda_\pm : \ W\Lambda_\pm = \pm\Lambda_\pm, \ \Lambda_\pm \in \mathbb{Z}^N\} \tag{3.38}$$

These sets form integer lattices of dimension n_+ and n_-. Thus they can be represented as $\Xi_\pm = V_\pm \mathbb{Z}^{n_\pm}$ where $V_\pm$ are $N \times n_\pm$ integer matrices. We then define the matrices $K_\pm$ as

$$K_\pm = V_\pm^T K V_\pm \tag{3.39}$$

Notice that $K_\pm$ are $n_\pm \times n_\pm$ matrices — precisely the dimension of the $+1$ and -1 eigenspaces of W.

The reason that the matrices $K_\pm$ are useful is that there is a one-to-one correspondence between their null vectors, which we denote by $\bar{\Lambda}_\pm$, and the even/odd null vectors of K, which we denote by $\Lambda_\pm$. This correspondence is given by

$$\Lambda_\pm = V_\pm \bar{\Lambda}_\pm \tag{3.40}$$

Given this correspondence, our task reduces to finding null vectors of $K_\pm$.

Proving $K_\pm$ have a complete set of null vectors

In this section, we show that K_+ and K_- both have a complete set of primitive null vectors $\{\bar{\Lambda}_\pm^{(1)}, ..., \bar{\Lambda}_\pm^{(n_\pm/2)}\}$. To establish this, it suffices to prove two claims: (1) $\mathrm{sig}(K_\pm) = 0$, and (2) the Abelian topological phases corresponding to the K-matrices $K_\pm$ have Lagrangian subgroups. Indeed, Ref. [42] showed that these two properties guarantee the existence of the required null vectors.

To see that $\mathrm{sig}(K_\pm) = 0$, observe that

$$\mathrm{sig}(K_-) = \nu_-, \quad \mathrm{sig}(K_+) = \mathrm{sig}(K) - \nu_- \tag{3.41}$$

The claim then follows from our assumption that $\nu_- = 0$, together with the fact that $\mathrm{sig}(K) = 0$ for any SPT edge.

Proving that the topological phases corresponding to $K_\pm$ have Lagrangian subgroups requires a bit more work. We accomplish this using a lemma, proven in Appendix B.2, which states that if a bosonic Abelian topological phase has vanishing chiral central charge and satisfies $a^2 = 1$ for all anyons a then it has a Lagrangian subgroup. To apply this lemma, we need to show that $a^2 = 1$ for all anyons a. This will follow if we can show that $2K_\pm^{-1}$ are integer matrices.

We now prove this claim for K_+ — the proof for K_- is similar. Let x be an n_+ component vector such that $K_+ x$ is an integer vector. Then $\Lambda_+^T K V_+ x$ is an integer for every $\Lambda_+ \in \Xi_+$.

At the same time, it is clear that $\Lambda_-^T K V_+ x = 0$ for every $\Lambda_- \in \Xi_-$ since $V_+ x$ is even under W, while Λ_- is odd under W. Noting that every integer vector y can be written as a linear combination $y = \frac{1}{2}(\Lambda_+ + \Lambda_-)$ with $\Lambda_\pm \in \Xi_\pm$, we deduce that $2y^T K V_+ x$ is always an integer for every integer vector y. It then follows that $2V_+ x$ is an integer vector since $\det K = \pm 1$. Hence $2x$ must be an integer vector (since $2V_+ x$ is clearly an element of Ξ_+). Thus, we have shown that if $K_+ x$ is an integer vector then $2x$ is an integer vector. The claim follows immediately.

Symmetric null vectors for K

So far we have shown that $K_\pm$ each have a complete set of primitive null vectors $\{\bar{\Lambda}_\pm^{(1)}, ..., \bar{\Lambda}_\pm^{(n_\pm/2)}\}$. As in Eq. 3.40, if we apply $V_\pm$ to these vectors, we can convert these to null vectors for K: $\{\Lambda_+^{(1)}, ..., \Lambda_+^{(n_+/2)}, \Lambda_-^{(1)}, ..., \Lambda_-^{(n_-/2)}\}$. The latter vectors automatically obey the first two properties listed in the beginning of section 3.3.2; the goal of this section is to show that they obey the third property — that is $(\Lambda_+^{(j)})^T \chi_+ = 0 \pmod 2$.

To this end, we show that we can always choose the $\bar{\Lambda}_+^{(j)}$ vectors so that

$$(\bar{\Lambda}_+^{(j)})^T \bar{\chi}_+ = 0 \pmod 2 \tag{3.42}$$

where $\bar{\chi}_+ = V_+^T \chi_+$. Then the property $(\Lambda_+^{(j)})^T \chi_+ = 0 \pmod 2$ follows immediately.

We establish Eq. (3.42) using the following lemma:

Lemma 1. *Suppose (K, W, χ) is a chiral boson edge theory with $\mathbb{Z}_2$ symmetry where K is an $n \times n$ bosonic K-matrix, $W = 1$ and χ is an n component integer vector. Furthermore, suppose we have stacked the system with a trivial SPT so that K and χ can be written in the form*

$$K = \tilde{K} \oplus \begin{pmatrix} 0 & 1 \\ 1 & 0 \end{pmatrix}, \quad \chi = \tilde{\chi} \oplus \begin{pmatrix} 1 \\ 0 \end{pmatrix} \tag{3.43}$$

If (i) K has $n/2$ linearly independent, primitive null vectors $\Lambda_1, ..., \Lambda_{n/2}$ and (ii) $\frac{1}{2}\chi^T K^{-1} \chi =$

0 (mod 2), *then there exist another set of* $n/2$ *linearly independent, primitive null vectors* $\Lambda'_1, ..., \Lambda'_{n/2}$ *with* $(\Lambda'_i)^T \chi = 0 \pmod 2$.

Proof. To begin, let $m = \frac{1}{4}\tilde{\chi}^T \tilde{K}^{-1} \tilde{\chi}$. By assumption m is an integer. Next, define w to be the following n component integer vector:

$$w = \det \tilde{K} \cdot \begin{pmatrix} \tilde{K}^{-1}\tilde{\chi} \\ -2m \\ 1 \end{pmatrix} \tag{3.44}$$

The vector w has two important properties. First, w obeys $w^T K w = 0$. Second, w has the property that

$$Kw = \det \tilde{K} \cdot \left[\chi - \begin{pmatrix} 0 \\ \vdots \\ 0 \\ 2m \end{pmatrix} \right] \tag{3.45}$$

The latter property means that if Λ is an integer vector with $\Lambda^T K w = 0$, then we will automatically have

$$\Lambda^T \chi = 0 \pmod 2 \tag{3.46}$$

This is very useful since ultimately we want to find null vectors satisfying Eq. (3.46).

The next step is to use the fact that K has $n/2$ linearly independent, primitive null vectors $\Lambda_1, ..., \Lambda_{n/2}$. Let $\mathcal{V}$ be the real-linear subspace defined by

$$\mathcal{V} = \{v : \ v = \sum_i a_i \Lambda_i + aw, \ v^T K w = 0\} \tag{3.47}$$

It is easy to see that $\mathcal{V}$ is at least $n/2$ dimensional. To see this, note that either w is linearly independent from $\Lambda_1, ..., \Lambda_{n/2}$ or it is linearly dependent. In the former case, $\mathcal{V}$ has $n/2 + 1$

generators and 1 constraint, while in the latter case, it has $n/2$ generators and no constraint since in this case $v^T K w$ follows from the null property of the Λ_i's. Thus, in either case $\mathcal{V}$ has dimension $n/2$.

Given that $\mathcal{V}$ is defined by integer constraints ($v^T K w = 0$) and integer generators (Λ_i, w), and given that it is $n/2$ dimensional, it follows that $\mathcal{V} \cap \mathbb{Z}^n$ is an $n/2$ dimensional integer lattice. Let $\Lambda'_1, ..., \Lambda'_{n/2}$ be generators of this lattice. By construction these vectors are linearly independent and primitive, and have the null property $(\Lambda'_i)^T K \Lambda'_j = 0$. Furthermore, $(\Lambda'_i)^T K w = 0$ so Λ'_i obeys Eq. (3.46).

□

This lemma applies directly in our case if we use $K = K_+$, $\chi = \bar{\chi}_+$ and $n = n_+$. Indeed,

$$\frac{1}{2}\bar{\chi}_+^T K_+^{-1} \bar{\chi}_+ = \frac{1}{2}\chi_+^T K^{-1} \chi_+ = 0 \pmod 2 \tag{3.48}$$

where the last equality follows from our assumption that $\nu = 0 \pmod 2$ and $\nu_- = 0$.

Primitivity

At this point, we have constructed $N/2$ linearly independent null vectors of K, denoted $\{\Lambda_+^{(1)}, ..., \Lambda_+^{(n_+/2)}, \Lambda_-^{(1)}, ..., \Lambda_-^{(n_-/2)}\}$ satisfying the following properties:

1. $W^T \Lambda_\pm^{(i)} = \pm \Lambda_\pm^{(i)}$
2. $\chi_+^T \Lambda_+^{(i)} = 0 \pmod 2$
3. The subsets of even and odd vectors, namely $\{\Lambda_+^{(i)}\}$ and $\{\Lambda_-^{(i)}\}$, are both primitive.

In this section, we use these null vectors to construct a perturbation of the form

$$\sum_{i=1}^{N/2} U \cos(M_i^T K \Phi - \alpha_i) \tag{3.49}$$

which gaps the edge but does not break the $\mathbb{Z}_2$ symmetry explicitly or spontaneously.

Naively one might think that we could simply set $\{M_i\} = \{\Lambda_\pm^{(i)}\}$ and the resulting perturbation (3.49) would do the job. Indeed, this perturbation is manifestly symmetric (for appropriate choice of α_i) and furthermore it gaps the edge for sufficiently large U. The problem is that, while the subsets $\{\Lambda_+^{(i)}\}$ and $\{\Lambda_-^{(i)}\}$ are both primitive, the complete set of vectors, $\{\Lambda_\pm^{(i)}\}$ is not necessarily primitive. As a result, the ground state of the gapped edge may have some degeneracy and therefore we cannot rule out the possibility that the perturbation breaks the symmetry *spontaneously*. To rule out this possibility we now show how to construct a closely related perturbation of the form (3.49) where $\{M_1, ..., M_{N/2}\}$ is primitive.

The first step is to consider the real subspace spanned by $\{\Lambda_\pm^{(i)}\}$. Let Υ be the set of all integer vectors that belong to this subspace. Clearly Υ is an $N/2$ dimensional lattice. Furthermore, Υ is invariant under W since $W\Lambda_\pm^{(i)} = \pm\Lambda_\pm^{(i)}$. Therefore, if we pick a basis for Υ, then the action of W on the basis vectors defines an $(N/2) \times (N/2)$ integer matrix that squares to the identity. Now, in appendix B.3 we show that any integer matrix that squares to the identity can be put in the simple canonical form B.58. Applying this argument to W, it follows that we can find another basis for Υ, denoted $\{M_1, ..., M_{N/2}\}$ such that the action of W on the M_i's takes the form

$$\begin{aligned} WM_{2i-1} = M_{2i}, \quad WM_{2i} = M_{2i-1}, \quad 1 \le i \le q \\ WM_i = -M_i, \quad 2q+1 \le i \le 2q+r \\ WM_i = M_i, \quad 2q+r+1 \le i \le N/2 \end{aligned} \tag{3.50}$$

for some non-negative integers q, r with $2q + r \le N/2$. We can now write down the desired

perturbation:

$$\sum_{i=1}^{q}\Big[U\cos(M_{2i-1}^{T}K\Phi)+U\cos(M_{2i}^{T}K\Phi-\alpha_{2i})\Big] \\ +\sum_{i=2q+1}^{2q+r}U\cos(M_{i}^{T}K\Phi-\alpha_{i})+\sum_{i=2q+r+1}^{N/2}U\cos(M_{i}^{T}K\Phi) \tag{3.51}$$

Here the α_{2i} phases in the first term are fixed by requiring that

$$e^{iM_{2i-1}^{T}K\Phi}\to e^{iM_{2i}^{T}K\Phi}\cdot e^{-i\alpha_{2i}},\quad 1\le i\le q \tag{3.52}$$

under the $\mathbb{Z}_2$ symmetry. Likewise, the α_i phases in the second term are fixed by requiring that

$$e^{iM_{i}^{T}K\Phi}\to e^{-iM_{i}^{T}K\Phi}\cdot e^{2i\alpha_{i}},\quad 2q+1\le i\le 2q+r \tag{3.53}$$

Let us explain why the above perturbation (3.51) has the required properties: that is, (a) it gaps the edge for sufficiently large U; (b) it does not break the Z_2 symmetry explicitly; and (c) it does not break the symmetry spontaneously. To see that it gaps the edge, note that the M_i's obey $M_i^TKM_j=0$ since they are linear combinations of the $\Lambda_{\pm}^{(i)}$'s. To see that the perturbation does not break the Z_2 symmetry explicitly, note that the first two terms of (3.51) are manifestly invariant under under the $\mathbb{Z}_2$ symmetry, so we only have to worry about the last term, $\sum_{i=2q+r+1}^{N/2}U\cos(M_i^TK\Phi)$. To analyze the symmetry transformation properties of this term, note that $WM_i=M_i$ in this case so this term transforms as

$$e^{iM_{i}^{T}K\Phi}\to e^{iM_{i}^{T}K\Phi}\cdot e^{i\pi M_{i}^{T}\chi_{+}},\quad 2q+r+1\le i\le N/2 \tag{3.54}$$

Thus, the crucial question is to determine the parity of $M_i^T\chi_+$. To this end, note that each of the above M_i's can be written as a linear combination, $M_i=\sum_j a_{ij}\Lambda_+^{(j)}$ since $W^TM_i=M_i$.

Furthermore, the expansion coefficients, a_{ij}, are all integers since the set $\{\Lambda_+^{(i)}\}$ is primitive. Therefore, since $(\Lambda_+^{(i)})^T\chi_+$ is even (property 2 above), we conclude that $M_i^T\chi_+$ is also even. Hence, the term $\sum_{i=2q+r+1}^{N/2} U\cos(M_i^T K\Phi)$ is even under the Z_2 symmetry, as required.

All that remains is to show that the above perturbation (3.51) does not break the Z_2 symmetry spontaneously. This follows from the fact that the set $\{M_1, ..., M_{N/2}\}$ is primitive, which in turn follows from the fact that these vectors span the lattice Υ.

3.3.3 Proving $K = W = \sigma^x$ is gapped

In this section we prove that the theory described by $K = W = \sigma^x$ can be gapped without breaking the $\mathbb{Z}_2$ symmetry. The reason for this is actually quite simple to understand, and follows from the fact that the theory has a hidden $SU(2)_L \times SU(2)_R$ symmetry. This symmetry group contains an element U such that

$$U : \cos(\Theta_1) \to \frac{1}{\sqrt{2}}(\cos(\Theta_1) + \cos(\Theta_2)) \tag{3.55}$$

Because the theory with the perturbation $\cos(\Theta_1)$ is gapped, it follows from the symmetry of the spectrum that the perturbation $\frac{1}{\sqrt{2}}(\cos(\Theta_1) + \cos(\Theta_2))$ will also open up a gap. Furthermore, because the latter operator is invariant under the $\mathbb{Z}_2$ symmetry, it follows that this theory has a gapped, symmetric edge.

The origin of this symmetry is due to the fact that the three operators

$$\begin{aligned} J^x &= \cos(\Theta_1 + \Theta_2) \\ J^y &= \sin(\Theta_1 + \Theta_2) \\ J^z &= \frac{i}{2}\partial_x(\Theta_1 + \Theta_2) \end{aligned} \tag{3.56}$$

form a level-1 SU(2) current algebra.[14] Furthermore, the vector

$$b = \begin{pmatrix} e^{i\Theta_1} \\ e^{i\Theta_2} \end{pmatrix} \tag{3.57}$$

transforms as a doublet under this symmetry. From this it follows that there exists an operator U such that $e^{i\Theta_1} \to \frac{1}{\sqrt{2}}(e^{i\Theta_1} + e^{i\Theta_2})$. Because this matrix is real, taking the complex conjugate gives you the transformation $e^{-i\Theta_1} \to \frac{1}{\sqrt{2}}(e^{-i\Theta_1} + e^{-i\Theta_2})$. Together, these transformations produce the transformation given in Eq. 3.55. We prove the existence of this $\mathrm{SU}(2)_R$ symmetry and the transformation law of b in Appendix B.1.

3.4 Abelian $\mathbb{Z}_2$ SETs

In this section we discuss the extension of our results to bosonic, Abelian $\mathbb{Z}_2$ SETs. The main difference from the SPT case is that we no longer assume $|\det K| = 1$. Also, we will now work with an *equivalence class* $[\chi_+]$ of vectors satisfying Eqs. 3.21. Two vectors χ_+ and χ'_+ are equivalent if

$$\Lambda^T \chi'_+ = \Lambda^T \chi_+ \pmod 2 \tag{3.58}$$

for every integer Λ_+ with $W\Lambda_+ = \Lambda_+$.

The main result of this section, then, is that an Abelian $\mathbb{Z}_2$ SET parametrized by $\{K, W, [\chi_+]\}$ can have a gapped, symmetric boundary if the following criteria are satisfied:

1. $\mathrm{sig}(K) = 0$.

2. K has a Lagrangian subgroup invariant under S.

3. $0 \in \mathcal{S}$, where

$$\mathcal{S} = \{\nu(\chi_+) : \chi_+ \in [\chi_+]\} \tag{3.59}$$

and $\nu(\chi_+)$ is defined as

$$\nu(\chi_+) = \frac{1}{2}\chi_+^T K^{-1}\chi_+ + \frac{1}{4}\text{sig}((1-W^T)K(1-W)) \tag{3.60}$$

We now prove that these criteria are sufficient for having a gapped boundary. The proof that they are necessary will be included in a future publication.

3.4.1 Proof of sufficiency

The proof that these criteria are sufficient for a gapped edge is very similar to the proof in the SPT case. In particular, we show that when $\nu^{\text{set}} = 0$, we can find null vectors that gap the boundary explicitly. We break up the proof into two parts by defining $\nu^{\text{set}}(\chi_+) = \nu_+^{\text{set}}(\chi_+) + \nu_-^{\text{set}} \mod 2$ with

$$\nu_+^{\text{set}}(\chi_+) = \frac{1}{2}\chi_+^T K^{-1}\chi_+ \tag{3.61}$$

$$\nu_-^{\text{set}} = \frac{1}{4}\text{sig}((1-W^T)K(1-W)) \tag{3.62}$$

and we first prove the claim when $\nu_-^{\text{set}} = 0$. In particular, when $\nu_-^{\text{set}} = 0$ and there exists a $\chi_+ \in [\chi_+]$ such that $\nu^{\text{set}}(\chi_+)$ is even, then we prove that there exists a set of linearly independent vectors $\{\Lambda_+^{(1)}, ..., \Lambda_+^{(n_+/2)}, \Lambda_-^{(1)}, ..., \Lambda_-^{(n_-/2)}\}$ with three properties:

1. The vectors are mutually null: $(\Lambda_\pm^{(j)})^T K \Lambda_\pm^{(k)} = 0$ for all j, k.
2. $W\Lambda_\pm^{(j)} = \pm\Lambda_\pm^{(j)}$.
3. $(\Lambda_+^{(j)})^T \chi_+ = 0 \pmod 2$.

Following the proof in the SPT case, we first break up the problem of finding null vectors into finding null vectors for the even and odd subspaces. Conveniently, we can define the matrices $K_\pm$ exactly as we did in 3.3.2, with no change from the SPT case.

The next step in the proof is to show that these matrices $K_\pm$ have Lagrangian subgroups. It requires additional work to prove this in the SET case since $|\det(K)| \geq 1$, so the proof in section 3.3.2 cannot be applied directly. Nevertheless, the fact that $K_\pm$ have Lagrangian subgroups still holds in the SET case and we provide a proof of this in Appendix B.5.

From here, the argument that there exist $N/2$ symmetric null vectors when $\nu_+^{\text{set}} = 0 \mod 2$ given in section 3.3.2 still holds in the SET case. It then follows that we can gap the edge when $\nu_-^{\text{set}} = 0$ and $\nu_+^{\text{set}} = 0 \mod 2$. To generalize to the $\nu_-^{\text{set}} \neq 0$ we can use the same trick that was used in section 3.3.3 to stack with trivial systems and reduce to the $\nu_-^{\text{set}} = 0$ case.

CHAPTER 4

SOLVABLE MODELS FOR NEUTRAL MODES IN FRACTIONAL QUANTUM HALL EDGES

4.1 Introduction

One of the most important properties of quantum Hall states is that they have gapless edge modes. Every state has at least one such mode, but the structure of these modes varies from state to state. For example, the Laughlin states are believed to have a single chiral edge mode,[65] while integer quantum Hall states have multiple chiral edge modes — one for every filled Landau level.[19]

A particularly interesting edge theory is realized by the $\nu = 2/3$ fractional quantum Hall state. This state is believed to have two *counter-propagating* chiral edge modes — one which looks like the edge mode of a $\nu = 1$ integer quantum Hall state, and one which looks like the edge mode of a $\nu = 1/3$ Laughlin state, but with opposite chirality.[64, 66, 52, 26] This edge theory poses a basic puzzle because it naively predicts charge propagation in both directions along the edge, in disagreement with experiment.[2]

A possible resolution to this problem was put forth by Kane, Fisher and Polchinski.[29] In that work, the authors argued that what is missing from the previous picture is impurity-induced electron scattering between the two edge modes. The authors showed that impurity scattering can drive the edge to a special disorder dominated fixed point where one of the edge modes is electrically *neutral* while the other carries charge; the charge mode propagates in the direction determined by the external magnetic field while the neutral mode propagates in the opposite 'upstream' direction. This mode structure can explain why current flow is only observed in one direction on the 2/3 edge. It is also consistent with experiments on the $\nu = 2/3$ edge which have found evidence for upstream neutral modes,[4] though the picture has been complicated by more recent studies which suggest that the 2/3 edge may have multiple charge modes, perhaps as a result of edge reconstruction.[56] Also, we should

mention that other studies have detected neutral modes in quantum Hall states where they were not expected theoretically.[61, 25]

The main theoretical justification for the neutral mode proposal of Ref. [29] comes from a renormalization group (RG) analysis of the fixed point edge theory which shows that the fixed point has no relevant perturbations. This calculation proves that the fixed point has a finite basin of attraction; as long as the edge lies in this basin of attraction, impurity scattering will drive the system to the fixed point with a neutral mode.

While this analysis is powerful, it leaves some important questions unanswered. In particular, it does not give a microscopic picture for how a neutral mode emerges from impurity scattering. In this chapter, we seek to provide such a picture in the context of concrete models.

The models we consider are built out of two counter-propagating chiral Luttinger liquids together with a collection of discrete impurity scatterers. Our main result is an exact solution of these models in the limit of infinitely strong impurity scattering, which we obtain using a formalism introduced in Ref. [15]. From this solution, we explicitly derive the existence of a neutral mode and we determine all of its microscopic properties including its velocity. Importantly, we also study the stability of the neutral mode and we show that it survives at finite, but sufficiently strong impurity scattering, as long as this scattering has a random spatial dependence.

Our results apply to a particular class of fractional quantum Hall (FQH) edge theories of which the $\nu = 2/3$ edge is a special case. Specifically, the edge theories that we analyze are those described by a K-matrix[66] of the form $K = \begin{pmatrix} k_1 & 0 \\ 0 & -k_2 \end{pmatrix}$ where k_1 is an odd integer and $k_2 = k_1 + 2$.[1] These edge theories correspond to a class of Abelian quantum hall states with filling fraction $\nu = \frac{1}{k_1} - \frac{1}{k_2}$. The $\nu = 2/3$ edge corresponds to the case $k_1 = 1$ and $k_2 = 3$.

1. Much of our analysis applies to general odd k_1, k_2 but our most important conclusions rely on the assumption that $|k_2 - k_1| = 2$, for reasons explained in Appendix C.1.

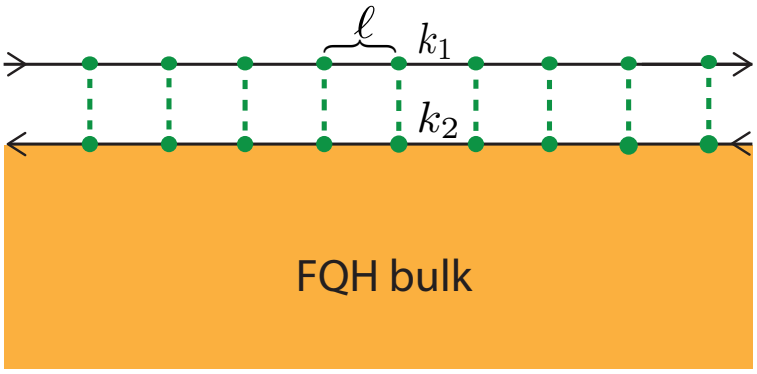

Figure 4.1: Toy model for a FQH edge with impurity scattering: two counter-propagating chiral Luttinger liquids with parameters k_1 and k_2 together with a regular lattice of impurity scatterers with spacing ℓ.

The structure of the paper is as follows. In section 4.2 we present the models that we study and we summarize our main results. In section 4.3 we solve our simplest model — a minimal toy model — in the infinite scattering limit and derive the existence of a neutral mode. In section 4.4 we study the toy model with finite but large impurity scattering and we show that the neutral mode survives in this case. Finally, in section 4.5 we consider more general and realistic models and we show that our main results still hold. We conclude in section 4.6 and mention a few directions for future work.

4.2 Models and main results

As we mentioned previously, we focus our analysis on FQH edge theories that have filling fraction $\nu = \frac{1}{k_1} - \frac{1}{k_2}$ and that are described by a K-matrix of the form $K = \begin{pmatrix} k_1 & 0 \\ 0 & -k_2 \end{pmatrix}$ where k_1 is an odd integer and $k_2 = k_1 + 2$. In the absence of impurity scattering, the edges of these states can be modeled as two counterpropagating chiral Luttinger liquids which look like the edge modes of the $1/k_1$ and $1/k_2$ Laughlin states, but with opposite chiralities.[66] Our goal is to study how impurity scattering in these systems can produce a neutral mode using concrete models.

We start with a minimal toy model which consists of two counterpropagating chiral

Luttinger liquids together with a periodic lattice of impurity scatterers with lattice spacing ℓ (Fig. 4.1). The Hamiltonian is

$$\begin{aligned} H &= H_0 - U\sum_j \cos(k_1\phi_1(j\ell) + k_2\phi_2(j\ell) - \alpha_j), \\ H_0 &= \frac{v}{4\pi}\int_{-\infty}^{\infty} dx\Big(k_1(\partial_x\phi_1)^2 + k_2(\partial_x\phi_2)^2\Big) \end{aligned} \tag{4.1}$$

where ϕ_1, ϕ_2 obey commutation relations

$$\begin{aligned} [\phi_1(x), \partial_y\phi_1(y)] &= -\frac{2\pi i}{k_1}\delta(x-y) \\ [\phi_2(x), \partial_y\phi_2(y)] &= \frac{2\pi i}{k_2}\delta(x-y) \\ [\phi_1(x), \partial_y\phi_2(y)] &= 0 \end{aligned} \tag{4.2}$$

Let us explain the different terms in the Hamiltonian. The first term, H_0, is a bosonized representation of the two chiral Luttinger liquid edge modes in a normalization convention where the electron creation operators are $\psi_1^\dagger = e^{-ik_1\phi_1}$, and $\psi_2^\dagger = e^{ik_2\phi_2}$. The second term — the sum of cosines — describes a lattice of impurities that scatter electrons from one mode to the other (Fig. 4.1). The only parameters in the model are v, U and $\{\alpha_j\}$: v is the velocity of the two edge modes, while U and $\{\alpha_j\}$ describe the amplitude and phase of the electron scattering associated with the j'th impurity. Notice that we allow the α_j phases to be different for each impurity, but we take the scattering strength U to be constant for simplicity.

What makes the above model useful is that we can study it in a well-controlled fashion and explicitly see that the impurity-induced electron scattering leads to an emergent neutral mode. First, consider the case where $U = 0$ so there is no scattering. In this case, the resulting edge theory has two decoupled modes, ϕ_1, ϕ_2. Both modes are charge-carrying, since the electron density operator is given by $\rho(x) = \frac{1}{2\pi}(\partial_x\phi_1 + \partial_x\phi_2)$. Next suppose we turn on a small U. The mode structure remains qualitatively the same as the $U = 0$ case

(assuming the α_j phases are chosen randomly) since it is easy to check that the scattering terms are irrelevant perturbations of the $U = 0$ edge theory.[2]

The more interesting case, and our focus in this chapter, is when U is *large*. In this case, we show that one of the low energy modes is charged and the other is neutral. We derive this result in two steps. In the first step, we solve the model exactly in the limit $U \to \infty$ using the formalism of Ref. [15]. The key point is that in this limit, the impurities act as elastic phonon scatterers similarly to a δ-function potential for non-interacting electrons. Consequently, the periodic lattice of impurities produces a phonon band structure just like a periodic potential for electrons. Working out this phonon band structure, we find that there are two low energy phonon modes, which are described by the following low energy Hamiltonian:

$$\overline{H}_{\text{eff}} = \frac{\bar{v}}{4\pi} \int_{-\infty}^{\infty} dx \ \left(\frac{1}{\nu} (\partial_x \phi_\rho)^2 + \frac{1}{k_2 - k_1} (\partial_x \phi_\sigma)^2 \right), \tag{4.3}$$

Here $\bar{v} = \frac{k_2 - k_1}{k_1 + k_2} v$ is the velocity of the two modes and ϕ_ρ, ϕ_σ are fields obeying commutation relations

$$\begin{aligned} [\phi_\rho(x), \partial_y \phi_\rho(y)] &= -2\pi i \nu \delta(x - y) \\ [\phi_\sigma(x), \partial_y \phi_\sigma(y)] &= 2\pi i (k_2 - k_1) \delta(x - y) \\ [\phi_\rho(x), \partial_y \phi_\sigma(y)] &= 0 \end{aligned} \tag{4.4}$$

In addition to the Hamiltonian, we also derive an expression for the (coarse-grained) density $\bar{\rho}$:

$$\bar{\rho}(x) = \frac{1}{2\pi} \partial_x \phi_\rho \tag{4.5}$$

Eqs. (4.3-4.5) tell us the complete low energy mode structure in the limit $U \to \infty$. Most

2. The critical scaling dimension for perturbations with random coefficients in 1D is 3/2 (see Ref. [16]) while the scaling dimension for the scattering term is $\Delta = (k_1 + k_2)/2$ which is always larger than 3/2.

importantly, they tell us that there are two decoupled low energy modes, ϕ_ρ and ϕ_σ, and that ϕ_ρ carries charge while ϕ_σ is *neutral*.

The second step in our derivation is to study what happens when U is large but finite. We analyze this case by adding correction terms to the $U \to \infty$ low energy theory (4.3). We then investigate the effects of these correction terms using a renormalization group (RG) analysis. In the most realistic case where the α_j are chosen randomly, we find that the correction terms have no effect except to renormalize the velocities of the charge and neutral modes. Hence, for random α_j, the charge/neutral mode structure persists at large but finite U. This is the main result for the first part of the paper.

In the second part of the paper, we generalize the toy model (4.1) in two ways. First, we define H_0 using an *arbitrary* velocity matrix V_{ij}:

$$H_0^{\text{gen}} = \frac{1}{4\pi} \int dx \sum_{i,j=1}^{2} V_{ij} \partial_x \phi_i \partial_x \phi_j \tag{4.6}$$

Here V can be any real, symmetric, positive definite 2×2 matrix. Physically, this extension allows the ϕ_1 and ϕ_2 modes to have arbitrary velocities and density-density coupling. Our second extension is to make the impurities randomly distributed, rather than regularly spaced. The total Hamiltonian is then

$$H^{\text{gen}} = H_0^{\text{gen}} - U \sum_j \cos(k_1 \phi_1(x_j) + k_2 \phi_2(x_j) - \alpha_j), \tag{4.7}$$

where x_j is the position of the jth impurity. Our main result for this part is that H^{gen} has a charge and a neutral mode at large U, just like the toy model H. In other words, our derivation generalizes to a more realistic setup with an arbitrary velocity matrix and randomly distributed scatterers.

4.3 Toy model: infinite U

In this section we solve the toy model (4.1) in the limit of infinite scattering strength, $U \to \infty$. Our main result is that the system has two low energy modes in this limit: a charge mode and a neutral mode. We show that these modes are described by the low energy theory (4.3-4.5).

4.3.1 Review of general formalism

Our solution of the toy model is based on a general formalism for solving quadratic Hamiltonians with large cosine terms, introduced in Ref. [15]. Below we briefly review some of the central results of this formalism before turning to our specific problem.

Consider a general Hamiltonian of the form

$$H = H_0 - U \sum_i \cos(C_i) \tag{4.8}$$

defined on some phase space $\{x_1, p_1, x_2, p_2, ...\}$. H_0 is a quadratic function of position and momentum variables $\{x_1, p_1, x_2, p_2, ...\}$ and the C_i are linear functions of these variables. The C_i's can be arbitrary except for two restrictions: (1) $\{C_1, C_2, ...\}$ are linearly independent, and (2) $[C_i, C_j]$ is an integer multiple of $2\pi i$ for all i, j (so that the cosine terms commute with one another). Ref. [15] showed how to find the low energy spectrum of Hamiltonians of this kind in the limit $U \to \infty$.

The basic idea behind the analysis of Ref. [15] is that the cosine terms act as *constraints* in the limit $U \to \infty$. These constraints force the arguments of the cosine terms to be locked to integer multiples of 2π at low energies. When this happens, the low energy spectrum of H can be described by an effective Hamiltonian H_{eff} acting within an effective Hilbert space $\mathcal{H}_{\text{eff}}$. Importantly, the effective Hamiltonian H_{eff} is *quadratic* and therefore can be diagonalized using elementary methods.

How do we construct the effective Hamiltonian and Hilbert space? The Hilbert space is

easy: $\mathcal{H}_{\text{eff}}$ is the subspace of the original Hilbert space consisting of all states $|\psi\rangle$ satisfying

$$\cos(C_i)|\psi\rangle = |\psi\rangle, \quad i = 1, 2, ... \tag{4.9}$$

As for the Hamiltonian, Ref. [15] described a simple recipe for simultaneously constructing and diagonalizing H_{eff}. The first step is to find all operators a that are linear combinations of the phase space variables $x_1, p_1, ...$ and that satisfy the equations

$$[a, H_0] = Ea + \sum_j \lambda_j [C_j, H_0] \tag{4.10}$$

$$[a, C_i] = 0, \quad \text{for all } i \tag{4.11}$$

where λ_j and E are arbitary scalars with $E \neq 0$. The above operators a have a simple physical meaning: they describe creation or annihilation operators for the effective Hamiltonian H_{eff}. The scalar E is the energy of the corresponding mode while the scalars λ_j can be thought of as Lagrange multipliers associated with the constraints imposed by the cosine terms.

Once the solutions to (4.10-4.11) have been identified, the next step is to separate them into two classes: 'annihilation operators' with $E > 0$ and 'creation operators' with $E < 0$. If $a_1, a_2, ...$ form a complete set of linearly independent annihilation operators, and $a_1^\dagger, a_2^\dagger, ...$ are the corresponding creation operators, then they should be normalized so that

$$[a_k, a_{k'}^\dagger] = \delta_{kk'}, \quad [a_k, a_{k'}] = [a_k^\dagger, a_{k'}^\dagger] = 0 \tag{4.12}$$

After these steps have been completed, the effective Hamiltonian H_{eff} can be written down

easily: according to Ref. [15], H_{eff} is simply given by[3]

$$H_{\text{eff}} = \sum_k E_k a_k^\dagger a_k \tag{4.13}$$

A cautionary note: while it is tempting to conclude that the energy spectrum of H_{eff} is identical to that of a collection of harmonic oscillators with frequencies E_k, this is not quite correct in general. The reason is that, in many cases H_{eff} has additional degeneracy, i.e. each occupation number eigenstate may be D-fold degenerate for some D. In this chapter we will focus on systems where $D = 1$ in order to avoid complications associated with this degeneracy. In fact, this is the reason that we restrict to the case $k_2 = k_1 + 2$ (see Appendix C.1).

4.3.2 Solving the toy model

We now use the above formalism to solve the toy model in the $U \to \infty$ limit. Here, H_0 is defined in Eq. (4.1), and the C_j's are defined by

$$C_j = k_1\phi_1(j\ell) + k_2\phi_2(j\ell) - \alpha_j \tag{4.14}$$

According to the general formalism, we need to find all operators a satisfying the following properties. First, a should be a linear combination of the phase space variables $\{\partial_x\phi_1, \partial_x\phi_2\}$:

$$a = \int_{-\infty}^{\infty} dx\ (f(x)\partial_x\phi_1 + g(x)\partial_x\phi_2) \tag{4.15}$$

3. More precisely, Eq. (4.13) is only guaranteed to hold if we make the additional assumption that the matrix $\mathcal{Z}_{ij} = \frac{1}{2\pi i}[C_i, C_j]$ has a non-vanishing determinant. This property holds for all the systems discussed in this chapter.

Second, a should obey Eqs. (4.10-4.11) for some λ_j, E with $E \neq 0$. Finally, given that Eqs. (4.10-4.11) have discrete translational symmetry,[4] $f(x)$ and $g(x)$ should obey the Bloch condition

$$f(x+\ell) = e^{-ik\ell} f(x), \quad g(x+\ell) = e^{-ik\ell} g(x) \tag{4.16}$$

where k is in the Brillouin zone $[-\pi/\ell, \pi/\ell]$.

Our task is thus to solve Eqs. (4.10-4.11) and (4.16). For clarity, we present the result first and then explain the derivation. In short, what we find is that there are an infinite number of solutions to these equations for each value of k in $[-\pi/\ell, \pi/\ell]$. We label these solutions by $a_{n,k}$ and $E_{n,k}$ where n is an integer index, $n = 0, \pm 1, \pm 2, ...$ These solutions take the form

$$a_{n,k} = \int_{-\infty}^{\infty} \frac{dx}{\sqrt{|E_{n,k}|}} e^{-ikx} (u_{n,k}(x)\partial_x \phi_1 + w_{n,k}(x)\partial_x \phi_2) \tag{4.17}$$

where $u_{n,k}$ and $w_{n,k}$ are periodic functions which we derive below. The energies $E_{n,k}$ are given by

$$E_{n,k} = \frac{n\pi v}{\ell} + \frac{(-1)^n v}{\ell} \arcsin\left(\frac{k_2 - k_1}{k_2 + k_1} \sin k\ell\right) \tag{4.18}$$

The solutions come in pairs with $a_{-n,-k} = a^\dagger_{n,k}$ and $E_{-n,-k} = -E_{n,k}$, with the $a_{n,k}$ operators obeying the standard commutation relations

$$[a_{n,k}, a^\dagger_{n',k'}] = \delta(k-k')\delta_{nn'}, \quad E_{n,k} > 0 \tag{4.19}$$

With these results in hand, we can immediately write down the effective Hamiltonian H_{eff} using the general formalism (4.13):

$$H_{\text{eff}} = \sum_n \int_{-\pi/\ell}^{\pi/\ell} dk\ \Theta(E_{n,k})\ E_{n,k} a^\dagger_{n,k} a_{n,k} \tag{4.20}$$

4. The only part of the toy model that breaks translational symmetry are the α_j phases, and these do not appear in Eqs. 4.10-4.11.

where Θ denotes the Heaviside step function.

Equations (4.17-4.20) tell us the complete low energy spectrum of the toy model in the limit $U \to \infty$. To understand the physical interpretation of this spectrum, note that phonons scatter off the impurities elastically in the limit $U \to \infty$, since in this limit the cosine terms can be modeled as hard constraints on the ϕ_1, ϕ_2 fields. Thus a lattice of impurities gives rise to a band structure for phonons just as a periodic potential gives rise to a band structure for electrons. The above results are consistent with this physical picture: the operators $a^\dagger_{n,k}, a_{n,k}$ (for $E_{n,k} > 0$) can be thought of as creation and annihilation operators for a phonon in band n with crystal momentum k. The energy of this phonon mode is given by $E_{n,k}$.

One thing that these equations do not tell us is the *degeneracy* of the different energy levels of H_{eff}. As we mentioned in the previous section, the phonon occupation numbers $\{a^\dagger_{n,k} a_{n,k}\}$ are not necessarily a complete set of observables; that is, every phonon occupation state may be D-fold degenerate for some D. We study this issue in Appendix C.1 using the general formalism of Ref. [15]. We find that for $|k_2 - k_1| = 2$, the toy model has no degeneracy: $D = 1$. In contrast, for $|k_2 - k_1| > 2$ we find that the model has an *extensive* degeneracy, i.e. D grows exponentially with the number of impurities. This degeneracy poses many complications, and is the reason that we restrict our analysis to the case $k_2 = k_1 + 2$.

We now solve Eqs. (4.10-4.11) and (4.16) and derive the results listed above. First, we plug (4.15) into (4.10), thereby obtaining the differential equations

$$\begin{aligned} f'(x) &= -i\frac{E}{v} f(x) - k_1 \sum_{j=-\infty}^{\infty} \lambda_j \delta(x - j\ell) \\ g'(x) &= i\frac{E}{v} g(x) - k_2 \sum_{j=-\infty}^{\infty} \lambda_j \delta(x - j\ell) \end{aligned} \tag{4.21}$$

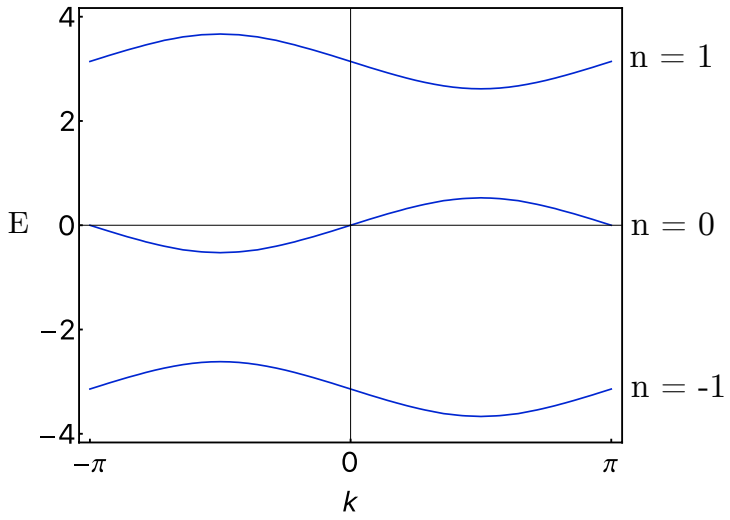

Figure 4.2: Phonon bandstructure of the toy model in the limit $U \to \infty$, for the case $k_1 = 1, k_2 = 3$ and $v = \ell = 1$. The zeros of the $n = 0$ band correspond to low energy phonon modes: $k = 0$ corresponds to a right-moving charge mode, while $k = \pi/\ell$ corresponds to a left-moving neutral mode.

Solving this system of equations, we obtain piecewise plane wave solutions of the form

$$\begin{aligned} f(x) &= A^{(j)} e^{-i\frac{E}{v}(x-j\ell)}, \\ g(x) &= B^{(j)} e^{i\frac{E}{v}(x-j\ell)}, \qquad j\ell \le x < (j+1)\ell \end{aligned} \tag{4.22}$$

To obtain the matching conditions between the $A^{(j)}, B^{(j)}$ coefficients, we note that Eq. (4.21) implies that

$$\begin{aligned} A^{(j)} &= A^{(j-1)} e^{-i\frac{E\ell}{v}} - \lambda_j k_1, \\ B^{(j)} &= B^{(j-1)} e^{i\frac{E\ell}{v}} - \lambda_j k_2 \end{aligned} \tag{4.23}$$

or equivalently

$$\frac{A^{(j)} - A^{(j-1)} e^{-i\frac{E\ell}{v}}}{k_1} = \frac{B^{(j)} - B^{(j-1)} e^{i\frac{E\ell}{v}}}{k_2} \tag{4.24}$$

Another matching condition for $A^{(j)}, B^{(j)}$ comes from the constraint (4.11): substituting

(4.15) into (4.11), and using an appropriate regularization (see appendix C.2), yields

$$\frac{A^{(j)} + A^{(j-1)}e^{-i\frac{E\ell}{v}}}{2} = \frac{B^{(j)} + B^{(j-1)}e^{i\frac{E\ell}{v}}}{2} \tag{4.25}$$

Using the two constraints (4.24) and (4.25), we can solve for $A^{(j)}$ and $B^{(j)}$ in terms of $A^{(j-1)}$ and $B^{(j-1)}$:

$$\begin{pmatrix} A^{(j)} \\ B^{(j)} \end{pmatrix} = T \cdot D(E\ell) \cdot \begin{pmatrix} A^{(j-1)} \\ B^{(j-1)} \end{pmatrix} \tag{4.26}$$

where

$$T = \frac{1}{k_2 - k_1} \begin{pmatrix} k_2 + k_1 & -2k_1 \\ 2k_2 & -k_1 - k_2 \end{pmatrix} \tag{4.27}$$

and

$$D(x) = \begin{pmatrix} e^{-ix/v} & 0 \\ 0 & e^{ix/v} \end{pmatrix}$$

Each of the matrices, T, $D(E\ell)$ and their product $T \cdot D(E\ell)$, have a simple interpretation. The matrix T can be interpreted as the transfer matrix corresponding to a single impurity: it relates the mode amplitudes just to the right of the impurity to those just to the left. Likewise $D(E\ell)$ can be interpreted as a propagator that describes how the amplitudes change in between the impurities. Finally, $T \cdot D(E\ell)$ can be interpreted as a transfer matrix corresponding to a *unit cell*: it relates the mode amplitudes at the end of the unit cell to those at the beginning of the unit cell.

To proceed further, we impose the Bloch condition (4.16), which implies that

$$\begin{pmatrix} A^{(j)} \\ B^{(j)} \end{pmatrix} = e^{-ijk\ell} \begin{pmatrix} A \\ B \end{pmatrix} \tag{4.28}$$

where $A \equiv A^{(0)}$ and $B \equiv B^{(0)}$. Combining (4.26) and (4.28), we arrive at the eigenvalue

equation

$$T \cdot D(E\ell) \cdot \begin{pmatrix} A \\ B \end{pmatrix} = e^{-ik\ell} \begin{pmatrix} A \\ B \end{pmatrix} \tag{4.29}$$

Equation (4.29) encodes all the information about the phonon band structure and is the main result of our calculation. All that is left is to solve this equation. A quick way to do this is to note that $\det(T) = -1$ while $\det(D) = 1$, so $\det(T \cdot D) = -1$. It follows that if $T \cdot D$ has an eigenvalue $e^{-ik\ell}$, then its other eigenvalue must be $-e^{ik\ell}$. Hence, $\mathrm{Tr}(T \cdot D)$ must be equal to $-2i\sin(k\ell)$. Comparing this value of the trace with the explicit form of $T \cdot D$, we derive the relation

$$\frac{k_2 + k_1}{k_2 - k_1} \sin\left(\frac{E\ell}{v}\right) = \sin k\ell \tag{4.30}$$

We can see that for each $k \in [-\pi/\ell, \pi/\ell]$, there are an infinite number of E's that obey this equation. These solutions are precisely the $E_{n,k}$'s given in Eq. 4.18. The corresponding expressions for A, B can be obtained by straightforward algebra:

$$\begin{pmatrix} A_{n,k} \\ B_{n,k} \end{pmatrix} = \begin{pmatrix} k_2 + k_1 + (k_2 - k_1)e^{i(k+E_{n,k}/v)\ell} \\ 2k_2 \end{pmatrix} \tag{4.31}$$

Putting this all together, we conclude that the most general creation/annihilation operators are of the form (4.17) where

$$\begin{aligned} u_{n,k}(x) &= \frac{A_{n,k}}{\mathcal{N}_{n,k}} e^{i(k-E_{n,k}/v)\{x\}} \\ w_{n,k}(x) &= \frac{B_{n,k}}{\mathcal{N}_{n,k}} e^{i(k+E_{n,k}/v)\{x\}} \end{aligned} \tag{4.32}$$

and where $\{x\}$ is defined to be the distance to the nearest impurity to the left of x (i.e. if $j\ell \leq x < (j+1)\ell$ then $\{x\} = x - j\ell$). The normalization constant $\mathcal{N}_{nk}$ can be determined

by demanding that a_{nk} obeys the commutation relations (4.19):

$$\mathcal{N}_{n,k} = \frac{2\pi}{\sqrt{v}} \left(\frac{|A_{n,k}|^2}{k_1} + \frac{|B_{n,k}|^2}{k_2} \right)^{1/2} \tag{4.33}$$

4.3.3 Low energy phonon modes

The most important feature of the band structure derived in the previous section (Fig. 4.2) is that the $n = 0$ phonon band crosses $E = 0$ in two places: $k = 0$ and $k = \pi/\ell$. These crossings imply that the system has two low energy phonon modes with opposite chiralities. We now derive a low energy Hamiltonian that describes these modes.

In order to be precise, we first need to specify the low energy Hilbert space $\overline{\mathcal{H}}_{\text{eff}}$ for this Hamiltonian. We do this in the obvious way: we define the Hilbert space $\overline{\mathcal{H}}_{\text{eff}}$ to be the subspace spanned by phonon excitations in the $n = 0$ band with

$$|k| \leq \Lambda \quad \text{or} \quad |k - \pi/\ell| \leq \Lambda$$

where Λ is some momentum cutoff with $\Lambda \ll 1/\ell$.

Likewise, we define the low energy Hamiltonian $\overline{H}_{\text{eff}}$ by projecting H_{eff} onto the low energy Hilbert space. The result of this projection is that all the creation and annihilation operators in H_{eff} drop out except for those with $n = 0$ and with k near 0 or π. We will relabel these low energy operators as $a_{\rho k}$ and $a_{\sigma k}$ where

$$a_{\rho,k} \equiv a_{0,k}, \quad a_{\sigma,k} = a_{0,k+\pi/\ell} \tag{4.34}$$

and where $|k| \leq \Lambda$. Expressing H_{eff} in terms of these variables and linearizing the dispersion, we derive the low energy Hamiltonian

$$\overline{H}_{\text{eff}} = \int_0^\Lambda dk \;\; \bar{v}k(a^\dagger_{\rho,k} a_{\rho,k} + a^\dagger_{\sigma,-k} a_{\sigma,-k}) \tag{4.35}$$

where the (renormalized) velocity $\bar{v}$ is given by

$$\bar{v} = \frac{k_2 - k_1}{k_1 + k_2} v \tag{4.36}$$

Note that the modes at $k = 0$ and $k = \pi/\ell$ have opposite velocities $\pm\bar{v}$.

4.3.4 Expression for density operator

We now derive an expression for the charge density $\rho(x) = \frac{1}{2\pi}(\partial_x\phi_1 + \partial_x\phi_2)$ in terms of $a_{\rho,k}$ and $a_{\sigma,k}$. This expression is interesting because it tells us that the ρ ($k = 0$) mode carries *charge* while the σ ($k = \pi/\ell$) mode is *neutral*.

The first step is to note that $\rho(x)$ can be expanded as a linear combination of the $a_{n,k}$ operators, that is:

$$\rho(x) = \sum_n \int_{-\frac{\pi}{\ell}}^{\frac{\pi}{\ell}} dk\ \rho_{n,k}(x) a_{n,k} \tag{4.37}$$

Here the $\rho_{n,k}(x)$ are unknown functions that we will determine below. The existence of such an expansion follows from the completeness of the $a_{n,k}$ operators: any linear combination of $\partial_x\phi_1$ and $\partial_x\phi_2$ that commutes with the C_j's can always be expanded in terms of the $a_{n,k}$.[15]

Next we find the expansion coefficients $\rho_{n,k}(x)$. To do this, we take the commutator of Eq. (4.37) with $a_{-n,-k}$, which gives

$$[\rho(x), a_{-n,-k}] = \rho_{n,k}(x) \cdot \mathrm{sgn}(E_{n,k}) \tag{4.38}$$

Evaluating the commutator using the expression for $a_{n,k}$ (4.17), we obtain

$$\begin{aligned}\rho_{n,k}(x) &= -\frac{i\mathrm{sgn}(E_{n,k})}{\sqrt{|E_{n,k}|}} \\ &\times \partial_x \left(e^{ikx} \left[\frac{u_{-n,-k}(x)}{k_1} - \frac{w_{-n,-k}(x)}{k_2} \right] \right) \\ &= \frac{\sqrt{|E_{n,k}|}}{v} e^{ikx} \left(\frac{u_{-n,-k}(x)}{k_1} + \frac{w_{-n,-k}(x)}{k_2} \right) \end{aligned} \tag{4.39}$$

where the second equality follows from the differential equation (4.21). Putting this together, we can write $\rho(x)$ as

$$\rho(x) = \sum_n \int_{-\frac{\pi}{\ell}}^{\frac{\pi}{\ell}} dk \ \sqrt{|E_{n,k}|} e^{ikx} z_{n,k}(x) a_{n,k} \tag{4.40}$$

where

$$z_{n,k}(x) = \frac{u_{-n,-k}(x)}{vk_1} + \frac{w_{-n,-k}(x)}{vk_2} \tag{4.41}$$

At this point, we have found an expression for $\rho(x)$ in terms of the $a_{n,k}$ operators; to complete the calculation we need to go to lower energies and translate Eq. (4.40) into an analogous expression for $\rho(x)$ in terms of $a_{\rho,k}$ and $a_{\sigma,k}$. More precisely, since our low energy theory has a momentum cutoff Λ, we will not be interested in the microscopic density $\rho(x)$, but rather in a *coarse-grained* version of this quantity, which we will denote by $\bar{\rho}(x)$. The coarse-grained density $\bar{\rho}(x)$ is defined by spatially averaging $\rho(x)$ over a region of size $1/\Lambda$.[5]

Our task is thus to find the expression for $\bar{\rho}(x)$ in terms of $a_{\rho,k}$ and $a_{\sigma,k}$. To this end, we need to *spatially average* the expression for $\rho(x)$ given in Eq. (4.40), and then *project* this expression to the low energy Hilbert space $\overline{\mathcal{H}}_{\text{eff}}$. The spatial averaging step can be accomplished by making two changes to Eqs. (4.40), namely (1) restricting the integral to $|k| \leq \Lambda$, and (2) replacing $z_{n,k}(x) \to \bar{z}_{n,k}$, where $\bar{z}_{n,k}$ is defined by averaging $z_{n,k}(x)$ over

5. The details of this spatial averaging procedure are not important for our purposes: the only property that we will assume below is that $\bar{\rho}$ has identical Fourier components as ρ for wave vectors $|k| \leq \Lambda$ and has vanishing Fourier components for $|k| \gtrsim \Lambda$.

a unit cell. The projection step can be accomplished by simply throwing out all the terms involving $a_{n,k}$ for $n \neq 0$.

After performing both steps, the end result is:

$$\bar{\rho}(x) = \int_{-\Lambda}^{\Lambda} dk \ \sqrt{|E_{0,k}|} e^{ikx} \bar{z}_{0,k} a_{0,k} \tag{4.42}$$

The final step is to compute $\bar{z}_{0,k}$. To do this, note that since we are only interested in small k modes, i.e. $|k| \leq \Lambda \ll 1/\ell$, we can make the approximation

$$\bar{z}_{0,k} \approx \bar{z}_{0,0} = \frac{\bar{u}_{0,0}}{vk_1} + \frac{\bar{w}_{0,0}}{vk_2} \tag{4.43}$$

Similarly, we can approximate $\sqrt{|E_{0,k}|} \approx \sqrt{\bar{v}|k|}$. Substituting this into Eq. (4.42) and using the expressions for $u_{n,k}, w_{n,k}$ and $\bar{v}$ (4.32, 4.36), we derive

$$\bar{\rho}(x) = \frac{\sqrt{\nu}}{2\pi} \int_{-\Lambda}^{\Lambda} dk \ \sqrt{|k|} e^{ikx} a_{\rho,k} \tag{4.44}$$

Here we have used the identification $a_{0,k} \equiv a_{\rho,k}$.

4.3.5 Charge and neutral modes

To complete our derivation, we now define two real-space fields $\partial_x \phi_\rho$ and $\partial_x \phi_\sigma$, which we label the *charge* and *neutral* modes:

$$\partial_x \phi_\rho(x) = \sqrt{\nu} \int_{-\Lambda}^{\Lambda} dk \ \sqrt{|k|} e^{ikx} a_{\rho,k} \tag{4.45}$$

$$\partial_x \phi_\sigma(x) = \sqrt{k_2 - k_1} \int_{-\Lambda}^{\Lambda} dk \sqrt{|k|} e^{ikx} a_{\sigma,k} \tag{4.46}$$

One can check that these fields obey the commutation relations

$$[\phi_\rho(x), \partial_y \phi_\rho(y)] = -2\pi i \nu \delta(x-y)$$
$$[\phi_\sigma(x), \partial_y \phi_\sigma(y)] = 2\pi i (k_2 - k_1)\delta(x-y)$$
$$[\phi_\rho(x), \partial_y \phi_\sigma(y)] = 0$$

where the above '$\delta(x)$' is actually a regularized δ function that only has Fourier components smaller than Λ. In terms of these fields, the Hamiltonian (4.35) becomes

$$\overline{H}_{\text{eff}} = \frac{\bar{v}}{4\pi} \int_{-\infty}^{\infty} dx \ \left(\frac{1}{\nu} (\partial_x \phi_\rho)^2 + \frac{1}{k_2 - k_1} (\partial_x \phi_\sigma)^2 \right),$$

while the (coarse-grained) density operator (4.44) is

$$\bar{\rho}(x) = \frac{1}{2\pi} \partial_x \phi_\rho$$

This completes our derivation of the real space low energy theory (4.3-4.5). It also completes our derivation of the neutral mode: indeed, it is obvious that ϕ_σ is electrically neutral since it does not appear in the above expression for the charge density.

It is natural to ask: what is the origin of the neutral mode in our calculation? For the above model, this question has a simple answer: the presence of a neutral mode can be traced to the fact that the phonon bands cross $E = 0$ at both $k = 0$ and $k = \pi/\ell$. The key point is that the $k = \pi/\ell$ mode is *guaranteed* to be electrically neutral on average, due to its spatial oscillations.

4.4 Toy model: finite U

In this section, we analyze the toy model (4.1) at large but *finite* scattering strength U. Our main result is that the charge/neutral mode structure persists at finite U, as long as the α_j

phases are chosen randomly.

4.4.1 RG analysis of low energy theory

The key idea behind our analysis is that the low energy effective theory at finite U can be obtained by adding correction terms to the low energy theory at $U = \infty$ (4.3). Given this fact, all we have to do is compute these 'finite U corrections' and study their effects on (4.3). Before doing this, we first orient ourselves by analyzing the effects of *arbitrary* charge-conserving perturbations on the low energy theory (4.3). This will help us distinguish between important and unimportant corrections.

We begin by enumerating all local, charge-conserving operators in the low energy theory (4.3). To start, it is useful to think about simple examples and 'non-examples' of these operators. In particular, we note that the operators $\partial_x\phi_\sigma$ and $\partial_x\phi_\rho$ are valid examples, but $e^{i\text{const.}\cdot\phi_\rho}$ is not since it does not commute with $\int dx\partial_x\phi_\rho$ and therefore breaks charge conservation. Another important example is $e^{im\phi_\sigma}$. This operator is charge-conserving for all m but it is only a legitimate low energy operator when m is an integer, since it is only in this case that it commutes with the constraints e^{iC_j} that define the low energy Hilbert space (4.9). One way to see this is to rewrite $\int dx\partial_x\phi_\sigma$ as

$$\begin{aligned}\int_{-\infty}^{\infty} dx\ \partial_x\phi_\sigma &= \sqrt{k_2-k_1}\int_{-\infty}^{\infty} dx \int_{-\Lambda}^{\Lambda} dk\sqrt{|k|}e^{ikx}a_{\sigma,k} \\ &= \sum_j (-1)^j \int_{j\ell}^{(j+1)\ell} dx(k_1\partial_x\phi_1 + k_2\partial_x\phi_2) \\ &= \sum_j 2(-1)^{j+1}(C_j+\alpha_j) \end{aligned} \tag{4.47}$$

(Here the second equality comes from plugging in the definition of $a_{\sigma,k}$ (4.17,4.34) and simplifying). From this identity, we can see that

$$\Big[\sum_j (-1)^{j+1}C_j, \phi_\sigma\Big] = \pi(k_1-k_2) \tag{4.48}$$

It follows that $\exp(im\phi_\sigma)$ commutes with $\exp(i\sum_j (-1)^{j+1} C_j)$ only if m is an integer multiple of $2/(k_2 - k_1)$. Since we specialize to the case $k_2 - k_1 = 2$, we conclude that m has to be an integer, as claimed above.

Putting together the above examples, we deduce that the most general charge-conserving operator can be parameterized as

$$e^{im\phi_\sigma} f(\{\partial_x^k \phi_\sigma, \partial_x^l \phi_\rho\}) \tag{4.49}$$

where m is an integer and f is a monomial built out of derivatives of ϕ_σ and ϕ_ρ. Our next task is to understand the perturbative effect of these operators on the low energy theory (4.3). We do this with a renormalization group (RG) approach. First, we note that the scaling dimension of $e^{im\phi_\sigma}$ is $\Delta = m^2$ (here we again use the fact that $k_2 - k_1 = 2$). This fact implies that all the operators in (4.49) with $|m| \geq 2$ have scaling dimensions larger than 2 and are thus irrelevant in the RG sense. We can therefore restrict our attention to the operators with $m = 0, \pm 1$, of which the only marginal or relevant ones are:

$$\begin{aligned} &\partial_x \phi_\rho, \quad \partial_x \phi_\sigma, \quad e^{\pm i\phi_\sigma}, \quad (\partial_x \phi_\rho)^2, \quad (\partial_x \phi_\sigma)^2, \\ &\partial_x \phi_\rho \partial_x \phi_\sigma, \quad e^{\pm i\phi_\sigma} \partial_x \phi_\rho \end{aligned} \tag{4.50}$$

Let us consider each of these perturbations. The first three terms are unimportant since they can be 'gauged away' — that is, eliminated from the Hamiltonian by an appropriate redefinition of fields. This is obvious for $\partial_x \phi_\rho$ and $\partial_x \phi_\sigma$: these terms can be eliminated by completing the square in the Hamiltonian (4.3). As for $e^{\pm i\phi_\sigma}$, the fact that this term can be gauged away follows from an observation of Ref. [29], namely that when $|k_1 - k_2| = 2$, the three operators $\{\int dx \cos(\phi_\sigma), \int dx \sin(\phi_\sigma), \int dx \partial_x \phi_\sigma\}$ generate an $SU(2)$ symmetry group that leaves the Hamiltonian (4.3) invariant. Like any $SU(2)$ generators, these three operators transform like a three component vector under the symmetry that they generate. In particular, this means that we can rotate the operator $\cos(\phi_\sigma)$ into $\partial_x \phi_\sigma$ using the $SU(2)$

symmetry. The latter term can be gauged away, hence $\cos(\phi_\sigma)$ can also be gauged away.

The next two perturbations, $(\partial_x\phi_\rho)^2, (\partial_x\phi_\sigma)^2$, are also relatively unimportant since their only effect is to shift the charge and neutral mode velocities. Thus, the only perturbations we need to worry about are $\partial_x\phi_\rho\partial_x\phi_\sigma$ and $e^{\pm i\phi_\sigma}\partial_x\phi_\rho$. These perturbations *do* have an important effect: they couple the charge and neutral modes so that both of the resulting hybridized modes are charge-carrying. [6] Thus, these perturbations are dangerous from our perspective because they destroy the decoupled charge/neutral mode structure if they are present.

4.4.2 Fate of neutral mode

The next step is to compute the finite U corrections for the impurity model (4.1) and determine whether the two 'dangerous' perturbations discussed above, namely $\partial_x\phi_\rho\partial_x\phi_\sigma$ and $e^{\pm i\phi_\sigma}\partial_x\phi_\rho$, are generated. This calculation is technical so we postpone it to the next section, and skip to the main result: what we find is that these perturbations *do* appear as finite U corrections but with spatially dependent coefficients. In particular, $\partial_x\phi_\rho\partial_x\phi_\sigma$ appears in the form

$$\sum_j (-1)^j \partial_x\phi_\rho\partial_x\phi_\sigma(j\ell) \tag{4.51}$$

with a coefficient that changes sign every unit cell. Meanwhile $e^{\pm i\phi_\sigma}\partial_x\phi_\rho$ appears in the form

$$\sum_j \cos(\phi_\sigma(j\ell) - \beta_j)\partial_x\phi_\rho(j\ell) \tag{4.52}$$

where the β_j are determined by the original α_j phases via the relation

$$\beta_{j+1} - \beta_j = (-1)^j(\alpha_{j+1} - \alpha_j) \tag{4.53}$$

6. This hybridization effect is obvious for $\partial_x\phi_\rho\partial_x\phi_\sigma$; to see why it occurs for $e^{\pm i\phi_\sigma}$, note that these three operators form a multiplet under the $SU(2)$ symmetry mentioned above.

The alternating coefficient in Eq. (4.51) has a very important consequence: it suppresses the effect of $\partial_x\phi_\rho\partial_x\phi_\sigma$, effectively rendering it *irrelevant*. Likewise, the β_j phases in (4.52) can also lead to cancellations that suppress this perturbation, but these cancellations are more delicate and depend on the values of α_j. Thus to determine the fate of the charge/neutral mode structure, we need to fix a choice of α_j. Here we focus on two possibilities: (a) $\alpha_j = j\Phi$ for some Φ, and (b) random α_j. Physically, case (a) corresponds to a situation where an identical amount of magnetic flux Φ threads between each pair of impurities, between the ϕ_1, ϕ_2 edge modes. Likewise, case (b) corresponds to random magnetic flux and can be thought of as capturing some aspects of a more realistic random impurity system.

Interestingly these two cases lead to different physics. In the uniform flux case (a), we obtain $\beta_{j+1} - \beta_j = (-1)^j\Phi$, so we can take $\beta_{2j} = 0$ and $\beta_{2j+1} = \Phi$. Substituting this into (4.52), we see that in the long distance limit, the finite U corrections generate a term of the form

$$[\cos(\phi_\sigma) + \cos(\phi_\sigma - \Phi)]\partial_x\phi_\rho \tag{4.54}$$

Evidently there is no cancellation (for generic Φ) so the $e^{\pm i\phi_\sigma}\partial_x\phi_\rho$ perturbation is not suppressed. Therefore, the charge and neutral modes will become hybridized at finite U. In other words, the charge/neutral mode structure does *not* persist at finite U in this case.

On the other hand, in the random flux case (b), the β_j phases are also random and independent, so the operators $e^{\pm i\phi_\sigma}\partial_x\phi_\rho$ appear with random phases. These random phases make $e^{\pm i\phi_\sigma}\partial_x\phi_\rho$ irrelevant, since it has a scaling dimension, $\Delta = 2$, which is larger than the critical dimension of 3/2 for perturbations with random coefficients.[16] Therefore, in this case, both of the dangerous perturbations are suppressed and hence the charge and neutral mode survive at finite U in this case.

4.4.3 Finite U corrections

To complete the discussion, we need to compute the finite U corrections and derive Eqs. (4.51) and (4.52). Before doing this, we first review the general formalism for these corrections.

In Ref. [15] it was argued that the low energy spectrum of (4.8) for large, finite U can be obtained by adding appropriate correction terms to the $U = \infty$ effective Hamiltonian H_{eff} (4.13). These correction terms can always be written in the following general form:[7]

$$\sum_{\boldsymbol{m}} e^{i\sum_j m_j \Pi_j} \epsilon_{\boldsymbol{m}}(\{a_k, a_k^\dagger\})) \tag{4.55}$$

Here the sum runs over integer vectors $\boldsymbol{m} = (m_1, m_2, ...)$ and the $\epsilon_{\boldsymbol{m}}$ are some unknown functions of $\{a_k, a_k^\dagger\}$ which also depend on U. Also, Π_j is defined by

$$\Pi_j = \frac{1}{2\pi i} \sum_i \mathcal{N}^{-1}_{ji} [C_i, H_0] \tag{4.56}$$

where $\mathcal{N}$ is the matrix $\mathcal{N}_{ji} = -\frac{1}{(2\pi)^2}[C_j, [C_i, H_0]]$. Note that (4.55) does not tell us the functional form of $\epsilon_{\boldsymbol{m}}(a_k, a_k^\dagger)$: this is system dependent and cannot be determined without more calculation.

To understand where the expression (4.55) comes from, note that when U is finite, we expect that there is a small amplitude for the system to tunnel between the minima of the cosine terms, i.e. $C_j \to C_j - 2\pi m_j$. Thus, the corrections to H_{eff} should be a sum of the most general possible operators describing tunneling processes of this kind. Eq. (4.58) is precisely such a sum of (general) tunneling operators. Indeed, one can see that (4.55) gives a matrix element for the tunneling process $C_j \to C_j - 2\pi m_j$ using the commutation relation

$$[C_j, \Pi_i] = 2\pi i \delta_{ji} \tag{4.57}$$

7. This expression holds assuming the matrix $\mathcal{Z}_{ij} = \frac{1}{2\pi i}[C_i, C_j]$ has a non-vanishing determinant, as is the case for all the systems discussed in this chapter.

(See Ref. [15] for more details).

We now apply the above general formalism to the lattice impurity model (4.1). For simplicity, we start with the case where only one of the impurities has a finite value of U while the others have $U = \infty$. In this case, we only have to think about the finite U corrections associated with a single impurity — say, the jth impurity. Thus, the general expression (4.55) reduces to:

$$\sum_{m=-\infty}^{\infty} e^{im\Pi_j} \epsilon_m(\{a_{n,k}, a_{n,k}^\dagger\}) \tag{4.58}$$

where Π_j is defined by

$$\Pi_j = 2\pi i \frac{[C_j, H_0]}{[C_j, [C_j, H_0]]} \tag{4.59}$$

and where ϵ_m are some unknown functions of $\{a_{n,k}, a_{n,k}^\dagger\}$ which also depend on U. [8]

Equivalently, the finite U corrections can be written in the real space form

$$\sum_{m=-\infty}^{\infty} e^{im\Pi_j} f_m(\partial_x^k \phi_1(j\ell), \partial_x^l \phi_2(j\ell)) \tag{4.60}$$

where the function f_m obtained by expressing $\epsilon_m(\{a_{n,k}, a_{n,k}^\dagger\})$ in terms of $\partial_x\phi_1, \partial_x\phi_2$.

Next, consider the case where *all* the impurities have the same finite value of U. For large U, we expect the dominant corrections to be independent tunneling processes associated with single impurities. Therefore, in this limit, we expect the finite U corrections to be a sum of the single impurity corrections (4.58) over all j:

$$\sum_{m,j} e^{im\Pi_j} f_m(\partial_x^k \phi_1(j\ell), \partial_x^l \phi_2(j\ell)) \tag{4.61}$$

Our main task is to translate the correction terms (4.61) into the low energy theory with

8. Here the reason that the Π_j operator takes a simpler form is that the matrix $\mathcal{N}_{ji} = -\frac{1}{(2\pi)^2}[C_j, [C_i, H_0]]$ is diagonal.

two linearly dispersing phonon modes (4.3). We start with the operator $f_m(\partial_x^k \phi_1, \partial_x^l \phi_2)$. To translate this operator into the low energy theory, we note that $\partial_x \phi_1$ and $\partial_x \phi_2$ are linearly related to $a_{n,k}, a_{n,k}^\dagger$, which are in turn linearly related to $\partial_x \phi_\rho$ and $\partial_x \phi_\sigma$. Hence the f_m operator corresponds to some function of the derivatives of ϕ_ρ and ϕ_σ, evaluated at $j\ell$. Next, consider the operator $e^{i\Pi_j}$. Translating this operator into the low energy theory requires more sophisticated arguments. First, we use the relation $[C_i, \Pi_j] = 2\pi i \delta_{ij}$ together with the identity (4.47) to deduce that

$$\left[\int dx \partial_x \phi_\sigma, e^{i\Pi_j} \right] = 4\pi (-1)^j e^{i\Pi_j} \tag{4.62}$$

Writing down the most general charge-conserving operator in the low energy theory that is consistent with these commutation relations, we derive

$$e^{i\Pi_j} = e^{i(-1)^j (\phi_\sigma(j\ell) - \beta_j)} (1 + ...) \tag{4.63}$$

where β_j is some unknown phase and the '...' includes terms built out of derivatives of ϕ_σ, ϕ_ρ. To fix the value of the β_j phases, or more precisely, the *relative* values of these phases, consider the operator

$$\mathcal{O} = \Pi_j + \Pi_{j+1} + C_j - C_{j+1} + \alpha_j - \alpha_{j+1} \tag{4.64}$$

The operator $\mathcal{O}$ has two important properties: (i) it is linear in the fields $\partial_x \phi_1, \partial_x \phi_2$, and (ii) it commutes with C_j for all j. (Here the second property follows from the commutation relation $[C_j, C_i] = i\pi(k_2 - k_1) \cdot \mathrm{sgn}(j - i)$). Given these two properties, it follows that $\mathcal{O}$ can be expanded as a linear combination of $a_{n,k}, a_{n,k}^\dagger$ since $a_{n,k}, a_{n,k}^\dagger$ form a complete basis for the set of operators satisfying (i), (ii).[15] This means that we have

$$\Pi_j + \Pi_{j+1} = \alpha_{j+1} - \alpha_j + C_{j+1} - C_j + \sum_{n,k} (\lambda_{n,k} \cdot a_{n,k} + h.c) \tag{4.65}$$

for some constants $\lambda_{n,k}$. If we now exponentiate both sides of this equation and take the ground state expectation value in the limit $U \to \infty$, we see that

$$\arg(\langle e^{i\Pi_j} e^{i\Pi_{j+1}} \rangle) = \alpha_{j+1} - \alpha_j \tag{4.66}$$

since $e^{iC_j} = e^{iC_{j+1}} = 1$ in this limit. Comparing this result to the expression (4.63), we deduce that $\beta_{j+1} - \beta_j = (-1)^j(\alpha_{j+1} - \alpha_j)$ as in Eq. (4.53).

Putting this all together, we conclude that the finite U corrections (4.61) take the following form in the low energy theory:

$$\sum_{m,j} e^{im(-1)^j(\phi_\sigma(j\ell)-\beta_j)} \tilde{f}_m(\partial_x^k \phi_\rho(j\ell), (-1)^j \partial_x^l \phi_\sigma(j\ell)) \tag{4.67}$$

Here β_j is given by Eq. (4.53) and $\tilde{f}_m$ are some unknown functions. The reason for the factor of $(-1)^j$ multiplying $\partial_x^l \phi_\sigma$ is that ϕ_σ describes a mode near $k = \pi/\ell$, and therefore the relation between ϕ_σ and ϕ_1, ϕ_2 alternates sign at every impurity. The same reasoning explains why there is no factor of $(-1)^j$ multiplying $\partial_x^k \phi_\rho$ since ϕ_ρ describes a mode near $k = 0$.

From Eq. (4.67), we can immediately read off the correction terms that are proportional to the two 'dangerous' perturbations, $\partial_x\phi_\rho\partial_x\phi_\sigma$ and $e^{\pm i\phi_\sigma}\partial_x\phi_\rho$. Specifically, we can see that $\partial_x\phi_\rho\partial_x\phi_\sigma$ appears in the $m = 0$ terms, and takes the form $\sum_j (-1)^j \partial_x\phi_\rho(j\ell)\partial_x\phi_\sigma(j\ell)$. Likewise, $e^{\pm i\phi_\sigma}\partial_x\phi_\rho$ appears in the $m = \pm 1$ terms and takes the form $\sum_j \cos(\phi_\sigma(j\ell) - \beta_j)\partial_x\phi_\rho(j\ell)$. This completes our derivation of Eqs. (4.51) and (4.52).

4.5 Generalized models

Thus far we have focused on the toy model (4.1). This model has several special (and unrealistic) properties: (i) the impurities are arranged in a perfect lattice, and (ii) the two modes ϕ_1 and ϕ_2 move at the same speed v and are decoupled from one another. We now

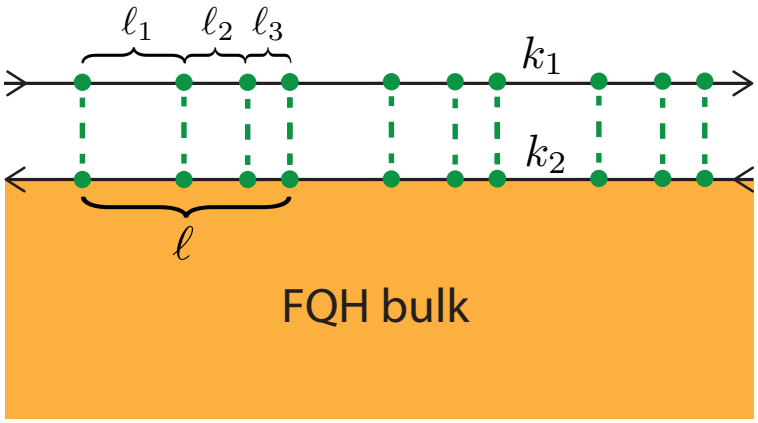

Figure 4.3: Generalized impurity lattice model with three impurities per unit cell. The unit cell has length ℓ while the spacings between the impurities are ℓ_1, ℓ_2 and ℓ_3.

investigate whether the charge and neutral modes persist under more realistic conditions. We build up to the most realistic case in several steps. First, in section 4.5.1, we consider what happens when the velocity matrix is arbitrary, the impurities form a lattice with an arbitrary unit cell, and $U \to \infty$. Then, in section 4.5.2, we consider the case where the velocity matrix is arbitrary, the impurities are *randomly* positioned, and $U \to \infty$. Finally, in section 4.5.2, we consider the most realistic case of an arbitrary velocity matrix, random impurities and a finite U.

4.5.1 General impurity lattices

In this section we generalize the toy model in two ways. First, instead of focusing on the simplest possible impurity lattice, with only one impurity per unit cell, we consider a *general* lattice with m impurities in a unit cell of length ℓ with arbitrary spacing $\ell_1, ..., \ell_m$ (Fig. 4.3). Second, instead of assuming that the two modes ϕ_1 and ϕ_2 are decoupled from one another and move with the same speed v, we consider an arbitrary velocity matrix V_{ij}. That is, we consider a Hamiltonian of the form H^{gen} (4.7), with the impurities arranged in a general lattice.

Structure of low energy modes

We begin by analyzing the phonon modes for these more general systems. Our main result is that when $U \to \infty$ these systems have two low energy phonon modes, whose creation/annihilation operators we denote by $a_{\rho,k}$ and $a_{\sigma,k}$ (see below for their definitions). These modes are described by an effective Hamiltonian of the form

$$\overline{H}_{\text{eff}} = \int_0^\Lambda dk \;\; (v_\rho k a^\dagger_{\rho,k} a_{\rho,k} + v_\sigma k a^\dagger_{\sigma,-k} a_{\sigma,-k}) \tag{4.68}$$

where $v_\rho, v_\sigma > 0$ are defined below and $\Lambda \ll 1/\ell$ is a momentum cutoff.

The calculation is very similar to the one for the toy model. Indeed, Bloch's theorem guarantees that the phonon creation and annihilation operators $a_{n,k}$ take the same form as before:

$$a_{n,k} = \int \frac{dx}{\sqrt{|E_{n,k}|}} e^{-ikx} (u_{n,k}(x)\partial_x\phi_1 + w_{n,k}(x)\partial_x\phi_2) \tag{4.69}$$

where k takes values in the Brillouin zone $[-\pi/\ell, \pi/\ell]$ and $u_{n,k}(x), w_{n,k}(x)$ are periodic functions with period ℓ. The effective Hamiltonian also takes the same form as before:

$$H_{\text{eff}} = \sum_n \int_{-\pi/\ell}^{\pi/\ell} dk \; \Theta(E_{n,k}) \; E_{n,k} a^\dagger_{n,k} a_{n,k}$$

Thus, all we have to do is find the phonon energies $E_{n,k}$ and the Bloch functions $u_{n,k}(x), w_{n,k}(x)$. Proceeding in exactly the same way as in section 4.3.2, these quantities can be obtained by solving an eigenvalue equation of the form given in Eq. (4.29):

$$T_{\text{cell}}(E) \cdot \begin{pmatrix} A \\ B \end{pmatrix} = e^{-ik\ell} \begin{pmatrix} A \\ B \end{pmatrix} \tag{4.70}$$

where T_{cell} is the transfer matrix associated with a single unit cell. The only difference from the toy model is that the transfer matrix T_{cell} is more complicated due to the fact that the

unit cell contains m impurities, and the velocity matrix is more general. In particular, T_{cell} is given by

$$T_{\text{cell}}(E) = TD(E\ell_m)T \cdots TD(E\ell_1) \tag{4.71}$$

where $D(x) = e^{-iWx}$ and $W = KV^{-1}$ and $K = \begin{pmatrix} k_1 & 0 \\ 0 & -k_2 \end{pmatrix}$.

Eq. (4.70) tells us the entire phonon band structure, but for our purposes, we only need to understand the *low energy* phonon modes. Therefore, in what follows we will focus on solving (4.70) in the limit of small E. To this end, we expand $T_{\text{cell}}(E)$ to linear order in E. Using the fact that $T^2 = \mathbb{1}$, we obtain:

$$T_{\text{cell}}(E) = \begin{cases} T - iE(TW\ell_{\text{odd}} + WT\ell_{\text{even}}) & \text{if } m \text{ is odd} \\ \mathbb{1} - iE(W\ell_{\text{odd}} + TWT\ell_{\text{even}}) & \text{if } m \text{ is even} \end{cases} \tag{4.72}$$

where

$$\begin{aligned} \ell_{\text{odd}} &= \ell_1 + \ell_3 + \cdots \\ \ell_{\text{even}} &= \ell_2 + \ell_4 + \cdots \end{aligned} \tag{4.73}$$

From these expressions, we can readily compute the eigenvectors and eigenvalues of T_{cell}. First suppose m is odd. In this case, perturbation theory gives the following eigenvalues for T_{cell}:

$$1 - iE\ell/v_\rho, \quad -1 - iE\ell/v_\sigma \tag{4.74}$$

where

$$v_\rho = \frac{2}{\text{Tr}(TW + W)}, \quad v_\sigma = \frac{2}{\text{Tr}(TW - W)} \tag{4.75}$$

Substituting these expressions into Eq. (4.70), we see that there are two low energy phonon modes, which are located near $k = 0$ and $k = \pi/\ell$ and have velocities v_ρ and $-v_\sigma$ respectively

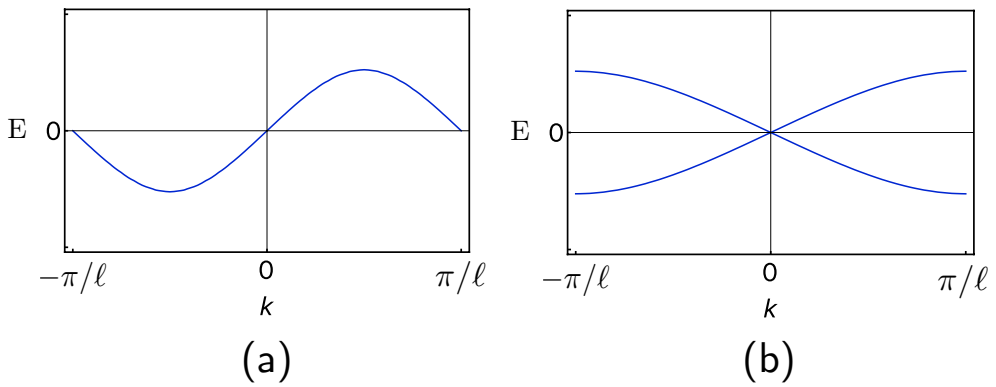

Figure 4.4: A schematic figure illustrating the difference between band structures with an odd and even number of impurities per unit cell. In the odd case (a), the phonon bands have zeros at $k = 0$ and $k = \pi/\ell$. In the even case (b), the phonon bands have both zeros at $k = 0$.

(Fig. 4.4(a)).

Similarly, when m is even, perturbation theory gives the following eigenvalues for T_{cell}:

$$1 - iE\ell/v_\rho, \quad 1 + iE\ell/v_\sigma \tag{4.76}$$

where v_ρ^{-1} and $-v_\sigma^{-1}$ are the two eigenvalues of the matrix

$$\widetilde{W} = W\ell_{\text{odd}} + TWT\ell_{\text{even}}, \tag{4.77}$$

Plugging these expressions into Eq. (4.70), we see that there are again two low energy phonon modes, but now both are located near $k = 0$ with velocities v_ρ and $-v_\sigma$ (Fig. 4.4(b)).

Combining these results, we see that for either parity of m, the lowest energy modes are described by the effective Hamiltonian (4.68) — where $a_{\rho,k}$ and $a_{\sigma,k}$ are the creation/annihilation operators for the two low energy modes. Note that the definitions of $a_{\rho,k}$ and $a_{\sigma,k}$ are different depending on whether m is odd or even due to the fact that the modes are located in different places in k space. If m is odd, then

$$a_{\rho,k} \equiv a_{0,k}, \quad a_{\sigma,k} \equiv a_{0,k+\pi/\ell}$$

as in Eq. 4.34, while if m is even,

$$a_{\rho,k} \equiv a_{0,k}, \quad a_{\sigma,k} \equiv a_{1,k}$$

where '0' and '1' are the band indices for the two bands that pass through $k = 0$ and $E = 0$.

Expression for density operator

In order to understand how much charge is carried by these low energy modes, we now express the (coarse-grained) density operator $\bar{\rho}(x)$ in terms of $a_{\rho,k}$ and $a_{\sigma,k}$. As in section 4.3.4, the first step is to express the microscopic density operator $\rho(x) = \frac{1}{2\pi}(\partial_x\phi_1 + \partial_x\phi_2)$ in terms of $a_{n,k}$. This step closely parallels the derivation of Eq. (4.40), and the result takes a similar form:

$$\rho(x) = \sum_n \int_{-\frac{\pi}{\ell}}^{\frac{\pi}{\ell}} dk \ \sqrt{|E_{n,k}|} e^{ikx} z_{n,k}(x) a_{n,k} \tag{4.78}$$

where

$$z_{n,k}(x) = \begin{pmatrix} 1 & 1 \end{pmatrix} \cdot V^{-1} \cdot \begin{pmatrix} u_{-n,-k}(x) \\ w_{-n,-k}(x) \end{pmatrix} \tag{4.79}$$

As before, the quantity that we want to compute is the *coarse-grained* density $\bar{\rho}(x)$, obtained by spatially averaging $\rho(x)$ over a length scale of order $1/\Lambda$, where Λ is a momentum cutoff much smaller than $1/\ell$. To perform this spatial averaging step, we restrict the integral in (4.78) to $|k| \leq \Lambda$, and replace $z_{n,k}(x) \to \bar{z}_{n,k}$ where $\bar{z}_{n,k}$ is defined by averaging $z_{n,k}(x)$ over a unit cell. This gives:

$$\bar{\rho}(x) = \sum_n \int_{-\Lambda}^{\Lambda} dk \ \sqrt{|E_{n,k}|} e^{ikx} \bar{z}_{n,k} a_{n,k} \tag{4.80}$$

To complete the calculation, we need to project the above expression to the Hilbert space generated by the low energy phonon modes. This projection step gives a different

result depending on whether m is odd or even. If m is odd, then just as in section 4.3.4, there is only one low energy mode with $|k| \leq \Lambda$, namely $a_{\rho,k}$ ($\equiv a_{0,k}$), so we obtain

$$\bar{\rho}(x) = \int_{-\Lambda}^{\Lambda} dk \ \sqrt{|v_\rho k|} e^{ikx} \bar{z}_{\rho,k} a_{\rho,k} \tag{4.81}$$

On the other hand, if m is even, then there are two low energy modes with $|k| \leq \Lambda$, namely $a_{\rho,k}$ ($\equiv a_{0,k}$) and $a_{\sigma,k}$ ($\equiv a_{1,k}$) so we derive

$$\bar{\rho}(x) = \int_{-\Lambda}^{\Lambda} dk \ e^{ikx} (\sqrt{|v_\rho k|} \bar{z}_{\rho,k} a_{\rho,k} + \sqrt{|v_\sigma k|} \bar{z}_{\sigma,k} a_{\sigma,k}) \tag{4.82}$$

Here $z_{\rho,k}, z_{\sigma,k}$ are defined by

$$\begin{aligned} z_{\rho,k}(x) &= \begin{pmatrix} 1 & 1 \end{pmatrix} \cdot V^{-1} \cdot \begin{pmatrix} u_{\rho,-k}(x) \\ w_{\rho,-k}(x) \end{pmatrix} \\ z_{\sigma,k}(x) &= \begin{pmatrix} 1 & 1 \end{pmatrix} \cdot V^{-1} \cdot \begin{pmatrix} u_{\sigma,-k}(x) \\ w_{\sigma,-k}(x) \end{pmatrix} \end{aligned} \tag{4.83}$$

while $\bar{z}_{\rho,k}$ and $\bar{z}_{\sigma,k}$ are defined by averaging $z_{\rho,k}(x)$ and $z_{\sigma,k}(x)$ over a unit cell.

Conditions for neutral mode

With this preparation we are ready to tackle the main question: determining the conditions under which the σ mode is electrically neutral. Our main result is that the σ mode is neutral in two cases: (a) m is odd, or (b) m is even and

$$\ell_{\text{odd}} = \ell_{\text{even}} \tag{4.84}$$

where ℓ_{odd} and ℓ_{even} are defined as in Eq. (4.73).

We start with case (a). This case is quite simple since when m is odd, $a_{\sigma,k}$ does not appear

at all in the expression for $\bar{\rho}$ as we can see from Eq. (4.81). It thus follows immediately that the σ mode is neutral in this case.

Case (b) is more subtle. Indeed, when m is even, $a_{\sigma,k}$ *does* appear in $\bar{\rho}$ (4.82) so to determine the amount of charge carried by the σ mode, we need to compute the coefficient $\bar{z}_{\sigma,k}$ that multiplies $a_{\sigma,k}$. In fact, since we are interested in low energy properties, the relevant quantity is the $k \to 0$ limit of this coefficient, $\bar{z}_{\sigma,0}$.

We compute this quantity in three steps. First, we find the eigenvectors of $T_{\text{cell}}(E)$ (4.71) in the $E \to 0$ limit. To this end, recall from Eq. (4.72) that $T_{\text{cell}}(E)$ can be approximated by

$$T_{\text{cell}}(E) \approx \mathbb{1} - iE(W\ell_{\text{odd}} + TWT\ell_{\text{even}}) \tag{4.85}$$

Conveniently, this expression is easy to diagonalize when $\ell_{\text{odd}} = \ell_{\text{even}}$. Indeed, in this case, one can check that

$$[T, W\ell_{\text{odd}} + TWT\ell_{\text{even}}] = 0 \tag{4.86}$$

since $T^2 = \mathbb{1}$. It follows that the eigenvectors of $T_{\text{cell}}(E)$ are the same as T, namely: $(1\ 1)^T$ and $(k_1\ k_2)^T$.

Next, we substitute the above eigenvectors into the expressions for the Bloch functions, u, w. These expressions, which can be derived in a similar fashion to Eqs. (4.32), are as follows:

$$\begin{pmatrix} u(x) \\ w(x) \end{pmatrix} = e^{ik\{x\}} \cdot e^{-iEW(x-x_j)} \cdot \begin{pmatrix} A^{(j)} \\ B^{(j)} \end{pmatrix}, \tag{4.87}$$

where

$$\begin{pmatrix} A^{(j)} \\ B^{(j)} \end{pmatrix} = TD(E\ell_j) \cdots TD(E\ell_1) \cdot \begin{pmatrix} A \\ B \end{pmatrix} \tag{4.88}$$

Here we assume that x is located between the jth and $j+1$st impurities, i.e. $x_j \leq x < x_{j+1}$,

and $\{x\}$ is defined by $\{x\} = x - p\ell$, for $p\ell \leq x < (p+1)\ell$.

We start with the second eigenvector. Letting $(A\ B) = (k_1\ k_2)$ and $E = k = 0$ in Eqs. (4.87-4.88) gives

$$\begin{pmatrix} u(x) \\ w(x) \end{pmatrix} = \pm \begin{pmatrix} k_1 \\ k_2 \end{pmatrix} \tag{4.89}$$

with the sign *alternating* across each impurity. This alternating sign is due to the fact that $(k_1\ k_2)^T$ is an eigenvector of T with eigenvalue -1. Likewise, letting $(A\ B) = (1\ 1)$ gives

$$\begin{pmatrix} u(x) \\ w(x) \end{pmatrix} = \begin{pmatrix} 1 \\ 1 \end{pmatrix} \tag{4.90}$$

Note that the sign does not alternate in this case since $(1\ 1)^T$ is an eigenvector of T with eigenvalue $+1$.

To complete the calculation, we identify $(k_1\ k_2)$ with the σ mode and $(1\ 1)$ with the ρ mode and then we average the above Bloch functions over a unit cell and plug them into (4.83) to obtain $\bar{z}_{\sigma,0}$ and $\bar{z}_{\rho,0}$. We start with σ: in this case, the averaging step gives $\bar{u}_{\sigma,0} = \bar{w}_{\sigma,0} = 0$ since there is *perfect cancellation* between the '+' and '−' signs due to the fact that $\ell_{even} = \ell_{odd}$. Hence, when we plug this into (4.83), we obtain $\bar{z}_{\sigma,0} = 0$. We conclude that the σ mode is neutral in the low energy, long wavelength limit, to lowest order in k. For comparison, if we repeat this calculation for the ρ mode, the averaging step gives $\bar{u}_{\rho,k} = \bar{w}_{\rho,k} \neq 0$ since the sign does not alternate in this case. It follows that $\bar{z}_{\rho,0} \neq 0$, so the ρ mode carries charge in the low energy, long wavelength limit.

4.5.2 Random impurities

In this section, we consider systems with *randomly* distributed impurities. We start with the $U \to \infty$ case and then consider the case where U is large but *finite*.

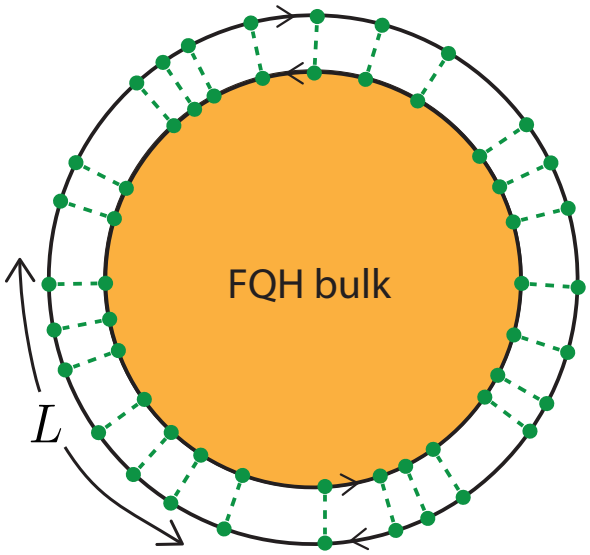

Figure 4.5: Random impurity model: two counter-propagating chiral Luttinger liquids in a circular geometry of length L, together with M randomly positioned impurity scatterers.

Infinite U

Given the results from the previous section, one might expect random impurity systems to have a neutral mode in the limit $U \to \infty$ since the 'even' and 'odd' spacings are equal on average. Here we show that this intuition is correct.

Our basic setup is as follows. We consider a circular edge of circumference L with M randomly positioned impurities. We denote the spacing between the impurities by $\ell_1, ..., \ell_M$, and the average spacing by $\bar{\ell} = L/M$ (Fig. 4.5). We show that this system supports two low energy phonon modes, one of which is neutral and one of which is charged, and neither of which is localized.

The first step in our analysis is to view the random system as an impurity lattice consisting of a single unit cell of length L. We can then carry over all of our results on impurity lattices by simply setting $\ell = L$, $m = M$, and $k = 0$. In particular, if we make these substitutions in (4.70), we obtain the eigenvalue equation

$$T_{sys}(E) \cdot \begin{pmatrix} A \\ B \end{pmatrix} = \begin{pmatrix} A \\ B \end{pmatrix} \tag{4.91}$$

where

$$T_{sys}(E) = TD(E\ell_M)T \cdots TD(E\ell_1) \tag{4.92}$$

is the transfer matrix describing the entire system. As before, every solution (E, A, B) to this eigenvalue equation defines a phonon creation/annihilation operator with energy E.

The next step is to solve the above eigenvalue equation in the limit $E \to 0$. We do this with the help of the following approximate expression for T_{sys}:

$$T_{sys}(E) = \exp\Big[-\frac{iEL}{2}(W + TWT) + O(E^{\frac{4}{3}} L \bar{\ell}^{\frac{1}{3}} \|W\|^{\frac{4}{3}}) \Big] \tag{4.93}$$

Here $\|W\|$ is defined as the magnitude of the largest eigenvalue of W (see Appendix C.3 for a derivation).

To use (4.93), we substitute it into (4.91) and neglect the error term. This approximation is justified at sufficiently low energies, i.e.,

$$E \ll \frac{1}{L^{3/4} \bar{\ell}^{1/4} \|W\|} \tag{4.94}$$

The result of the substitution is:

$$\exp\left[-\frac{iEL}{2}(W + TWT) \right] \cdot \begin{pmatrix} A \\ B \end{pmatrix} = \begin{pmatrix} A \\ B \end{pmatrix} \tag{4.95}$$

Next, we observe that the following commutator vanishes, as in Eq. (4.86):

$$[T, W + TWT] = 0$$

It follows that the matrix on the left hand side of (4.95) has the same eigenvectors as T,

namely $\begin{pmatrix}1\\1\end{pmatrix}, \begin{pmatrix}k_1\\k_2\end{pmatrix}$. Thus,

$$\begin{pmatrix}A\\B\end{pmatrix} = \begin{pmatrix}1\\1\end{pmatrix} \text{ or } \begin{pmatrix}k_1\\k_2\end{pmatrix} \tag{4.96}$$

Plugging these eigenvectors into (4.95), we can extract the corresponding energies with straightforward linear algebra:

$$E_{\rho n} = v_\rho \cdot \frac{2\pi n}{L}, \quad \text{or} \quad E_{\sigma n} = v_\sigma \cdot \frac{2\pi n}{L} \tag{4.97}$$

where v_ρ, v_σ are given by the formulas in (4.75) and $n = 1, 2, ...$, etc.

We can now derive both of our claims about the low energy phonon modes — namely (1) they are not localized and (2) one is charged and the other is neutral. To see that the low energy phonon modes are not localized, notice that the energy levels in (4.97) are equally spaced with a spacing proportional to $1/L$: this level spacing indicates that the localization length ξ is larger than the system size L for any E satisfying (4.94). To see that the σ mode is neutral, notice that the eigenvector $\begin{pmatrix}k_1\\k_2\end{pmatrix}$ associated with the σ mode is an eigenvector of T with eigenvalue -1. As a result, the phonon creation/annihilation operators for this mode are of the form $a_{\sigma n} = \int dx(f_{\sigma n}(x)\partial_x\phi_1 + g_{\sigma n}(x)\partial_x\phi_2)$ where $f_{\sigma n}$ and $g_{\sigma n}$ alternate signs at each impurity. Like in section 4.5.1, these alternating signs suppress the contribution of the $a_{\sigma n}$ operator to the coarse-grained density $\bar{\rho}$ since the even and odd spacings are equal on average. It follows that the σ mode is neutral.

Finite U

We now consider the same setup as above, but with finite scattering strength U. Our main result is that the charge and neutral modes continue to persist at sufficiently large U.

Like the toy model, we study the effect of finite U by adding appropriate correction terms to the $U \to \infty$ low energy theory. For the random impurity model, the latter theory can be read off from the phonon dispersion relations (4.97): these expressions imply that the $U \to \infty$ low energy theory is a variant of $\overline{H}_{\rm eff}$ (4.3) where the ρ and σ modes have velocities v_ρ and v_σ instead of $\bar{v}$.

Since the low energy theory is almost the same as for the toy model, most of our analysis of finite U corrections can be repeated without change. As before, there are only two kinds of correction terms we need to worry about: $\partial_x\phi_\rho\partial_x\phi_\sigma$ and $e^{\pm i\phi_\sigma}\partial_x\phi_\rho$. Also as before, both of these terms are generated by finite U corrections, but with spatially dependent coefficients. The first term, $\partial_x\phi_\rho\partial_x\phi_\sigma$, appears in a combination of the form

$$\sum_j (-1)^j c_j \partial_x\phi_\rho\partial_x\phi_\sigma(x_j) \tag{4.98}$$

while $e^{\pm i\phi_\sigma}\partial_x\phi_\rho$ appears in a combination of the form

$$\sum_j d_j \cos(\phi_\sigma(x_j) - \beta_j)\partial_x\phi_\rho(x_j) \tag{4.99}$$

The only difference between these expressions and Eqs. (4.51) and (4.52) is that the coefficients c_j, d_j are j-dependent. This inhomogeneity is expected since each impurity experiences a different local environment due to the random spacing.

The rest of the argument is identical to the one for the toy model. As before, the alternating signs in the first expression and the random[9] β_j phases in the second expression have the effect of suppressing these two perturbations, making them *irrelevant* in the RG sense. Since these are the only perturbations that can hybridize the charge and neutral mode, we conclude that the charge and neutral mode structure persists at sufficiently large U, as claimed above.

9. We assume that the α_j are random for this model.

4.6 Conclusion

In this chapter we have presented a microscopic derivation of the neutral mode in various FQH edges, including the $\nu = 2/3$ edge. Our derivation applies to a particular set of models which consist of two counter-propagating chiral Luttinger liquids together with a collection of discrete impurity scatterers. Our main result is an *exact* solution of these models in the limit of infinitely strong impurity scattering. From this solution, we have explicitly shown that the low energy theory of these systems consists of decoupled charge and neutral modes. In addition we have shown that the charge and neutral modes survive at finite but sufficiently strong scattering as long as this scattering has a random spatial dependence.

It is interesting to circle back and compare our results with the original neutral mode analysis of Kane, Fisher, and Polchinski.[29] In that work, the authors studied a model similar to the random impurity model H^{gen} (4.7) for the case $k_1 = 1$ and $k_2 = 3$, i.e. the $\nu = 2/3$ state. Instead of a discrete set of scatterers, Ref. [29] considered a continuum scattering term of the form $\int dx(\xi(x)e^{ik_1\phi_1+ik_2\phi_2} + \text{H.c})$ where $\xi(x)$ is a Gaussian random variable with $\overline{\xi^*(x)\xi(x')} = U^2\delta(x-x')$ for some U.[10] While this model is not identical to H^{gen}, it is similar enough that we can compare results on a qualitative level. From this comparison we can see that the two works consider different parameter regimes. Ref. [29] established the existence of a neutral mode for the case where U is arbitrary but the velocity matrix V has the special property that the edge theory has nearly decoupled charge and neutral modes in the *absence* of electron scattering. In contrast, we derive the neutral mode for large U but *arbitrary* V. This difference in parameter regimes implies a conceptual difference between our two analyses: while Ref. [29] established the stability of the charge and neutral mode structure to small perturbations, we show that electron scattering can produce charge and neutral modes out of a system whose bare ($U = 0$) mode structure is completely different. In this sense, the results in this chapter are complementary to those of Ref. [29].

10. Here we have modified the notation of Ref. [29], where $\overline{\xi^*(x)\xi(x')} = W\delta(x-x')$, so that it is consistent with this paper.

One of the main achievements of this work has been to show that our models capture a nontrivial effect of impurity scattering, namely the emergent neutral mode. But impurity scattering also has another important effect on FQH edges: it provides a mechanism for equilibrating the chemical potential of different edge modes. Such equilibration is a crucial property of multi-mode edges and in fact is necessary to explain their observed quantized Hall conductance.[29, 8, 27] Thus, it is natural to ask whether our models capture this equilibration physics. The answer to this question depends on whether we consider finite or infinitely strong impurity scattering. In the case of finite scattering strength, we believe that our models do exhibit equilibration, as would be expected for any sufficiently generic system. On the other hand, in the case of infinite scattering strength, our models do not display equilibration since they are *integrable* (in fact quadratic) in this limit. Thus, while the infinite scattering limit provides an exactly solvable model for the neutral mode, it does not provide a model for edge equilibration physics.

We envision several directions for future work. One direction would be to extend our analysis to systems with more than two edge modes, such as the Jain states with filling fraction $n/(2n \pm 1)$ or a $\nu = 2/3$ state with edge reconstruction.[56] Many of these states are predicted to have neutral modes based on the same kind of RG analysis as in the original $\nu = 2/3$ proposal.[28, 54] Similarly, it would be interesting to apply our approach to systems with Majorana modes such as the anti-Pfaffian state.[44, 41]

Another direction would be to study the $\nu = 4/5$ edge. This example is interesting because, in our language, it corresponds to the case $k_1 = 1$ and $k_2 = 5$, so in particular it has $k_2 - k_1 > 2$. As we mentioned earlier, when $k_2 - k_1$ is larger than 2, the infinite scattering limit exhibits an extensive ground state degeneracy in addition to charge and neutral modes. This degeneracy poses basic challenges for determining whether the charge and neutral modes survive at finite scattering strength. Thus, a new approach may be needed to understand this case.

CHAPTER 5

CONCLUSION

5.1 Summary of results

In this thesis we investigated symmetry enriched topological phases. We addressed the problem of characterizing these phases by building exactly solvable models that realize them and by analyzing their edge theories.

In chapter 2 we presented a construction for building exactly solvable models of SET phases. This construction applied to a broad class of phases, namely 2D bosonic SET phases with finite, unitary onsite symmetry group. An important quality of this construction is its generality – we conjectured that the construction could be used to realize every SET phase in this class whose underlying topological can be realized by a string-net model. The models produced by this construction had a number of nice properties: they are exactly solvable, and they are closely related to the well studied string-net models. We illustrated our construction with a number of examples, including a model for the toric code with a $\mathbb{Z}_2$ symmetry that permutes the e and m particles.

In the third chapter we examined the edge theories of $\mathbb{Z}_2$ SPT and SET phases, and we addressed the question of when they can and cannot be gapped. For the case of $\mathbb{Z}_2$ SPT phases, we derived an invariant ν and proved that the edge can be gapped without breaking the symmetry if and only if $\nu = 0$. We then generalized these results to $\mathbb{Z}_2$ SET phases and proved that if the theory has a Lagrangian subgroup invariant under the symmetry, and a slightly modified invariant which we called ν^{set} is equal to zero, then the boundary can be gapped without breaking the symmetry. Our derivation relied on building perturbations that could explicitly gap the boundary, and proving that when the conditions are not satisfied no such perturbations exist.

In the last chapter, we investigated the phenomenon of decoupled charge and neutral modes which occurs in certain fractional quantum Hall states, including the $\nu = 2/3$ state.

These states pose a basic puzzle because a clean edge theory predicts charge propagation in both directions, contradicting experiments that detect charge propagation in only one direction. One solution to this problem, which was first introduced in Ref. [29], is to introduce imputing backscattering between the counterpropagating modes. We presented concrete models for impurity backscattering in these edge states. We solved these models in a particular limit, and were able to explicitly demonstrate the emergence of decoupled charge and neutral modes in this context. We then analyzed a sequence of increasingly realistic models, and proved that the decoupled charge and neutral modes persisted as long as the impurities were sufficiently strong and randomly distributed.

5.2 Future directions

One interesting direction for future work would be to study the results of chapter 3 in the context of the models introduced in chapter 2. In particular, it would be interesting to consider the symmetry enriched string-net models in a system with boundary, and explicitly derive an edge theory from the bulk, in a manner similar to Ref. [43]. For some simple SET phases, such as the toric code phase with the $e \leftrightarrow m$ symmetry, it would be interesting to analyze the corresponding spin model for the edge and provide an alternative derivation for why the edge must be gapless.

Another interesting direction would be to generalize the results of chapter 3 to fermionic SPTs and SETs. Preliminary work in this direction, to be included in a future publication, suggests that the bosonic SPT results generalize nicely to the fermionic case. In particular, we believe that the invariant ν takes the same form for fermionic SPTs, and also captures the $\mathbb{Z}_8$ classification in this case. More work needs to be done to prove the results for fermions since some of our derivation relied on the fact that the K-matrix was bosonic.

Finally, we believe that it would be interesting to extend the results of chapter 3 to non-Abelian phases. This case is more complicated because there is no longer a simple way to parametrize all the edge theories, unlike the K-matrix description for Abelian phases. As

a result, a more promising direction would be to determine if the edge can be gapped by analyzing the bulk data. In particular, we believe that the notion of a Lagrangian subgroup has a non-Abelian analogue known as a Lagrangian algebra. Such a Lagrangian algebra would need to be invariant under the symmetry, and we also expect there to be a non-Abelian generalization of the invariant ν, although it may be significantly more complicated in the general case.

APPENDIX A

APPENDICES FOR CHAPTER 2

A.1 Ground state degeneracy

In this appendix we calculate the degeneracy of the symmetric toric code on a sphere and torus and discuss the generalization to higher genus surfaces.[1] To begin, recall that the ground state degeneracy can be expressed using the following formula:

$$D = \mathrm{Tr}\left(\prod_l P_l \prod_v Q_v \prod_p B_p\right) \tag{A.1}$$

Next, observe that the operator $\prod_l P_l \prod_v Q_v$ projects onto the space of states that obey the fusion rules at each vertex and whose plaquette spin domain walls coincide with σ strings. Denoting this space of states by $\mathcal{X}$, we can simplify the calculation by only tracing over this space:

$$D = \mathrm{Tr}_{\mathcal{X}}\left(\prod_p B_p\right) \tag{A.2}$$

Next, recall that B_p is a sum of three terms: $B_p = \frac{1}{4}(1 + B_p^{\psi} + \sqrt{2}B_p^{\sigma}\tau_p^x)$. However, $B_p^{\sigma}\tau_p^x$ is clearly traceless because it contains the operator τ_p^x. We can therefore ignore this term in the trace and Eq. (A.2) simplifies further to

$$D = \mathrm{Tr}_{\mathcal{X}}\left(\prod_p \frac{1}{4}(1 + B_p^{\psi})\right) \tag{A.3}$$

To calculate the trace, it is convenient to use the basis states $|\{\tau_p^z, \mu_l\}\rangle$. We first note that

$$\langle \text{tadpole}| \prod_p \frac{1}{4}(1 + B_p^{\psi})|\text{tadpole}\rangle = 0 \tag{A.4}$$

1. To define the symmetric toric code on a sphere or on other surfaces, we generalize the model from the honeycomb lattice to an arbitrary trivalent lattice in the obvious way.

where $|\text{tadpole}\rangle$ is any basis state $|\{\tau_p^z, \mu_l\}\rangle$ in $\mathcal{X}$ containing a σ loop with an odd number of ψ strings ending on it (these are states for which $f(X) = 0$ in Eq. (2.18). We will not prove this result here, but it is easy to show using expression (2.9) for B_p^ψ.

From (A.4) it follows that the only basis states in $\mathcal{X}$ that contribute to the trace are the *no-tadpole* states, i.e. states in which every σ loop has an even number of ψ strings ending on it. Denoting this set of no-tadpole states by $\mathcal{Z}$, we derive

$$D = \sum_{Z \in \mathcal{Z}} \langle Z | \prod_p \frac{1}{4}(1 + B_p^\psi) | Z \rangle \tag{A.5}$$

Expanding out the product, we obtain

$$D = \frac{1}{4^N} \sum_{Z \in \mathcal{Z}} \sum_R \langle Z | \prod_{p \in R} B_p^\psi | Z \rangle \tag{A.6}$$

where N is the number of plaquettes and the second sum runs over subsets R of the set of plaquettes. To proceed further, we note that

$$\langle Z | \prod_{p \in R} B_p^\psi | Z \rangle = 0 \text{ or } 1 \tag{A.7}$$

for any no-tadpole state $Z \in \mathcal{Z}$ and any subset of plaquettes R. Again, we will not prove this identity here, but it can be derived using (2.9). Combining (A.6) and (A.7), we can rewrite D as

$$D = \frac{M}{4^N} \tag{A.8}$$

where M is the number of pairs $(|Z\rangle, R)$ such that $\prod_{p \in R} B_p^\psi |Z\rangle = |Z\rangle$.

Our problem is now to compute M. Conveniently, this counting problem can be reduced to a simple group theory calculation. The key point is that we can think of each operator $\prod_{p \in R} B_p^\psi$ as an element of the group $G = (\mathbb{Z}_2)^N$ since $(B_p^\psi)^2 = 1$, and since the B_p^ψ operators commute with one another. From this point of view, the B_p^ψ operators define an action of

the group $G = (\mathbb{Z}_2)^N$ on the subpace spanned by the no-tadpole states. In fact, the B_p^ψ operators also define a group action on the *set* $\mathcal{Z}$ (as opposed to the subspace spanned by $\mathcal{Z}$) since one can easily see that when the operator B_p^ψ acts on a no-tadpole state, it always gives back another no-tadpole state (up to a $\pm$ sign, which we will ignore).

With this identification, the problem of computing M is equivalent to finding the number of fixed points of the above group action for each group element $g \in (\mathbb{Z}_2)^N$ and then summing over all g. Conveniently, the latter quantity can be related to the number of orbits of the group action via Burnside's lemma:

$$M = |(\mathbb{Z}_2)^N| \cdot (\text{number of orbits of group action}) \tag{A.9}$$

All that remains is to find the number of orbits of the above group action. To this end, we observe that the B_p^ψ operators do not affect the σ strings or the spins τ_p^z, so there is at least one orbit for each configuration of σ loops and τ_p^z spins. In fact, in a spherical geometry, it is not hard to see that there is *exactly* one orbit for each configuration of σ loops and τ_p^z spins. It follows that the number of orbits is 2^N since there are 2^{N-1} different configurations of σ loops and there are 2 possibilities for the τ^z spins for each σ loop confiuration. Substituting this into (A.9) and (A.8), we immediately derive

$$D_{\text{sphere}} = \frac{2^N \cdot 2^N}{4^N} = 1 \tag{A.10}$$

In contrast, on a torus the situation is different because there are 4 orbits for each configuration of σ loops and τ_p^z spins. This additional factor of 4 comes from the fact that the B_p^ψ operators do not affect the parity of the number of ψ strings wrapping around the two non-contractible cycles of the torus; the 4 orbits correspond to the four possibilities of even/odd parity for each of the two cycles. We conclude that the number of orbits is $4 \cdot 2^N$, which gives a degeneracy of

$$D_{\text{torus}} = 4 \tag{A.11}$$

More generally, on a surface of genus g, the number of non-contractible cycles is $2g$, so the number of orbits is $4^g \cdot 2^N$ and the degeneracy is $D_g = 4^g$.

A.2 Derivation of ground state wave function

In this appendix we explain how to derive formula (2.18) for the ground state wave function of the symmetric toric code model. The first step is to solve the three eigenvalue equations in (2.16), each of which tells us something about the structure of the ground state $|\Psi\rangle$. The first equation, $P_l|\Psi\rangle = |\Psi\rangle$, implies that the only configurations $|\{\tau_p^z, \mu_l\}\rangle$ that appear in $|\Psi\rangle$ are those with $\mu_l = \sigma$ along the domain walls of the τ_p^z spins. The second equation, $Q_v|\Psi\rangle = |\Psi\rangle$, tells us that the only configurations that appear in $|\Psi\rangle$ are those in which the μ_l states obey the fusion rules at every vertex (Fig. 2.2). The last equation, $B_p|\Psi\rangle = |\Psi\rangle$, is more subtle and tells us something about the relative amplitudes of the configurations in the ground state. In fact, this equation tells us that these amplitudes are equal to the corresponding ground state amplitudes of the doubled Ising string-net model:

$$\Psi(\{\tau_p^z, \mu_l\}) = \Psi^{di}(\{\mu_l\}) \tag{A.12}$$

Here Ψ^{di} denotes the ground state of the doubled Ising string-net model and $|\{\mu_l\}\rangle$ denotes a string-net basis state with string occupations specified by μ_l.

To prove Eq. (A.12), it suffices to show that the $|\Psi\rangle$ defined in Eq. (A.12) satisfies $B_p|\Psi\rangle = |\Psi\rangle$. To this end, we make three observations. The first observation is that the $|\Psi\rangle$ defined in Eq. (A.12) is symmetric under the $\mathbb{Z}_2$ symmetry S so it can be expanded as a linear combination of *symmetrized* states, defined by:

$$|\{\mu_l\}, \mathrm{sym}\rangle \equiv \frac{1}{\sqrt{2}}(|\{\tau_p^z, \mu_l\}\rangle + |\{-\tau_p^z, \mu_l\}\rangle) \tag{A.13}$$

Furthermore, Eq. (A.12) tells us that the expansion coefficients in this linear combination

are given by

$$\langle \{\mu_l\}, \mathrm{sym} | \Psi \rangle = \sqrt{2} \langle \{\mu_l\} | \Psi^{di} \rangle \tag{A.14}$$

The second observation is that the matrix elements of B_p between symmetrized states are identical to the corresponding matrix elements of the plaquette operator B_p^{di} in the doubled Ising string-net model:

$$\langle \{\mu_l'\}, \mathrm{sym} | B_p | \{\mu_l\}, \mathrm{sym} \rangle = \langle \{\mu_l'\} | B_p^{di} | \{\mu_l\} \rangle \tag{A.15}$$

Indeed, this identity follows easily from the definition of B_p^{di} — namely $B_p^{di} \equiv a_1 B_p^1 + a_\psi B_p^\psi + a_\sigma B_p^\sigma$. The third and final observation is that the doubled Ising ground state obeys $B_p^{di} |\Psi^{di}\rangle = |\Psi^{di}\rangle$. Putting these three observations together, the claim follows immediately.

With Eq. (A.12) in hand, all we have to do to derive formula (2.18) is to compute the ground state wave function of the doubled Ising string-net model and show that it agrees with (2.18). This computation is discussed in section 2.3.1.

A.3 The other toric code with $e \leftrightarrow m$ symmetry

Previous work has shown that there are *two* distinct toric code phases that have a $\mathbb{Z}_2$ symmetry that exchanges e and m.[3] However, we have only discussed how to realize one of these phases — namely the symmetric toric code. In this appendix, we briefly explain how to realize the other phase.

First we need to describe the $\mathbb{Z}_2$-extensions corresponding to the two phases. The $\mathbb{Z}_2$ extension for the symmetric toric code is $\mathcal{D} = \{1, \psi, \sigma\}$ with fusion rules and F-symbols coming from the Ising fusion category. In comparison, the $\mathbb{Z}_2$ extension for the other toric code phase is also $\mathcal{D} = \{1, \psi, \sigma\}$ but with F-symbols coming from the $(\mathrm{Ising})^3$ fusion category.[33] Note that the two extensions are nearly identical to one another, with the only difference being that they have slightly different F-symbols.

Because the two extensions are so similar, the corresponding lattice models are also

closely related. Indeed, using the general construction from section 2.4, we find that the Hamiltonian for the other toric code phase is identical to that of the symmetric toric code except that the B_p^σ term given in Eq. (2.10) is replaced with

$$B_{p,ghijkl}^{\sigma,g'h'i'j'k'l'}(abcdef) = \delta_{\sigma gg'} \cdots \delta_{\sigma ll'} \cdot (-2)^{-\frac{Np\sigma}{4}} (-1)^{N_{p2}} \tag{A.16}$$

(Here, the only change is $2 \to -2$). This minor change in the Hamiltonian also leads to a minor modification of the ground state wave function. Instead of Eq. (2.18) we have

$$\Psi(X) \equiv \langle X|\Psi\rangle = (-\sqrt{2})^{N_\sigma(X)} f(X). \tag{A.17}$$

Everything else, including the form of the string operators, is identical to the symmetric toric code case.

To see that these two models belong to distinct SET phases, consider their corresponding gauge theories. By construction, gauging the symmetric toric code model gives a system with Ising$\times\overline{\text{Ising}}$ anyons, while gauging the other model gives a system with $(\text{Ising})^3 \times (\overline{\text{Ising}})^3$ anyons. Since these two gauge theories have distinct braiding statistics, it follows that the two ungauged models cannot be smoothly connected without closing the energy gap or breaking the symmetry. [43]

A.4 Derivation of string operators

In this appendix, we derive the W_e and W_m string operators (2.19), (2.22). We do this in two steps: first we construct string operators for the doubled Ising string-net model, and then we translate these over to the symmetric toric code using the connection between the two models.

To begin, we need to understand the relationship between the anyon excitations in the two systems. Given that the doubled Ising string-net model is equivalent to the *gauged* toric code

model, we know that one of the anyon excitations of the former system can be identified with the $\mathbb{Z}_2$ gauge charge in the latter system. The obvious candidate is $\psi\bar{\psi}$ since this is the only Abelian excitation with bosonic statistics. With this identification, we immediately deduce that the anyons $\{\sigma, \bar{\sigma}, \sigma\bar{\psi}, \bar{\sigma}\psi\}$ correspond to $\mathbb{Z}_2$ gauge fluxes since they have mutual statistics of π with respect to $\psi\bar{\psi}$. Likewise, the remaining anyons, $\{1, \psi, \bar{\psi}, \psi\bar{\psi}, \sigma\bar{\sigma}\}$, correspond to zero-flux excitations since they have mutual statistics of 0 with respect to $\psi\bar{\psi}$.

Consider the latter set of anyons $\{1, \psi, \bar{\psi}, \psi\bar{\psi}, \sigma\bar{\sigma}\}$ and the string operators $\{W_1, W_\psi, W_{\bar{\psi}}, W_{\psi\bar{\psi}}, W_{\sigma\bar{\sigma}}\}$ that create them. Because these anyons do not involve any gauge flux, it follows that they can be 'ungauged' and mapped onto excitations of the symmetric toric code model. In terms of string operators, this means we can ungauge $\{W_1, W_\psi, W_{\bar{\psi}}, W_{\psi\bar{\psi}}, W_{\sigma\bar{\sigma}}\}$ so as to construct string operators in the symmetric toric code model. In fact, by following the ungauging procedure described in section 2.3.4, one can show that this ungauging step is completely trivial in this case: to ungauge one of the above string operators, we simply embed them, without any changes, in the symmetric toric code Hilbert space. We will therefore abuse notation and use the same symbol W_a to denote a string operator and its ungauged counterpart.

After this ungauging step, $\{W_1, W_\psi, W_{\bar{\psi}}, W_{\psi\bar{\psi}}, W_{\sigma\bar{\sigma}}\}$ define string operators in the symmetric toric code model, which means they can be expanded as linear combinations of the four elementary string operators $\{W_1, W_e, W_m, W_{em}\}$. Conveniently, the coefficients in these linear combinations are fixed by general considerations (up to local operators acting at the ends of the strings):

$$\begin{aligned} W_\psi \sim W_{em}, \quad W_{\bar{\psi}} \sim W_{em}, \quad W_{\psi\bar{\psi}} \sim W_1 \\ W_{\sigma\bar{\sigma}} \sim W_e + W_m \end{aligned} \tag{A.18}$$

Here, the first two relations follow from the fact that W_ψ and $W_{\bar{\psi}}$ create fermions and therefore must map onto W_{em}, while the third relation follows from the fact that $\psi\bar{\psi}$ is a $\mathbb{Z}_2$

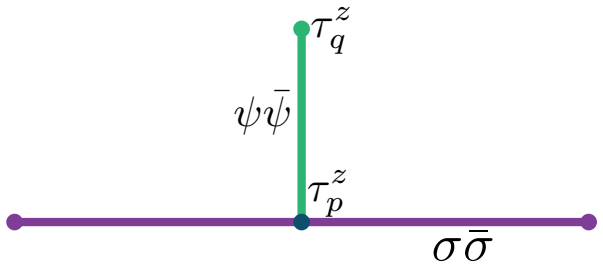

Figure A.1: The 'T-junction' operator $W_{\sigma\bar{\sigma}\perp\psi\bar{\psi}}$ is made up of two string operators $W_{\sigma\bar{\sigma}}$, $W_{\psi\bar{\psi}}$ which meet at a point p.

gauge charge, which is trivial in the ungauged theory. As for the last relation, this follows from two observations: (1) $\sigma\bar{\sigma}$ has mutual statistics π with respect to ψ, and (2) $W_{\sigma\bar{\sigma}}$ is *even* under the $\mathbb{Z}_2$ symmetry (as is every gauge invariant operator). The first observation implies that $W_{\sigma\bar{\sigma}}$ must be a linear combination of W_e and W_m (since these are the only anyons with mutual statistics π with respect to em), while the second observation implies that the coefficents of W_e, W_m are equal.

The last equation (A.18) is especially useful since it provides a route to constructing $W_e + W_m$. This is nice because if we can also find the difference $W_e - W_m$, then we can obtain W_e and W_m individually. The problem is that $W_e - W_m$ is *odd* under the $\mathbb{Z}_2$ symmetry, so it has no counterpart in the doubled Ising string-net model (i.e., it cannot be gauged). To get around this obstacle, we consider the related operator $(W_e - W_m)\tau_q^z$. This operator is *even* under the symmetry so it can be gauged and hence translated into the doubled Ising string-net model. A natural guess is that its gauged counterpart is the 'T-junction' operator $W_{\sigma\bar{\sigma}\perp\psi\bar{\psi}}$ consisting of a $\psi\bar{\psi}$ string ending on a $\sigma\bar{\sigma}$ string (Fig. A.1). Thus we have

$$W_{\sigma\bar{\sigma}\perp\psi\bar{\psi}} \sim (W_e - W_m)\tau_q^z \tag{A.19}$$

Eqs. (A.18) and (A.19) form the backbone of our derivation. The rest is straightforward: we will simply construct the two operators $W_{\sigma\bar{\sigma}}$, and $W_{\sigma\bar{\sigma}\perp\psi\bar{\psi}}$ using the general string-net formalism[48] and then plug them into (A.18) and (A.19) and solve for W_e and W_m.

We begin with $W_{\sigma\bar{\sigma}}$. This operator is easiest to describe using the graphical representation discussed in Ref. [48]. Let $|X\rangle$ be some Ising string-net state on the honeycomb lattice and let γ be a path drawn on the links of this lattice. To compute $W^{\gamma}_{\sigma\bar{\sigma}}|X\rangle$, the first step is to shift the path γ slightly so that it no longer lies exactly on the honeycomb lattice. The precise way in which γ is shifted is not important, but we will use a convention where γ is shifted to the 'left', where 'left' is defined with respect to some arbitrary orientation of γ. The second step is to insert a '$\sigma\bar{\sigma}$' string along the path γ and to resolve all the resulting crossings using the local rules

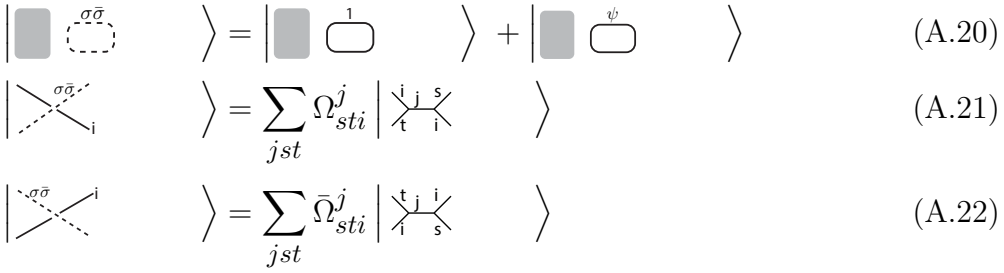

(A.20)

(A.21)

(A.22)

Here $\Omega^{j}_{sti} = \bar{\Omega}^{j}_{sti}$ is a four index tensor characterizing the string operator whose only nonzero values are

$$\Omega^{0}_{000} = \Omega^{2}_{220} = \Omega^{0}_{222} = \Omega^{1}_{021} = \Omega^{1}_{201} = 1, \quad \Omega^{2}_{002} = -1$$

where $0 =$ vacuum, $1 = \sigma$ and $2 = \psi$.

After resolving the crossings using the above rules, the result is a linear combination of doubled Ising string-net states, each of which is slightly displaced from the honeycomb lattice. The last step is to 'fuse' these strings onto the links of the honeycomb lattice using the rules (2.32-2.35). Denoting the resulting linear combination of states by $\sum_j c_j|Y_j\rangle$, the action of $W_{\sigma\bar{\sigma}}$ is then defined by $W_{\sigma\bar{\sigma}}|X\rangle = \sum_j c_j|Y_j\rangle$.

By examining the above local rules, we can read off the basic structure of the $W_{\sigma\bar{\sigma}}$ string operator. For example, Eq. (A.20) implies that whenever we resolve the $\sigma\bar{\sigma}$ string, it is always in either the 1 or ψ channel. Meanwhile, the fact that $\Omega^{1}_{st1} = 0$ unless $s = 0$ and

$t = 2$ (or vice versa) tells us that $\sigma\bar{\sigma}$ alternates between the 1 channel and the ψ channel every time it crosses a σ string. Putting these two observations together, it follows that $W_{\sigma\bar{\sigma}}$ can be written as a sum of two pieces

$$W_{\sigma\bar{\sigma}} = W_1 + W_2 \tag{A.23}$$

where W_1 inserts an alternating $1 - \psi - 1 - \psi \cdots$ string and W_2 inserts an alternating $\psi - 1 - \psi - 1 \cdots$ string (with alternations occurring every time the path γ crosses a σ string).

Now imagine we ungauge the operator $W_{\sigma\bar{\sigma}}$. As we mentioned earlier, this ungauging process simply amounts to embedding $W_{\sigma\bar{\sigma}}$ within the larger Hilbert space of the symmetric toric code. Although the operator is unchanged, this new context allows us to rewrite $W_{\sigma\bar{\sigma}}$ in a slightly different form. To see this, recall that W_1 and W_2 alternate between 1 and ψ each time they cross a σ string. At the same time, we know that the σ strings coincide with plaquette spin domain walls (at least for low energy states, which is all that we care about) so crossing a σ string means moving from a domain where $\tau^z = +(-)$ to one where $\tau^z = -(+)$. We can therefore choose a convention in which one component, say W_1, is in the ψ channel in the $\tau^z = +$ domain and W_2 is in the ψ channel in the $\tau^z = -$ domain. Labeling these two components by $W_{\psi+}$ and $W_{\psi-}$ respectively, we can write

$$W_{\sigma\bar{\sigma}} = W_{\psi+} + W_{\psi-} \tag{A.24}$$

We now repeat this analysis for the second operator, $W_{\sigma\bar{\sigma}\perp\psi\bar{\psi}}$. However, before we can do that, we need to discuss $W_{\psi\bar{\psi}}$. This operator can be described using the same graphical representation as $W_{\sigma\bar{\sigma}}$. The only difference is that in this case, the first rule is replaced by

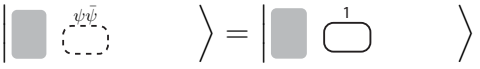

(A.25)

and the $\Omega, \bar{\Omega}$ tensors are different. In particular, the only nonzero values of $\Omega^j_{sti} = \bar{\Omega}^j_{sti}$ are

$$\Omega^0_{000} = \Omega^2_{002} = 1, \quad \Omega^1_{001} = -1 \tag{A.26}$$

in this case. Translating this graphical definition into algebra, one can see that the action of $W_{\psi\bar{\psi}}$ is very simple:

$$W_{\psi\bar{\psi}} = (-1)^{N_{\sigma\times}} \tag{A.27}$$

where $N_{\sigma\times}$ is an operator that is diagonal in the string-net basis and that counts the total number of σ strings that cross γ.

With this preparation, we are now ready to discuss the operator $W_{\sigma\bar{\sigma}\perp\psi\bar{\psi}}$. In the graphical representation, this operator inserts a T-junction made up of $\sigma\bar{\sigma}$ and $\psi\bar{\psi}$ strings. Crossings are then resolved using the $\sigma\bar{\sigma}$ and $\psi\bar{\psi}$ rules listed above. Translating this graphical definition into the notation of (A.23) and (A.27), one finds:

$$W_{\sigma\bar{\sigma}\perp\psi\bar{\psi}} = (W_1 - W_2)(-1)^{N_{\sigma\times}}\eta_p \tag{A.28}$$

where $\eta_p = \pm 1$ depending on whether W_1 is in the ψ channel or 1 channel at the point p where $\psi\bar{\psi}$ attaches to $\sigma\bar{\sigma}$ (Fig. A.1).

Now consider ungauging $W_{\sigma\bar{\sigma}\perp\psi\bar{\psi}}$ — that is, embedding this operator in the Hilbert space of the symmetric toric code. In this new context, we can rewrite $(-1)^{N_{\sigma\times}}$ as

$$(-1)^{N_{\sigma\times}} = \tau^z_p \tau^z_q \tag{A.29}$$

since the σ strings coincide with the plaquette spin domain walls at low energies (Fig. A.1). We can also rewrite $(W_1 - W_2)\eta_p$ as:

$$(W_1 - W_2)\eta_p = (W_{\psi+} - W_{\psi-})\tau^z_p \tag{A.30}$$

Multiplying (A.29) and (A.30) together and using (A.28), we derive

$$W_{\sigma\bar{\sigma}\perp\psi\bar{\psi}} = (W_{\psi+} - W_{\psi-})\tau_q^z \tag{A.31}$$

We now have everything we need to compute W_e and W_m. Combining equations (A.18, A.19, A.24, A.31) we derive:

$$W_e \sim W_{\psi+}, \quad W_m \sim W_{\psi-} \tag{A.32}$$

As a final step, we multiply the string operators by the projector P_γ from (2.20) which projects onto low energy states where σ strings are bound to domain walls and fusion rules are obeyed. While this step is not strictly necessary, it ensures that the string operators are especially well-behaved. After this step, we have:

$$\begin{aligned} W_e^\gamma &= \mathcal{P}_\gamma W_{\psi+} \mathcal{P}_\gamma \\ W_m^\gamma &= \mathcal{P}_\gamma W_{\psi-} \mathcal{P}_\gamma \end{aligned} \tag{A.33}$$

To go from the above expressions (A.33) to the formulas (2.19) and (2.22) in the main text is simply a matter of conversion from the graphical representation to an algebraic representation. In particular the (-1) factors associated with the first 3 vertices in Fig. 2.5 ($e1$, $e2$ and $e3$) arise from fusing the strings created by $W_{\psi+}$ onto the honeycomb lattice. Likewise, the (-1) factors from the last three vertices ($e4$, $e5$ and $e6$) come from the fact that $\Omega_{002}^2 = -1$ for the $\sigma\bar{\sigma}$ string.

APPENDIX B

APPENDICES FOR CHAPTER 3

B.1 Derivation of SU(2) symmetry

In this appendix we seek to establish two claims. First, we will prove that the three operators from Eq. 3.56 generate an SU(2) symmetry of the system. Second, we will prove that the vector $b^T = (e^{i\Theta_1}, e^{i\Theta_2})$ transforms as a doublet under this symmetry.

B.1.1 Review: the SU(2) symmetry

In this section we review the derivation of an SU(2) symmetry in the free chiral boson CFT [14]. We will find it convenient to work in holomorphic coordinates, defining a new field

$$\varphi(z) = \frac{1}{\sqrt{2}}(\Theta_1 + \Theta_2) \tag{B.1}$$

$$\varphi(\bar{z}) = \frac{1}{\sqrt{2}}(\Theta_1 - \Theta_2) \tag{B.2}$$

This bosonic field has an operator product with itself given by

$$\varphi(z)\varphi(w) \sim -\ln(z-w) \tag{B.3}$$

The related operator

$$H = i\partial\varphi(z) \tag{B.4}$$

has a scaling dimension equal to 1 because

$$\langle \partial\varphi(z)\partial\varphi(w)\rangle = \frac{1}{(z-w)^2} \tag{B.5}$$

In addition, the two operators

$$E^{\pm} = e^{\pm i\sqrt{2}\varphi(z)} \tag{B.6}$$

also have scaling dimension 1. To see this, we note simply that

$$\langle E^+(z)^\dagger E^+(w)\rangle = \langle E^-(z)^\dagger E^-(w)\rangle \tag{B.7}$$

$$= \exp[2\langle\varphi(z)\varphi(w)\rangle] = \frac{1}{(z-w)^2} \tag{B.8}$$

Furthermore, because these operators are chiral, their anti-holomorphic scaling dimensions are zero and thus $s = h - \bar{h} = 1$. That is, all three operators have spin-1. We can compute the full set of OPEs with help from the relation

$$: e^{A_1} :: e^{A_2} := e^{\langle A_1 A_2\rangle} : e^{A_1+A_2} : \tag{B.9}$$

which is valid for functions A_i which are linear in the creation/annihilation operators, such as the field φ. Using this relation (and leaving off the normal ordering symbols) we find

$$E^+(z)E^-(w) = e^{2\langle\varphi(z)\varphi(w)\rangle} e^{i\sqrt{2}(\varphi(z)-\varphi(w))} \tag{B.10}$$

$$= \frac{1}{(z-w)^2} \exp\left(i\sqrt{2} \sum_{n\geq 1} \frac{(z-w)^n}{n!} \partial^n \varphi(w) \right) \tag{B.11}$$

where in the second equality we evaluated the correlation function in term 1, and Taylor expanded the argument of term 2. The full set of OPEs now becomes

$$E^+(z)E^-(w) \sim \frac{1}{(z-w)^2} + \frac{\sqrt{2}H(w)}{z-w} \tag{B.12}$$

$$H(z)E^\pm(w) \sim \frac{\pm\sqrt{2}E^\pm(w)}{z-w} \tag{B.13}$$

$$H(z)H(w) \sim \frac{1}{(z-w)^2} \tag{B.14}$$

These OPEs match the SU(2) level one operator algebra in the Cartan-Weyl basis $(J_z, J_\pm)$.

The spin basis

Let's now analyze these operators in the spin basis

$$J^x(z) \equiv \cos[\sqrt{2}\varphi(z)] = \frac{1}{2}(E^+(z) + E^-(z)) \tag{B.15}$$

$$J^y(z) \equiv \sin[\sqrt{2}\varphi(z)] = \frac{1}{2i}(E^+(z) - E^-(z)) \tag{B.16}$$

$$J^z(z) = \frac{i}{\sqrt{2}}\partial\varphi \tag{B.17}$$

We now consider the set of OPEs with these operators. First we have the diagonal terms

$$\begin{aligned} J^x(z)J^x(w) &\sim \frac{1}{2(z-w)^2} \\ J^y(z)J^y(w) &\sim \frac{1}{2(z-w)^2} \\ J^z(z)J^z(w) &\sim \frac{1}{2(z-w)^2} \end{aligned} \tag{B.18}$$

Meanwhile, the non-diagonal OPEs take the form

$$J^x(z)J^y(w) \sim \frac{i}{z-w}J^z(w) \tag{B.19}$$

$$J^x(z)J^z(w) \sim -\frac{i}{z-w}J^y(w) \tag{B.20}$$

$$J^y(z)J^z(w) \sim \frac{i}{z-w}J^x(w) \tag{B.21}$$

$$\tag{B.22}$$

Or, in more compact form

$$J^i(z)J^j(w) \sim i\epsilon^{ijk}\frac{J^k(w)}{z-w} \tag{B.23}$$

We now see that the OPE coefficients of $\frac{1}{z-w}$ are precisely the structure constants of the SU(2) algebra. This implies[14] that they generate an SU(2) symmetry which transforms operators in the theory.

B.1.2 Transformation law for b

In this section we prove that the vector

$$b = \begin{pmatrix} e^{i\Theta_1} \\ e^{i\Theta_2} \end{pmatrix} \tag{B.24}$$

transforms as a doublet under the SU(2) symmetry generated by:

$$J^x(z) = \cos(\sqrt{2}\varphi(z)) \tag{B.25}$$

$$J^y(z) = \sin(\sqrt{2}\varphi(z)) \tag{B.26}$$

$$J^z(z) = \frac{i}{\sqrt{2}}\partial\varphi(z) \tag{B.27}$$

To determine how the vector b transforms under this SU(2) symmetry, recall that a tensor operator transforming under the spin-s representation of SU(2) consists of a set of operators, $O_l,\ l = 1, ..., 2s+1$ such that

$$[\mathcal{J}_a, O_l] = O_i[\mathcal{J}_a^s]_{ij} \tag{B.28}$$

where $[\mathcal{J}_a^s]$ is the spin-s representation of the generator of the symmetry. We will use this to show that b transforms as a doublet under $\mathrm{SU}(2)_R$. In this case, we have two operators $O_1 = e^{i\Theta_1}$ and $O_2 = e^{i\Theta_2}$. For now, let's just consider the transformation of b under the *global* $\mathrm{SU}(2)_R$. To isolate the global piece we expand the generators of the local symmetry as a Laurent series

$$J^i(z) = \sum_n z^{-(n+1)} J_n^i \tag{B.29}$$

Using contour integration, we find

$$J_m^i = \frac{1}{2\pi i}\oint z^m J^i(z)dz \tag{B.30}$$

where the contour encloses the origin. Now, to consider how b transforms under the global

$\mathrm{SU}(2)_R$, we only need to calculate the commutators (Eq. B.28) with J_0^i, that is,

$$J_0^i = \frac{1}{2\pi i}\oint J^i(z)dz \tag{B.31}$$

Because J_0^i is a contour integral of a purely holomorphic function, we can use CFT techniques to calculate the commutators in Eq. B.28. More specifically, if

$$A = \oint dz a(z) \tag{B.32}$$

then

$$[A, b(w)] = \oint_w a(z)b(w)dz \tag{B.33}$$

where $a(z)b(w)$ is the (normal ordered) OPE and the contour encloses the point w. We will now use formula B.33 to compute the commutators.

$$[J_0^x, O_1] = \frac{1}{2\pi i}[\oint dz \cos[\sqrt{2}z], e^{i\Theta_1(w,\bar{w})}] \tag{B.34}$$

$$= \frac{1}{2\pi i}e^{i\varphi(\bar{w})/\sqrt{2}}[\oint dz \cos[\sqrt{2}z], e^{i\varphi(w)/\sqrt{2}}] \tag{B.35}$$

$$= \frac{1}{2\pi i}e^{i\varphi(\bar{w})/\sqrt{2}}\Big(\frac{1}{2}[\oint dz e^{i\sqrt{2}\varphi(z)}, e^{i\varphi(w)/\sqrt{2}}] \tag{B.36}$$

$$+ \frac{1}{2}[\oint dz e^{-i\sqrt{2}\varphi(z)}, e^{i\varphi(w)/\sqrt{2}}]\Big) \tag{B.37}$$

$$= \frac{1}{2\pi i}e^{i\varphi(\bar{w})/\sqrt{2}}\Big(\frac{1}{2}\oint dz e^{i\sqrt{2}\varphi(z)}e^{i\varphi(w)/\sqrt{2}} \tag{B.38}$$

$$+ \frac{1}{2}\oint dz e^{-i\sqrt{2}\varphi(z)}e^{i\varphi(w)/\sqrt{2}}\Big) \tag{B.39}$$

To analyze these OPEs we will once again use the relation

$$:e^{A_1}::e^{A_2}:=e^{\langle A_1 A_2\rangle}:e^{A_1+A_2}: \tag{B.40}$$

Applying this relation we immediately see that the first term contains no singular terms, and therefore the contour integral will give zero. The non-zero contribution comes from the

second term. We have

$$[J_0^x, O_1] = \frac{1}{2\pi i} e^{i\varphi(\bar{w})/\sqrt{2}} \frac{1}{2} \oint dz \frac{e^{-i(2\varphi(z)-\varphi(w))/\sqrt{2}}}{z-w} \tag{B.41}$$

$$= \frac{1}{2} e^{i\varphi(w,\bar{w})} = \frac{1}{2} O_2 \tag{B.42}$$

A similar computation for O_2 shows that

$$[J_0^x, O_2] = \frac{1}{2} O_1 \tag{B.43}$$

Putting these results in the context of Eq. B.28 leads us to conclude

$$[J_0^x] = \frac{1}{2} \sigma^x \tag{B.44}$$

One can repeat this exercise for all other operators and one finds precisely

$$[J_0^i] = \frac{1}{2} \sigma^i \tag{B.45}$$

This proves that the vector b transforms under the spin-1/2 representation of the global $\mathrm{SU}(2)_R$ symmetry.

B.2 A lemma about bosonic Abelian topological phases

In this section we prove a lemma used earlier.

Lemma 2. *If a bosonic Abelian topological phase has a vanishing chiral central charge, and* $a^2 = 1$ *for all anyons* a*, then it has a Lagrangian subgroup.*

Proof. If each particle satisfies $a^2 = 1$ then it follows that the only possible *exchange* statistics are $\{0, \frac{\pi}{2}, \pi, \frac{3\pi}{2}\}$ modulo 2π since exchanging twice has to give you ± 1.

We can use this fact to prove that theory must contain at least one boson. And then, following an iterative procedure of condensing the boson and repeating the argument, we can show that the theory must contain a Lagrangian subgroup.

To prove that the theory has at least one boson, recall the relation between the self-statistics of the particles and the chiral central charge:

$$\frac{1}{\mathcal{D}}\sum_{i\in\mathcal{A}} d_i^2 e^{i\theta_i} = e^{2\pi i c_-/8}, \quad \mathcal{D} = \sqrt{\sum_{i\in\mathcal{A}} d_i^2} \tag{B.46}$$

where c_- is the *chiral central charge*. In the case at hand, we have $c_- = 0$, and we also know that $d_i = 1$ for all i because the phase is Abelian. Let $\mathcal{N}$ be the number of anyons, $\mathcal{N} = |\mathcal{A}|$. Then this formula can be rewritten as

$$\sum_{i\in\mathcal{A}} e^{i\theta_i} = \sqrt{\mathcal{N}} \tag{B.47}$$

Given that the possible values for θ_i are $\{0, \frac{\pi}{2}, \pi, \frac{3\pi}{2}\}$, it follows that for $\mathcal{N} > 1$, there are only solutions to the above equation if there exists at least one particle with $\theta_i = 0$ in addition to the identity particle, which we will call b.

The next step is to condense this boson b. After the condensation, there will be $\mathcal{N}/4$ particles. Furthermore, in the condensed phase, it will still be the case that all of the particles satisfy $a^2 = 1$, since this property can't change under condensation. Assuming the condensed phase is non-trivial, we can simply repeat the above argument to conclude that the condensed phase *also* has a boson b'. This boson can then also be condensed. This argument can be repeated until the condensed phase is trivial, proving that the original theory has a Lagrangian subgroup. □

B.3 Putting K, W, χ and χ_+ into standard form

The most general chiral boson edge theory can be parametrized by an $N \times N$ symmetric integer matrix K, an $N \times N$ integer matrix W, and an N component real vector χ satisfying the following constraints

$$W^T K W = K \tag{B.48}$$

$$W^2 = 1 \tag{B.49}$$

In this section we parametrize solutions to the above equation in such a way that W is in a simple block diagonal form. Putting W in a nice form will make it easier to derive the general form of the $\mathbb{Z}_2$ invariant.

To begin, we note that the condition that $W^2 = 1$ implies the eigenvalues of W are ± 1. Let n_+ be the number $+1$ eigenvalues and n_- be the number of -1 eigenvalues, so that $n_+ + n_- = N$. Next take $\{v_1, ..., v_{n_+}\}$ to be the basis for the $+1$ eigenspace. We also choose the v_i to be integer vectors, which we can always do because the $+1$ eigenspace is spanned by the columns of $1 + W$, an integer matrix. Furthermore, we choose the basis so that the $n_+ \times n_+$ minors of the matrix with columns $\{v_1, \ldots, v_{n_+}\}$ have no common factor. This ensures that we can extend $\{v_1, \ldots, v_{n_+}\}$ to an integer basis $\{v_1, \ldots, v_{n_+}, w_1, \ldots, w_{n_-}\}$ for the whole N dimensional space such that the matrix with columns $\{v_1, \ldots, v_{n_+}, w_1, \ldots, w_{n_-}\}$ has determinant ± 1.

Let U^{-1} be the matrix with columns $\{v_1, \ldots, v_{n_+}, w_1, \ldots, w_{n_-}\}$. We next make a change of basis $W \to UWU^{-1}$. After this change of basis W is in the form

$$W = \begin{pmatrix} \mathbf{1_n} & F \\ 0 & G \end{pmatrix} \tag{B.50}$$

where F is $n_+ \times n_-$ and G is $n_- \times n_-$. Using the fact that $W^2 = 1$, we can deduce that

$G^2 = 1$. Furthermore, because W is now an upper triangular matrix, $Tr(W) = Tr(\mathbf{1_{n_+}}) + Tr(\mathbf{G}) = n_+ - n_-$. This implies that $Tr(G) = -n_-$ and thus $G = -\mathbf{1_{n_-}}$ and thus W is of the form

$$W = \begin{pmatrix} \mathbf{1_{n_+}} & F \\ 0 & -\mathbf{1_{n_-}} \end{pmatrix} \tag{B.51}$$

The next step is to make another transformation $W \to UWU^{-1}$, where U is an integer matrix of the form

$$U = \begin{pmatrix} U_1 & 0 \\ 0 & U_2 \end{pmatrix} \tag{B.52}$$

and $\det(U_1) = \det(U_2) = \pm 1$. Under this transformation $F \to U_1 F U_2$ and U_1 and U_2 can be chosen so that F is a diagonal matrix. This follows from the Smith normal form of integer matrices. The next step is to make a transformation of the form $W \to UWU^{-1}$ where U is of the form

$$U = \begin{pmatrix} \mathbf{1_{n_+}} & Y \\ 0 & \mathbf{1_{n_-}} \end{pmatrix} \tag{B.53}$$

Under this transformation, $F \to F - 2Y$. We can thus then choose Y so that F has only 0's and 1's along the diagonal. We can therefore assume without loss of generality that F is of the form

$$F = \begin{pmatrix} \mathbf{1_{n_- - m}} & 0 \\ 0 & 0 \end{pmatrix} \tag{B.54}$$

where $m \leq p$. Altogether, then, we can conclude that W is of the form

$$W = \begin{pmatrix} \mathbf{1_{n_- - m}} & 0 & \mathbf{1_{n_- - m}} & 0 \\ 0 & \mathbf{1_{n_+ - n_- + m}} & 0 & 0 \\ 0 & 0 & \mathbf{-1_{n_- - m}} & 0 \\ 0 & 0 & 0 & \mathbf{-1_m} \end{pmatrix} \tag{B.55}$$

The final step is to make another transformation $W \to UWU^{-1}$ where U is of the form

$$U = \begin{pmatrix} \mathbf{1_{n_- - m}} & 0 & 0 & 0 \\ 0 & \mathbf{1_{n_+ - n_- + m}} & 0 & 0 \\ \mathbf{1_{n_- - m}} & 0 & \mathbf{1_{n_- - m}} & 0 \\ 0 & 0 & 0 & \mathbf{1_m} \end{pmatrix} \tag{B.56}$$

which puts W in the form

$$W = \begin{pmatrix} 0 & 0 & \mathbf{1_{n_- - m}} & 0 \\ 0 & \mathbf{1_{n_+ - n_- + m}} & 0 & 0 \\ \mathbf{1_{n_- - m}} & 0 & 0 & 0 \\ 0 & 0 & 0 & \mathbf{-1_m} \end{pmatrix} \tag{B.57}$$

Finally, after reordering the columns and rows we can put W in the following form:

$$W = \begin{pmatrix} \mathbf{-1_m} & 0 & 0 & 0 \\ 0 & \mathbf{1_{n_+ - n_- + m}} & 0 & 0 \\ 0 & 0 & 0 & \mathbf{1_{n_- - m}} \\ 0 & 0 & \mathbf{1_{n_- - m}} & 0 \end{pmatrix} \tag{B.58}$$

Using the $W^T K W = K$ relation and the fact that K is symmetric we find that K must be of the form

$$K = \begin{pmatrix} A & 0 & B & -B \\ 0 & C & D & D \\ B^T & D^T & E & F \\ -B^T & D^T & F & E \end{pmatrix} \tag{B.59}$$

where A, C, E and F are symmetric matrices, and the sizes of the matrices correspond to the blocks in the W matrix.

Lastly, it is possible to redefine our fields by shifting them so that we can put χ into the

following form

$$\chi = \begin{pmatrix} 0 \\ \chi_2 \\ 0 \\ 0 \end{pmatrix} \tag{B.60}$$

where χ_2 is an $n_+ - n_- + m$ dimensional vector of 1's and 0's. We now show how to compute χ_+ in this basis. This derivation parallels in many ways the derivation for the case $K = W = \sigma^x$ given in section 3.2.3. Because we can always pick a gauge such that $W\chi_+ = \chi_+$, we know that χ_+ can be parametrized in the form

$$\chi_+ = \begin{pmatrix} 0 \\ \chi_{+2} \\ \chi_{+3} \\ \chi_{+3} \end{pmatrix} \mod 2 \tag{B.61}$$

We can derive χ_+ by using a particular basis for $\{\Lambda_+\}$. The basis we pick is $\{e_{m+1}, \ldots, e_{n_+-n_-+2m}, f_1, \ldots f_{n_--m}\}$ where

$$f_i = e_{n_+-n_-+2m+i} + e_{n_++m+i} \quad \text{for} \quad i = 1, \ldots, n_- - m \tag{B.62}$$

Using this basis we can immediately see that $\chi_{+2} = \chi_2$ because $e^T_{m+i}\Theta = \Theta_{m+i}$ is a single field, so there is no additional commutator, and the shift of this field is simply given by the original shift vector χ_2. On the other hand

$$f_i^T\Theta = \Theta_{n_+-n_-+2m+i} + \Theta_{n_++m+i} \tag{B.63}$$

and we have the transformation

$$W : e^{i\Theta_{n_+ - n_- + 2m + i}} \to e^{i\Theta_{n_+ + m + i}} \tag{B.64}$$

$$W : e^{i\Theta_{n_+ + m + i}} \to e^{i\Theta_{n_+ - n_- + 2m + i}} \tag{B.65}$$

so we are in a situation entirely analogous to the one in section 3.2.3, and we simply need to compute the commutator

$$\begin{aligned} &[i\Theta_{n_+ - n_- + 2m + i}, i\Theta_{n_+ + m + i}] \\ &= i^3 \pi K_{n_+ - n_- + 2m + i, n_+ + m + i} \cdot \mathrm{sign}(m - n_-) \\ &= i\pi F_{ii} \end{aligned} \tag{B.66}$$

generalizing from the previous analysis of the case with a 2×2 K matrix, and using the fact that we are using a linearly independent basis for $\{\Lambda_+\}$ we see that this leads us precisely to a χ_+ of the form

$$\chi_+ = \begin{pmatrix} 0 \\ \chi_2 \\ \mathrm{diag}(F)/2 \\ \mathrm{diag}(F)/2 \end{pmatrix} \mod 2 \tag{B.67}$$

B.4 Proving ν is integer

In this appendix we prove that ν must be an integer. For simplicity we assume that $\nu_- = 0$. Also, we work in the standard basis where W and K are of the form (3.23)-(3.24). In this

case, the most general vectors $\Lambda_\pm \in \Xi_\pm$ take the form

$$\Lambda_+ = \begin{pmatrix} 0 \\ v \\ w \\ w \end{pmatrix}, \quad \Lambda_- = \begin{pmatrix} v \\ 0 \\ w \\ -w \end{pmatrix} \tag{B.68}$$

so the $V_\pm$ matrices are given by

$$V_+ = \begin{pmatrix} 0 & 0 \\ \mathbf{1} & 0 \\ 0 & \mathbf{1} \\ 0 & \mathbf{1} \end{pmatrix}, \quad V_- = \begin{pmatrix} \mathbf{1} & 0 \\ 0 & 0 \\ 0 & \mathbf{1} \\ 0 & -\mathbf{1} \end{pmatrix} \tag{B.69}$$

and hence $K_\pm$ are given by

$$K_+ = \begin{pmatrix} C & 2D \\ 2D^T & 2(E+F) \end{pmatrix} \tag{B.70}$$

$$K_- = \begin{pmatrix} A & 2B \\ 2B^T & 2(E-F) \end{pmatrix} \tag{B.71}$$

B.4.1 A special case

Before tackling the general case, we will first show that ν is an integer for the special case $\bar{\chi}_+ = \begin{pmatrix} 0 \\ \text{diag(F)} \end{pmatrix}$ (where $\bar{\chi}_+$ is defined by $\bar{\chi}_+ = V_+^T \chi_+$). The proof in this case requires several steps:

1. First we define two matrices:

$$J_+ = \begin{pmatrix} C & 2D \\ D^T & E+F \end{pmatrix}, \qquad I_+ = \begin{pmatrix} 2C & 2D \\ 2D^T & E+F \end{pmatrix} \tag{B.72}$$

   We note that

$$K_+^{-1} = 2 \cdot \begin{pmatrix} 1 & 0 \\ 0 & 1/2 \end{pmatrix} \cdot I_+^{-1} \cdot \begin{pmatrix} 1 & 0 \\ 0 & 1/2 \end{pmatrix} \tag{B.73}$$

   Combining this identity with the fact that $\bar{\chi}_+$ vanishes in the first argument, it follows that

$$2\nu = \bar{\chi}_+^T K_+^{-1} \bar{\chi}_+ = \frac{1}{2} \cdot \bar{\chi}_+^T I_+^{-1} \bar{\chi}_+ \tag{B.74}$$

   Thus, it suffices to show that $\frac{1}{2} \cdot \bar{\chi}_+^T I_+^{-1} \bar{\chi}_+$ is an even integer.

2. Next we note that we can make an integer change of basis so that I_+ takes the form

$$I_+ = \begin{pmatrix} 0 & A \\ A^T & B \end{pmatrix} \tag{B.75}$$

   where 0, A, B are square matrices, all of dimension $n_+/2$. To see this, recall that K_+ has $n_+/2$ linearly independent mutually null vectors (assuming it has dimension $n_+ \times n_+$), which implies that I_+ also has $n_+/2$ linearly independent mutually null vectors, which implies the above form.

3. In the above basis, the first $n_+/2$ components of $\bar{\chi}_+$ are all *even*. Indeed, this follows from two observations: (1) in the original basis, the components of $\bar{\chi}_+$ have the same parity as the diagonal elements of I_+, (2) this property is basis independent.

4. Given that the first $n_+/2$ components of $\bar{\chi}_+$ are all even in this basis, it follows that we can find another vector $\bar{\chi}'_+$ such that its first $n_+/2$ components all vanish and such

that $\bar{\chi}'_+ = \bar{\chi}_+ + 2l$ for some integer vector l.

5. Since the first $n_+/2$ components of $\bar{\chi}'_+$ all vanish, one can easily check that $\bar{\chi}'^T_+ I_+^{-1} \bar{\chi}'_+ = 0$. (This is because I_+^{-1} takes the form $\begin{pmatrix} 0 & * \\ * & * \end{pmatrix}$). Thus, our task reduces to showing that the difference

$$\frac{1}{2}(\bar{\chi}'^T_+ I_+^{-1} \bar{\chi}'_+ - \bar{\chi}^T_+ I_+^{-1} \bar{\chi}_+) \tag{B.76}$$

is an even integer.

6. The above difference can be rewritten as

$$2(l^T I_+^{-1} l + l^T I_+^{-1} \bar{\chi}_+) \tag{B.77}$$

We will now show that both of these terms are even integers. We do this by working in the *original* basis. First we note that in the original basis

$$\begin{aligned} 2I_+^{-1} &= \begin{pmatrix} 1 & 0 \\ 0 & 2 \end{pmatrix} \cdot J_+^{-1} \\ &= \begin{pmatrix} 1 & 0 \\ 0 & 0 \end{pmatrix} \cdot \begin{pmatrix} C^{-1} & 0 \\ * & (E+F)^{-1} \end{pmatrix} \pmod 2 \\ &= \begin{pmatrix} C^{-1} & 0 \\ 0 & 0 \end{pmatrix} \pmod 2 \end{aligned} \tag{B.78}$$

In particular, we can see that $2I_+^{-1}$ is an *even* matrix since C^{-1} is even (the inverse of an invertible even matrix is always even). Hence, the first term $2l^T I_+^{-1} l$ is an even integer. As for the second term, it is clear from the above expression for $2I_+^{-1}$ that $2l^T I_+^{-1} \bar{\chi}_+ = 0 \pmod 2$. This completes the proof of the special case.

B.4.2 The general case

We now consider the general case, where $\bar{\chi}_+$ is any vector of the form $\bar{\chi}_+ = \begin{pmatrix} l_1 \\ \text{diag(F)} + 2l_2 \end{pmatrix}$. Again, the proof required several steps:

1. In view of the result from the first section, it suffices to show that the difference

$$\begin{pmatrix} l_1 & \text{diag(F)} + 2l_2 \end{pmatrix} \cdot K_+^{-1} \begin{pmatrix} l_1 \\ \text{diag(F)} + 2l_2 \end{pmatrix} \tag{B.79}$$

$$- \begin{pmatrix} 0 & \text{diag(F)} \end{pmatrix} \cdot K_+^{-1} \begin{pmatrix} 0 \\ \text{diag(F)} \end{pmatrix} \tag{B.80}$$

   is an even integer.

2. This difference can be rewritten as

$$\begin{pmatrix} l_1 & 2l_2 \end{pmatrix} \cdot K_+^{-1} \begin{pmatrix} l_1 \\ 2l_2 \end{pmatrix} + \begin{pmatrix} 0 & \text{diag(F)} \end{pmatrix} \cdot K_+^{-1} \begin{pmatrix} 2l_1 \\ 4l_2 \end{pmatrix} \tag{B.81}$$

   Using $K_+^{-1} = J_+^{-1} \cdot \begin{pmatrix} 1 & 0 \\ 0 & 1/2 \end{pmatrix}$, we can rewrite this as

$$\begin{pmatrix} l_1 & 2l_2 \end{pmatrix} \cdot J_+^{-1} \begin{pmatrix} l_1 \\ l_2 \end{pmatrix} + \begin{pmatrix} 0 & \text{diag(F)} \end{pmatrix} \cdot J_+^{-1} \begin{pmatrix} 2l_1 \\ 2l_2 \end{pmatrix} \tag{B.82}$$

3. Clearly the second term is an even integer. Thus, it suffices to show that the first term is an even integer. To this end, note that

$$J_+^{-1} = \begin{pmatrix} C^{-1} & 0 \\ * & (E+F)^{-1} \end{pmatrix} \pmod 2 \tag{B.83}$$

so that

$$\begin{pmatrix} l_1 & 2l_2 \end{pmatrix} \cdot J_+^{-1} \begin{pmatrix} l_1 \\ l_2 \end{pmatrix} = l_1^T C^{-1} l_1 \pmod 2 \tag{B.84}$$

The latter quantity is clearly an integer since C^{-1} is an even matrix (the inverse of an invertible even matrix is always even). This completes the proof of the general case.

B.5 Proving $K_\pm$ have Lagrangian subgroups in the SET case

B.5.1 Statement of the result

Suppose we are given an $N \times N$ bosonic K-matrix K and a $\mathbb{Z}_2$ symmetry transformation W. In this section, we prove that if $K_\pm$ have vanishing signature and K has a Lagrangian subgroup that is invariant under the $\mathbb{Z}_2$ symmetry, then $K_\pm$ have Lagrangian subgroups.

We note that this result is what we need to prove that the SET criterion is *sufficient* for having a gapped, symmetric edge. Indeed, once we establish that $K_\pm$ have Lagrangian subgroups, the existence of the appropriate null vectors for K_+, K_- follows just as in the SPT case.

B.5.2 Proof

The argument is similar to one given in the appendix of the Ref. [42]. To begin, let $\mathcal{M}$ be a set of integer vectors forming a Lagrangian subgroup that is invariant under the symmetry. Then $\mathcal{M}$ has the following properties:

1. $m^T K^{-1} m'$ is an integer for any $m, m' \in \mathcal{M}$.
2. $m^T K^{-1} m$ is an *even* integer for any $m \in \mathcal{M}$.
3. If l is not equivalent to any element of $\mathcal{M}$, then $m^T K^{-1} l$ is non-integer for some $m \in \mathcal{M}$.

4. If $m \in \mathcal{M}$, then $W \cdot m$ is equivalent to $m' \in \mathcal{M}$ for some $m' \in \mathcal{M}$.

Define a set Γ by

$$\Gamma = \{v : \ v = m + K\Lambda, \ m \in \mathcal{M}, \ \Lambda \in \mathbb{Z}^N\} \tag{B.85}$$

Also, define two sets $\Gamma_\pm$ by $\Gamma_\pm = \Gamma \cap \Xi_\pm$. These sets have several important properties. First, all three are integer lattices, with Γ being of dimension N and $\Gamma_\pm$ being of dimension $n_\pm$. Second, $W\Gamma = \Gamma$, since this follows immediately from property (4) above. Finally, $\Gamma, \Gamma_\pm$ satisfy

$$\Gamma \subset \frac{1}{2}(\Gamma_+ + \Gamma_-) \tag{B.86}$$

In other words, every vector $v \in \Gamma$ can be written as a sum $v = \frac{1}{2}(v_+ + v_-)$ for some $v_\pm \in \Gamma_\pm$. This follows immediately by setting $v_\pm = (v \pm Wv)$.

To proceed further, we note that since $\Gamma_\pm$ are integer lattices of dimension $n_\pm$, they can be represented as $\Gamma_\pm = U_\pm \mathbb{Z}^{n_\pm}$ where $U_\pm$ are $N \times n_\pm$ integer matrices. Now consider the two matrices $P_\pm = U_\pm^T K^{-1} U_\pm$. It is easy to see that $P_\pm$ are symmetric integer matrices with vanishing signature, and only even numbers on the diagonal. Indeed, the fact that $P_\pm$ are integer matrices follows from property (1) of $\mathcal{M}$. Also, the fact that $P_\pm$ have only even elements on the diagonal, and have vanishing signature follows from the corresponding properties of K together with property (2) and our assumption that $K_\pm$ have vanishing signature.

In addition to the above properties, $P_\pm$ also have the property that $2P_\pm^{-1}$ is an *integer* matrix. We now prove this claim for P_+ — the proof for P_- is similar. To begin, suppose that x is a n_+ component vector with the property that $P_+ x$ is an integer vector. Then it follows that $v_+ K^{-1} U_+ x$ is integer for all $v_+ \in \Gamma_+$. At the same time, it is clear that $v_- K^{-1} U_+ x = 0$ for all $v_- \in \Gamma_-$. Indeed, this follows from the fact that $U_+ x$ is even under W. Combining these two observations we deduce that $v K^{-1} U_+ x$ is a *half-integer* for all $v \in \Gamma$: this follows from Eq. (B.86) above. The latter property implies that $2U_+ x \in \Gamma$, as this follows from property (3) above. At the same time, we know that $2U_+ x \in \Xi_+$, so we

conclude that $2U_+x \in \Gamma_+$. It then follows that $2x \in \mathbb{Z}^{n_+}$. Thus, we have shown that if P_+x is an integer vector then $2x \in \mathbb{Z}^{n_+}$. The claim follows immediately.

To summarize: we have shown that $P_\pm$ are symmetric even integer matrices with vanishing signature, and with the property that $2P_\pm^{-1}$ are integer matrices. This means that if we think of $P_\pm$ as K-matrices, then they describe bosonic topological phases with vanishing chiral central charge and with the property that $a^2 = 1$ for all anyons a. Therefore, according to the lemma proved in Appendix B.2, $P_\pm$ must have Lagrangian subgroups. This is turn means that $P_\pm$ have linearly independent null vectors $\{v_\pm^1, ..., v_\pm^{n_\pm/2}\}$. Now define

$$w_\pm^i = \det(K) \cdot K^{-1} U_\pm v_\pm^i \tag{B.87}$$

By construction, the $w_\pm^i$'s are null vectors for K. At the same time, they belong to $\Xi_\pm$, so they can be represented as

$$w_\pm^i = V_\pm \Lambda_\pm^i \tag{B.88}$$

We can now see that $\{\Lambda_\pm^1, ..., \Lambda_\pm^{n_\pm/2}\}$ are null vectors for $K_\pm$. Hence $K_\pm$ have a complete set of null vectors, implying that $K_\pm$ have Lagrangian subgroups. This completes the proof.

APPENDIX C

APPENDICES FOR CHAPTER 4

C.1 Degeneracy

In this chapter, we have made heavy use of the fact that the low energy spectrum of our models is described by non-interacting phonons in the limit $U \to \infty$. This result is correct for $k_2 - k_1 = 2$, but, as we mentioned earlier, it is not quite right for $k_2 - k_1 > 2$ due to an additional degeneracy in the energy spectrum. In this appendix we derive an explicit formula for this degeneracy: for a circular edge with $2N$ impurities and $k_1 \neq k_2$, we show that every phonon occupation state, including the ground state, has a degeneracy of

$$D = \left| \frac{k_2 - k_1}{2} \right|^{N-1} \tag{C.1}$$

in the limit $U \to \infty$. Notice that D grows exponentially with N when $k_2 - k_1 > 2$, so the degeneracy is *extensive* in this case.

C.1.1 General method for computing degeneracy

We begin by reviewing a method for computing degeneracy which applies to any Hamiltonian of the form (4.8). This method was derived in Ref. [15] and it goes as follows: the first step is to compute the commutator matrix

$$\mathcal{Z}_{ij} = \frac{1}{2\pi i}[C_i, C_j] \tag{C.2}$$

The second step is to make a linear change of variables,[1]

$$C_i' = \sum_j \mathcal{V}_{ij} C_j$$

such that (i) $\mathcal{V}$ is an integer matrix with determinant ± 1, and (ii) the matrix $\mathcal{Z}' = \frac{1}{2\pi i}[C_i', C_j']$ is in skew-normal form:

$$\mathcal{Z}' = \begin{pmatrix} 0 & -\mathcal{D} & 0 \\ \mathcal{D} & 0 & 0 \\ 0 & 0 & 0 \end{pmatrix} \tag{C.3}$$

where

$$\mathcal{D} = \begin{pmatrix} d_1 & 0 & \cdots & 0 \\ 0 & d_2 & \cdots & 0 \\ \vdots & \vdots & \vdots & \vdots \end{pmatrix} \tag{C.4}$$

and the d_i are all nonzero. Such a change of variables always exists, although it is not necessarily unique. After making this change of variables, the degeneracy can be computed as

$$D = \left| \prod_{i=1}^{N} d_i \right| \tag{C.5}$$

The intuition behind this procedure is that the degeneracy arises because the arguments of the cosine terms, i.e. the C_i, do not commute with one another; hence to compute the degeneracy, we need to carefully analyze the commutation relations of the C_i. For more details, we refer the reader to Ref. [15].

C.1.2 Application to impurity model

We now compute the degeneracy of our system of $2N$ impurities arranged in a disk geometry. Before we start, we first need to take care of a technical issue. This issue is that the above

1. In Ref. [15], this change of variables includes an offset, i.e. $C_i' = \sum_j \mathcal{V}_{ij} C_j + \chi_i$, but we do not need to include χ_i here as it does not play a role in the degeneracy computation.

method for computing degeneracy is designed for systems where all the degrees of freedom are continuous and real valued (e.g like x and p) but our system has two degrees of freedom that take integer values, namely the total charge on each edge mode:

$$Q_i = \frac{1}{2\pi} \int dx \partial_x \phi_i, \quad i = 1, 2 \tag{C.6}$$

Likewise, our system has two compact degrees of freedom that take values in $[0, 2\pi)$, namely $k_1\phi_1$ and $k_2\phi_2$.

Fortunately, there is a trick for dealing with this discrepancy, which was introduced by Ref. [15]. The trick is to treat all the degrees of freedom in our system as though they are real valued, and then enforce the quantization of Q_1, Q_2 and the compactness of ϕ_1, ϕ_2 at an energetic level by adding two more cosine terms to the Hamiltonian:

$$H \to H - U\cos(2\pi Q_1) - U\cos(2\pi Q_2)$$

In the limit $U \to \infty$, these cosine terms lock Q_1, Q_2 to integer values and also make the corresponding conjugate varables, ϕ_1, ϕ_2 compact.

With the help of this trick, it is straightforward to apply the above method to our system. All together, we have $2N + 2$ cosine terms $\cos(C_j)$ with

$$C_j = k_1\phi_1(x_j) + k_2\phi_2(x_j) - \alpha_j, \quad j = 1, ..., 2N$$
$$C_{2N+1} = 2\pi Q_1, \quad C_{2N+2} = 2\pi Q_2$$

To compute the corresponding commutator matrix $\mathcal{Z}_{ij}$, we need to fix a convention for the

commutation relations of ϕ_1, ϕ_2. We use the following convention:

$$[\phi_1(x_i), \phi_1(x_j)] = \frac{\pi i}{k_1}\mathrm{sgn}(i-j)$$
$$[\phi_2(x_i), \phi_2(y_j)] = -\frac{\pi i}{k_2}\mathrm{sgn}(i-j)$$

From the above commutation relations, we obtain

$$\mathcal{Z}_{ij} = \begin{pmatrix} 0 & c & c & \cdots & c & -1 & 1 \\ -c & 0 & c & \cdots & c & -1 & 1 \\ -c & -c & 0 & \cdots & c & -1 & 1 \\ \vdots & \vdots & \vdots & \vdots & \vdots & \vdots & \vdots \\ -c & -c & -c & \cdots & 0 & -1 & 1 \\ 1 & 1 & 1 & \cdots & 1 & 0 & 0 \\ -1 & -1 & -1 & \cdots & -1 & 0 & 0 \end{pmatrix} \tag{C.7}$$

where $c = \frac{k_2 - k_1}{2}$. The next step is to find a change of variables $C_i' = \sum_j \mathcal{V}_{ij} C_j$ such that $\mathcal{Z}_{ij}' = \frac{1}{2\pi i}[C_i', C_j'] = \mathcal{V} Z \mathcal{V}^T$ is in skew-normal form (C.3). One can check that following

change of variables does the job:

$$\begin{aligned}
C'_1 &= C_{2N+1} \\
C'_m &= C_{2m} - C_{2m-1}, \quad m = 2, ..., N \\
C'_{N+1} &= C_2 \\
C'_{N+m} &= (C_1 - C_2) + \sum_{k=1}^{m-1} (C_{2k+1} - C_{2k}), \ m = 2, ..., N \\
C'_{2N+1} &= C_1 - C_2 + C_3 - C_4 ... + C_{2N-1} - C_{2N} \\
&\quad + \frac{1+k_1}{2} C_{2N+1} + \frac{1+k_2}{2} C_{2N+2} \\
C'_{2N+2} &= -C_1 + C_2 - C_3 + C_4 ... - C_{2N-1} + C_{2N} \\
&\quad + \frac{1-k_1}{2} C_{2N+1} + \frac{1-k_2}{2} C_{2N+2}
\end{aligned} \tag{C.8}$$

The corresponding $\mathcal{D}$ matrix in (C.3) has dimension $N \times N$ with diagonal entries

$$d_1 = -1, \quad d_i = \frac{k_2 - k_1}{2}; \quad i = 2, \cdots, N$$

Substituting these values into the general formula for the degeneracy (C.5) gives $D = \left|\frac{k_2 - k_1}{2}\right|^{N-1}$. This completes our derivation of (C.1).

C.2 Regularizing the impurity scattering terms

In this appendix, we derive Eq. (4.25) from the constraint $[a, C_j] = 0$ by appropriately regularizing the impurity scattering terms. Our derivation closely follows a similar appendix in Ref. [15].

To see why we need to regularize at all, suppose we directly substitute the definition of a (4.15) into $[a, C_j] = 0$ and evaluate the commutator. The result is:

$$f(j\ell) = g(j\ell) \tag{C.9}$$

It is hard to make sense of this equation since the expressions for f and g (4.22) are discontinuous at $x = j\ell$ and hence $f(j\ell)$ and $g(j\ell)$ are not well-defined. What we will show below is that regularizing changes the above equation to the more sensible relation

$$\frac{f(j\ell^-) + f(j\ell^+)}{2} = \frac{g(j\ell^-) + g(j\ell^+)}{2} \tag{C.10}$$

Our regularization scheme is as follows: for each impurity scattering term $\cos(C_j)$, we replace $C_j = k_1\phi_1(j\ell) + k_2\phi_2(j\ell) - \alpha_j$ with

$$C_j = \int_{-\infty}^{\infty} dx\ \tilde{\delta}(x - j\ell)[k_1\phi_1(x) + k_2\phi_2(x)] - \alpha_j \tag{C.11}$$

where $\tilde{\delta}(x)$ is an approximation to a delta function, i.e. a narrowly peaked function with $\int \tilde{\delta}(x)dx = 1$. One can think of this replacement as effectively introducing a short distance cutoff into our model.

Once we make this substitution, we repeat the calculation in Eqs. (4.21 - 4.22) and solve for the functions f and g. We obtain

$$\begin{aligned} f(x) &= \sum_j A^{(j)} e^{-i\frac{E}{v}(x-j\ell)} \Big[\tilde{\Theta}_1(x - j\ell) - \tilde{\Theta}_1(x - (j+1)\ell)\Big] \\ g(x) &= \sum_j B^{(j)} e^{i\frac{E}{v}(x-j\ell)} \Big[\tilde{\Theta}_2(x - j\ell) - \tilde{\Theta}_2(x - (j+1)\ell)\Big] \end{aligned}$$

where $\tilde{\Theta}_1$ and $\tilde{\Theta}_2$ are regularized versions of the Heaviside step function:

$$\begin{aligned} \tilde{\Theta}_1(x) &= \int_{-\infty}^{x} e^{i\frac{E}{v}y}\tilde{\delta}(y)dy \\ \tilde{\Theta}_2(x) &= \int_{-\infty}^{x} e^{-i\frac{E}{v}y}\tilde{\delta}(y)dy \end{aligned} \tag{C.12}$$

Next we note that the constraint $[a, C_j] = 0$ gives

$$\int_{-\infty}^{\infty} dx\ [f(x) - g(x)]\tilde{\delta}(x - j\ell) = 0 \tag{C.13}$$

To complete the calculation, we need to substitute the above expressions for f and g into (C.13) and evaluate the resulting integral. We do this with the help of the following identity:

$$\begin{aligned}
&\lim_{\frac{E}{v}b\to 0} \int_{-\infty}^{\infty} dx\ \tilde{\Theta}_s(x - j\ell)\tilde{\delta}(x - j'\ell)e^{\pm i\frac{E}{v}x} \\
&= \begin{cases} 0 & j > j' \\ e^{\pm i\frac{E}{v}j'\ell} & j < j' \\ \frac{1}{2}e^{\pm i\frac{E}{v}j\ell} & j = j' \end{cases}
\end{aligned} \tag{C.14}$$

Here b is the characteristic width of the $\tilde{\delta}(x)$ function and s runs over the two values $s = 1, 2$. The justification for this identity for $j > j'$ and $j < j'$ is obvious; as for $j = j'$, we can prove it for $s = 1$ by noting that

$$\begin{aligned}
&\lim_{\frac{E}{v}b\to 0} \int_{-\infty}^{\infty} dx\ \tilde{\Theta}_1(x - j\ell)\tilde{\delta}(x - j\ell)e^{\pm i\frac{E}{v}x} \\
&= \lim_{\frac{E}{v}b\to 0} \int_{-\infty}^{\infty} dx \int_{-\infty}^{x} dy\ \tilde{\delta}(y - j\ell)\tilde{\delta}(x - j\ell)e^{i\frac{E}{v}(y-j\ell)\pm i\frac{E}{v}x} \\
&= e^{\pm i\frac{E}{v}j\ell} \lim_{\frac{E}{v}b\to 0} \int_{-\infty}^{\infty} dx \int_{-\infty}^{x} dy\ \tilde{\delta}(y - j\ell)\tilde{\delta}(x - j\ell) \\
&= \frac{1}{2}e^{\pm i\frac{E}{v}j\ell} \lim_{\frac{E}{v}b\to 0} \int_{-\infty}^{\infty} dx \int_{-\infty}^{\infty} dy\ \tilde{\delta}(y - j\ell)\tilde{\delta}(x - j\ell) \\
&= \frac{1}{2}e^{\pm i\frac{E}{v}j\ell}
\end{aligned} \tag{C.15}$$

The proof for $s = 2$ is similar.

Applying the above identity to (C.13) and simplifying, we arrive at the condition

$$\frac{A^{(j)} + A^{(j-1)}e^{-i\frac{E\ell}{v}}}{2} = \frac{B^{(j)} + B^{(j-1)}e^{i\frac{E\ell}{v}}}{2} \tag{C.16}$$

This is exactly Eq. 4.25, which we wished to derive.

C.3 Deriving the approximation (4.93)

In this appendix we derive Eq. (4.93), which gives an approximate expression for the transfer matrix T_{sys} for a system of M impurities randomly arranged on a circular edge of circumference L. As in the main text, we denote the spacing between the impurities by $\ell_1, ..., \ell_M$ so that

$$T_{sys}(E) = TD(E\ell_M)T \cdots TD(E\ell_1)$$

with $D(x) = e^{-iWx}$ and $W = KV^{-1}$.

For simplicity, we will assume that the number of impurities M is a power of 2. This allows us to factor M as $M = r \cdot (M/r)$ where r is a smaller power of 2. We can then write T_{sys} as a product of (M/r) terms, each of which involves r impurities. That is:

$$T_{sys}(E) = T_{M/r}(E) \cdots T_2(E) \cdot T_1(E) \tag{C.17}$$

where

$$\begin{aligned} T_1(E) &= TD(E\ell_r)T \cdots TD(E\ell_1) \\ T_2(E) &= TD(E\ell_{2r})T \cdots TD(E\ell_{r+1}) \\ &\vdots \end{aligned}$$

and so on. For the moment, we will leave the value of r unspecified; later we will choose r so as to obtain the best bound on the error in our approximations.

Next, we expand each $T_j(E)$ to linear order in E. Using the fact that $T^2 = \mathbb{1}$, this gives

$$T_j(E) \approx \mathbb{1} - iE(W\ell_{even,j} + TWT\ell_{odd,j})$$

where

$$\ell_{odd,j} = \ell_{jr-r+1} + \ell_{jr-r+3} + \cdots + \ell_{jr-1}$$
$$\ell_{even,j} = \ell_{jr-r+2} + \ell_{jr-r+4} + \cdots + \ell_{jr}$$

For a typical impurity distribution, the even and odd spacings are approximately equal:

$$\ell_{even,j} \approx \ell_{odd,j} \approx \frac{r\bar{\ell}}{2}$$

Hence, the above expression for $T_j(E)$ can be simplified to

$$T_j(E) \approx \mathbb{1} - \frac{riE\bar{\ell}}{2}[W + TWT] \tag{C.18}$$

Let us try to bound the total error in the above approximation. There are two errors we need to think about: the systematic error coming from expanding $T_j(E)$ to linear order in E and the statistical error coming from replacing $\ell_{even,j}$ and $\ell_{odd,j}$ by their typical value, $r\bar{\ell}/2$. The systematic error can be estimated by the quadratic term in the expansion of $T_j(E)$, which is of order $O(r^2E^2\bar{\ell}^2\|W\|^2)$ where $\|W\|$ is the magnitude of the largest eigenvalue of W. As for the statistical error, we expect this to be proportional to the typical size of the fluctuations in $\ell_{even,j}$ and $\ell_{odd,j}$, which are both of order $\sqrt{r}\bar{\ell}$, so we obtain the estimate $O(\sqrt{r}E\bar{\ell}\|W\|)$. To get an optimal bound on the total error, we choose r so that these two errors have the same size, i.e.

$$r \sim (E\bar{\ell}\|W\|)^{-\frac{2}{3}}$$

For this choice of r, both errors are of order $O(E^{\frac{2}{3}}\bar{\ell}^{\frac{2}{3}}\|W\|^{\frac{2}{3}})$, so that

$$T_j(E) = \mathbb{1} - \frac{riE\bar{\ell}}{2}(W + TWT) + O(E^{\frac{2}{3}}\bar{\ell}^{\frac{2}{3}}\|W\|^{\frac{2}{3}}) \tag{C.19}$$

Substituting the above expression (C.19) into (C.17), we derive

$$\begin{aligned} T_{sys}(E) &= \left[\mathbb{1} - \frac{riE\bar{\ell}}{2}(W + TWT) + O(E^{\frac{2}{3}}\bar{\ell}^{\frac{2}{3}}\|W\|^{\frac{2}{3}})\right]^{\frac{M}{r}} \\ &= \exp\left[-\frac{iME\bar{\ell}}{2}(W + TWT) + O(ME^{\frac{4}{3}}\bar{\ell}^{\frac{4}{3}}\|W\|^{\frac{4}{3}})\right] \\ &= \exp\left[-\frac{iEL}{2}(W + TWT) + O(E^{\frac{4}{3}}L\bar{\ell}^{\frac{1}{3}}\|W\|^{\frac{4}{3}})\right] \end{aligned} \tag{C.20}$$

which is exactly Eq. (4.93). We note that the error term in the above approximation is an *upper bound* and is likely larger than the true error.

REFERENCES

[1] Daniel Arovas, John R Schrieffer, and Frank Wilczek. Fractional statistics and the quantum hall effect. *Physical review letters*, 53(7):722, 1984.

[2] R. C. Ashoori, H. L. Stormer, L. N. Pfeiffer, K. W. Baldwin, and K. West. Edge magnetoplasmons in the time domain. *Phys. Rev. B*, 45(7):3894, 1992.

[3] Maissam Barkeshli, Parsa Bonderson, Meng Cheng, and Zhenghan Wang. Symmetry, defects, and gauging of topological phases. *arXiv preprint arXiv:1410.4540*, 2014.

[4] Aveek Bid, Nissim Ofek, Hiroyuki Inoue, Moty Heiblum, CL Kane, Vladimir Umansky, and Diana Mahalu. Observation of neutral modes in the fractional quantum hall regime. *Nature*, 466(7306):585–590, 2010.

[5] Parsa Bonderson. PhD thesis, Caltech, 2007.

[6] S. B. Bravyi and A. Y. Kitaev. Quantum codes on a lattice with boundary. *quant-ph/9811052*, 1998.

[7] F. J. Burnell, X. Chen, L. Fidkowski, and A. Vishwanath. Exactly soluble model of a 3d symmetry protected topological phase of bosons with surface topological order. *Phys. Rev. B*, 90:245122, 2014.

[8] M. Büttiker. Absence of backscattering in the quantum hall effect in multiprobe conductors. *Phys. Rev. B*, 38:9375–9389, Nov 1988.

[9] Liang Chang, Meng Cheng, Shawn X Cui, Yuting Hu, Wei Jin, Ramis Movassagh, Pieter Naaijkens, Zhenghan Wang, and Amanda Young. On enriching the levin–wen model with symmetry. *Journal of Physics A: Mathematical and Theoretical*, 48(12):12FT01, 2015.

[10] Xie Chen, Zheng-Cheng Gu, Zheng-Xin Liu, and Xiao-Gang Wen. Symmetry protected topological orders and the group cohomology of their symmetry group. *Physical Review B*, 87(15):155114, 2013.

[11] V. G. Drinfeld. Quantum groups. *Proceedings of the International Congress of Mathematicians, Berkeley*, pages 798–820, 1987.

[12] Torbjörn Einarsson. Fractional statistics on a torus. *Physical review letters*, 64(17):1995, 1990.

[13] Pavel Etingof, Dmitri Nikshych, Victor Ostrik, et al. Fusion categories and homotopy theory. *arXiv preprint arXiv:0909.3140*, 2009.

[14] Philippe Francesco, Pierre Mathieu, and David Sénéchal. *Conformal field theory*. Springer Science & Business Media, 2012.

[15] Sriram Ganeshan and Michael Levin. Formalism for the solution of quadratic hamiltonians with large cosine terms. *Phys. Rev. B*, 93(7):075118, 2016.

[16] T. Giamarchi and H. J. Schulz. Anderson localization and interactions in one-dimensional metals. *Phys. Rev. B*, 37:325–340, Jan 1988.

[17] Yuxiang Gu, Ling-Yan Hung, and Yidun Wan. Unified framework of topological phases with symmetry. *Physical Review B*, 90(24):245125, 2014.

[18] Jeongwan Haah. Local stabilizer codes in three dimensions without string logical operators. *Phys. Rev. A*, 83:042330, 2011.

[19] B. I. Halperin. Quantized hall conductance, current-carrying edge states, and the existence of extended states in a two-dimensional disordered potential. *Phys. Rev. B*, 25:2185–2190, Feb 1982.

[20] M. Z. Hasan and C. L. Kane. *Colloquium* : Topological insulators. *Rev. Mod. Phys.*, 82:3045–3067, 2010.

[21] M Zahid Hasan and Charles L Kane. Colloquium: topological insulators. *Reviews of Modern Physics*, 82(4):3045, 2010.

[22] Chris Heinrich, Fiona Burnell, Lukasz Fidkowski, and Michael Levin. Symmetry-enriched string nets: Exactly solvable models for set phases. *Physical Review B*, 94(23):235136, 2016.

[23] Chris Heinrich and Michael Levin. Solvable models for neutral modes in fractional quantum hall edges. *arXiv preprint arXiv:1702.08470*, 2017.

[24] Michael Hermele. String flux mechanism for fractionalization in topologically ordered phases. *Phys. Rev. B*, 90:184418, 2014.

[25] Hiroyuki Inoue, Anna Grivnin, Yuval Ronen, Moty Heiblum, Vladimir Umansky, and Diana Mahalu. Proliferation of neutral modes in fractional quantum hall states. *Nature communications*, 5, 2014.

[26] M. D. Johnson and A. H. MacDonald. Composite edges in the ν=2/3 fractional quantum hall effect. *Phys. Rev. Lett.*, 67:2060–2063, Oct 1991.

[27] C. L. Kane and Matthew P. A. Fisher. Contacts and edge-state equilibration in the fractional quantum hall effect. *Phys. Rev. B*, 52(24):17393, 1995.

[28] C. L. Kane and Matthew P. A. Fisher. Impurity scattering and transport of fractional quantum hall edge states. *Phys. Rev. B*, 51(19):13449, 1995.

[29] C. L. Kane, Matthew P. A. Fisher, and J Polchinski. Randomness at the edge: Theory of quantum hall transport at filling ν= 2/3. *Phys. Rev. Lett.*, 72(26):4129, 1994.

[30] Charles L Kane and Eugene J Mele. Quantum spin hall effect in graphene. *Physical review letters*, 95(22):226801, 2005.

[31] A. Kitaev and L. Kong. Models for Gapped Boundaries and Domain Walls. *Communications in Mathematical Physics*, 313:351–373, 2012.

[32] A Yu Kitaev. Fault-tolerant quantum computation by anyons. *Annals of Physics*, 303(1):2–30, 2003.

[33] Alexei Kitaev. Anyons in an exactly solved model and beyond. *Annals of Physics*, 321(1):2–111, 2006.

[34] K v Klitzing, Gerhard Dorda, and Michael Pepper. New method for high-accuracy determination of the fine-structure constant based on quantized hall resistance. *Physical Review Letters*, 45(6):494, 1980.

[35] J. B. Kogut. An introduction to lattice gauge theory and spin systems. *Rev. Mod. Phys.*, 51:659–713, 1979.

[36] Markus König, Steffen Wiedmann, Christoph Brüne, Andreas Roth, Hartmut Buhmann, Laurens W Molenkamp, Xiao-Liang Qi, and Shou-Cheng Zhang. Quantum spin hall insulator state in hgte quantum wells. *Science*, 318(5851):766–770, 2007.

[37] Tian Lan, Liang Kong, and Xiao-Gang Wen. Classification of 2+ 1d topological orders and spt orders for bosonic and fermionic systems with on-site symmetries. *arXiv preprint arXiv:1602.05946*, 2016.

[38] Tian Lan and Xiao-Gang Wen. Topological quasiparticles and the holographic bulk-edge relation in (2+ 1)-dimensional string-net models. *Physical Review B*, 90(11):115119, 2014.

[39] Lev Davidovich Landau. On the theory of phase transitions. i. *Zh. Eksp. Teor. Fiz.*, 11:19, 1937.

[40] Robert B Laughlin. Anomalous quantum hall effect: an incompressible quantum fluid with fractionally charged excitations. *Physical Review Letters*, 50(18):1395, 1983.

[41] Sung-Sik Lee, Shinsei Ryu, Chetan Nayak, and Matthew PA Fisher. Particle-hole symmetry and the ν= 5 2 quantum hall state. *Physical review letters*, 99(23):236807, 2007.

[42] Michael Levin. Protected edge modes without symmetry. *Physical Review X*, 3(2):021009, 2013.

[43] Michael Levin and Zheng-Cheng Gu. Braiding statistics approach to symmetry-protected topological phases. *Physical Review B*, 86(11):115109, 2012.

[44] Michael Levin, Bertrand I Halperin, and Bernd Rosenow. Particle-hole symmetry and the pfaffian state. *Physical review letters*, 99(23):236806, 2007.

[45] Michael Levin and Ady Stern. Classification and analysis of two-dimensional abelian fractional topological insulators. *Physical Review B*, 86(11):115131, 2012.

[46] Michael Levin and Xiao-Gang Wen. Fermions, strings, and gauge fields in lattice spin models. *Phys. Rev. B*, 67:245316, 2003.

[47] Michael Levin and Xiao-Gang Wen. Detecting topological order in a ground state wave function. *Phys. Rev. Lett.*, 96:110405, 2006.

[48] Michael A. Levin and Xiao-Gang Wen. String-net condensation: A physical mechanism for topological phases. *Phys. Rev. B*, 71:045110, 2005.

[49] Chien-Hung Lin and Michael Levin. Generalizations and limitations of string-net models. *Phys. Rev. B*, 89:195130, May 2014.

[50] Yuan-Ming Lu and Ashvin Vishwanath. Theory and classification of interacting integer topological phases in two dimensions: A chern-simons approach. *Physical Review B*, 86(12):125119, 2012.

[51] Yuan-Ming Lu and Ashvin Vishwanath. Classification and properties of symmetry-enriched topological phases: Chern-simons approach with applications to Z_2 spin liquids. *Phys. Rev. B*, 93:155121, 2016.

[52] A. H. MacDonald. Edge states in the fractional-quantum-hall-effect regime. *Phys. Rev. Lett.*, 64:220–223, Jan 1990.

[53] Andrej Mesaros and Ying Ran. Classification of symmetry enriched topological phases with exactly solvable models. *Phys. Rev. B*, 87:155115, 2013.

[54] Joel E Moore and Xiao-Gang Wen. Classification of disordered phases of quantum hall edge states. *Physical Review B*, 57(16):10138, 1998.

[55] X.-L. Qi and S.-C. Zhang. Topological insulators and superconductors. *Rev. Mod. Phys.*, 83:1057–1110, 2011.

[56] Ron Sabo, Itamar Gurman, Amir Rosenblatt, Fabien Lafont, Daniel Banitt, Jinhong Park, Moty Heiblum, Yuval Gefen, Vladimir Umansky, and Diana Mahalu. Edge reconstruction in fractional quantum hall states. *Nature Physics*, 2017.

[57] Marc D Schulz and Fiona J Burnell. Frustrated topological symmetry breaking: geometrical frustration and anyon condensation. *arXiv preprint arXiv:1510.08104*, 2015.

[58] N. Tarantino, N. H. Lindner, and L. Fidkowski. Symmetry fractionalization and twist defects. *New Journal of Physics*, 18(3):035006, 2016.

[59] J. C. Y. Teo, T. L. Hughes, and E. Fradkin. Theory of Twist Liquids: Gauging an Anyonic Symmetry. *ArXiv e-prints*, 2015.

[60] Daniel C Tsui, Horst L Stormer, and Arthur C Gossard. Two-dimensional magnetotransport in the extreme quantum limit. *Physical Review Letters*, 48(22):1559, 1982.

[61] Vivek Venkatachalam, Sean Hart, Loren Pfeiffer, Ken West, and Amir Yacoby. Local thermometry of neutral modes on the quantum hall edge. *Nature Physics*, 8(9):676–681, 2012.

[62] K. Walker and Z. Wang. (3+1)-tqfts and topological insulators. *Front. Phys.*, 7:1050, 2012.

[63] C. Wang and M. Levin. Topological invariants for gauge theories and symmetry-protected topological phases. *Phys. Rev. B*, 91:165119, 2015.

[64] X. G. Wen. Electrodynamical properties of gapless edge excitations in the fractional quantum hall states. *Phys. Rev. Lett.*, 64:2206–2209, Apr 1990.

[65] Xiao-Gang Wen. Chiral luttinger liquid and the edge excitations in the fractional quantum hall states. *Phys. Rev. B*, 41(18):12838, 1990.

[66] Xiao-Gang Wen. Topological orders and edge excitations in fractional quantum hall states. *Adv. Phys.*, 44(5):405, 1995.

[67] Xiao-Gang Wen. Quantum orders in an exact soluble model. *Phys. Rev. Lett.*, 90(1):016803, 2003.

[68] Xiao-Gang Wen and Qian Niu. Ground-state degeneracy of the fractional quantum hall states in the presence of a random potential and on high-genus riemann surfaces. *Physical Review B*, 41(13):9377, 1990.